Chronology of Planetesimal Differentiation

Based on the Timing of Achondrite Formation in the Early Solar System

by

Daniel Robert Dunlap

A Dissertation Presented in Partial Fulfillment
of the Requirements for the Degree
Doctor of Philosophy

Approved August 2019 by the
Graduate Supervisory Committee:

Meenakshi Wadhwa, Chair
Lindy Elkins-Tanton
Kip Hodges
Thomas Sharp
Steve Desch

ARIZONA STATE UNIVERSITY

May 2020

ABSTRACT

During the early Solar System many physiochemical processes were taking place that would shape the formation and evolution of rocky bodies. Growth of these rocky objects was rapid, with some growing to sizes of 10s – 1000s km ("planetesimals") in the first few million years. Because these objects formed early, they contained sufficient ^{26}Al (an isotope of Al with a short half-life of ~705,000 yrs) to heat the interiors to melting temperatures, resulting in the formation of the first igneous rocks in nacent Solar System. Depending on the size and time of accretion, some bodies experienced high degrees of melting (with some having global magma oceans) while others experienced lower degrees of partial melting, and yet others did not experience any melting at all. These varying degrees of heating and melting processes on early-formed planetesimals produced a variety of achondritic meteorite types. These achondrites have bulk compositions ranging from ultramafic to basaltic, with some rare types having more highly "evolved" (i.e., high-SiO_2) compositions. Determining the detailed chronology of their formation with fine time resolution is key for understanding the earliest stages of planet formation, and there are high resolution chronometers that are ideally suited for this application. Three such chronometers (i.e., the ^{26}Al-^{26}Mg, ^{53}Mn-^{53}Cr, and ^{207}Pb-^{206}Pb chronometers) are the focus of this work. Based on investigations of these chronometers in several achondritic meteorites, the implications for the formation and evolution of planetesimals in the early Solar System will be discussed.

DEDICATION

To Will Minnich, the voice of good reason, my drummer and best friend in the world and to my grandfather Dr. William Dunlap who never stopped learning.

ACKNOWLEDGMENTS

This work represents 6 years of my life. When I think about where path started there are two people I would like to thank first. Dr. Hap McSween and the late Dr. Larry Taylor for opening up this world for me. I will always remember those first BSE images of the enstatite chondrite I classified under their guidance. This experience and the knowledge and kindness they shared with me changed my life, and I will be eternally grateful.

I'd like to thank my committee members, Tom Sharp, Steve Desch, Kip Hodges, Lindy Elkins-Tanton, and most of all Mini Wadhwa. Thank you Mini for taking a chance on me and for helping steer my career and my science. I'd like to thank the Center for Meteorite Studies past and present staff members Susie Nowak and Rebecca Davis who helped in countless ways making sure we had everything we needed. To the ICGL staff; Rebekah Hines thanks for all your help since day one and for always being there to talk to and to Steve Romaniello, I seriously cannot thank you enough for your willingness to work with me and for all your help you taught me a great deal. To Kate Souders and Vinai Rai for you for all your help! To the students of CMS; Curtis Williams taking me under his wing and all the "pop quizzes", Prajkta Mane for countless lively debates, Kera "Squeaky" Tucker, Emilie Dunham, Zack Torrano, Souyma Rai, and Gabriel Franco thank you for being good friends and great scientists! Good luck with your future! I look forward to us working together again. Thanks to Cameron Mercer for being a true friend and confidant.

To my family Judy, John, and Beverly. Thank you for your constant love, support and patience. I know I didn't make it easy on you, but I hope I've made you proud. To my brother Lee, the strongest person I know. To all my friends in the SKM, roots run deep! I love you all.

.

TABLE OF CONTENTS

Page

LIST OF TABLES x

LIST OF FIGURES xi

CHAPTER

1 INTRODUCTION 1

1.1 The Formation and Growth of Planetesimals in the Early Solar System ... 1

1.2 Achondrites 2

1.2.1 Eucrites 3

1.2.2 Brachinites 4

1.2.3 Ungrouped Achondrites 7

1.3 High-Resolution Isotopic Chronometers 8

1.3.1 Relative Chronometers 8

1.3.2 ^{26}Al-^{26}Mg Systematics 9

1.3.3 ^{53}Mn-^{53}Cr Systematics 9

1.3.4 Pb-Pb and Uranium Systematics 14

1.4 Chronology of the Early Solar System 16

2 CHRONOLOGY OF UNGROUPED ACHONDRITES NORTHWEST AFRICA 11119 AND NORTHWEST AFRICA 7325/8486: DIFFERENTIATION HISTORY OF A PLANETESIMAL WITH A HETEROGENEOUSLY EVOLVED CRUST 18

CHAPTER Page

2.1 Introduction....18

2.2 Methods 22

2.2.1 Sample Preparation and Methods for Pb-Pb Analyses of NWA 11119 and NWA 8486.... 23

2.2.2 Sample Preparation and Methods for $^{238}U/^{235}U$ Analyses of NWA 11119 24

2.2.3 Sample Preparation and Methods for ^{53}Mn-^{53}Cr and $\varepsilon^{54}Cr$ Analyses of NWA 11119 25

2.2.4 Sample Preparation and Methods for ^{26}Al-^{26}Mg Analyses of NWA 7325.... 24

2.3 Results....28

2.3.1 Pb-Pb Systematics of NWA 11119 and NWA 8486 28

2.3.2 U-corrected Pb-Pb Age of NWA 11119 29

2.3.3 Pb-Pb Age of NWA 8486....33

2.3.4 ^{53}Mn-^{53}Cr and $\varepsilon^{54}Cr$ Systematics of NWA 11119 38

2.3.5 ^{26}Al-^{26}Mg Systematics of NWA 7325....39

2.4 Discussion....41

2.4.1 High-Resolution Chronology of NWA 11119 and NWA 7325/8486.. 41

2.4.2 Petrogenesis of the Silica-Rich Ungrouped Achondrite NWA 11119. 47

CHAPTER Page

2.4.3 NWA 11119 and NWA 7325/8486: Arguments for and Against a Shared Parent Body 49

2.4.4 Concordance and Implications for the Distribution of ^{267}Al in the Early Solar System 53

2.5 Conclusions 55

2.6 Supplementary Materials 56

2.6.1 Pb Methods for NWA 11119 56

2.6.2 Pb Methods for NWA 8486 58

2.6.3 Cr Methods 61

2.6.4 Supplementary Figures 65

2.6.5 Supplementary Tables 66

3 HIGH RESOLUTION CHRONOLOGY OF THE UNEQUILIBRATED EUCRITE NORTHWEST AFRICA 8661: TIMING OF BASALTIC CRUST FORMATION ON VESTA 67

3.1 Introduction 67

3.2 Petrography of NWA 8661 68

3.3 High-Resolution Chronology of NWA 8661 and its Implications 70

3.4 Supplementary Materials 77

3.4.1 NWA 8661 Sample Preparation 77

3.4.2 ^{26}Al-^{26}Mg Methods 77

3.4.3 ^{53}Mn-^{53}Cr Methods 79

CHAPTER Page

3.4.4 Pb-Pb Methods 80
3.4.5 Uranium Methods 82
3.4.6 Pb-Pb Systematics of NWA 8661 82
3.5 Supplementary Figures 85
3.6 Supplementary Tables 87

4 THE TIMING OF BRACHINITE FORMATION BASED ON SHORT-LIVED ISOTOPE SYSTEMATICS OF BRACHINA AND NORTHWEST AFRICA 4882 90
4.1 Introduction 90
4.2 Methods 91
4.2.1 ^{53}Mn-^{53}Cr Methods 91
4.2.2 ^{26}Al-^{26}Mg Methods 93
4.3 Results 94
4.3.1 Chromium Systematics of Brachina 94
4.3.2 Chromium Systematics of NWA 4882 95
4.3.3 ^{26}Al-^{26}Mg Systematics of Brachina and NWA 4882 96
4.4 Discussion 98
4.4.1 Chronology of Brachina and NWA 4882 98
4.4.2 Implications for the Petrogenesis of the Brachinite Parent Body 100
4.5 Conclusions 102

CHAPTER Page

5 PLANETESIMAL FORMATION AS A KEY TO UNDERSTANDING THE AGE OF THE SOLAR SYSTEM 104

5.1 Planetesimal Formation 104

5.1.1 Planetesimals as a Stage in Planet Formation 104

5.1.2 Timing of Planetesimal Formation 106

5.2 The Age of the Solar System 112

5.2.1 Challenges with Determining the Ages of CAIs 114

5.2.2 Estimating the Age of the Solar System 118

5.3 Initial Abundance of ^{53}Mn in the Early Solar System 129

5.4 Conclusions 134

REFERENCES 135

LIST OF TABLES

Table		Page
2.1	Pb Isotope Data for NWA 11119	30
2.2	Pb Isotope Data for NWA 8486	35
2.3	Mn-Cr Data for NWA 11119	38
2.4	Al-Mg Data for NWA 7325	40
S2.1	Uranium Isotope Data for NWA 11119	66
S3.1	Al-Mg Data for NWA 8661	87
S3.2	Mn-Cr Data for NWA 8661	87
S3.3	Pb Isotope Data for NWA 8661	88
S3.4	Uranium Isotope Data for NWA 8661	89
4.1	Mn-Cr Data for Brachina and NWA 4882	96
4.2	Al-Mg Data for Brachina and NWA 3882	97
5.1	^{26}Al-^{26}Mg and ^{53}Mn-^{53}Cr Systematics and Pb-Pb Ages of Achondrites	122
5.2	Calculations for the Estimation of the Age of the Solar System	122
5.3	Initial ^{53}Mn/^{55}Mn Calculation Parameters	123

LIST OF FIGURES

Figure		Page
2.1	NWA 11119 Pb-Pb Regression	31
2.2	NWA 11119 Pb-Pb Isochron	32
2.3	NWA 11119 Pb Model Ages	32
2.4	NWA 11119 $^{206}Pb/^{204}Pb$ vs Model Age	33
2.5	NWA 8486 Pb-Pb Regression	34
2.6	NWA 8486 Pb-Pb Isochron	37
2.7	NWA 8486/NWA 7325 Pb-Pb Isochron	37
2.8	NWA 11119 Mn-Cr Isochron	39
2.9	NWA 7325 Al-Mg Isochron	41
S2.1	Chromium Peak Postions (For Neptune)	65
S2.2	Chromium Isotope Long Term Reproducibility	66
3.1	NWA 8661 BSE Image	69
3.2a	NWA 8661 Al-Mg Isochron	71
3.2b	NWA 8661 Mn-Cr Isochron	71
3.2c	NWA 8661 Pb-Pb Isochron	71
3.2d	NWA 8661 Pb Model Ages	71
3.3	Eucrite Literature Age Comparison	74
S3.1	NWA 9661 Pyroxene Quadrilateral	85
S3.2	NWA 8661 Pb-Pb Isotope Regression	86

Figure Page

4.1 Brachinite Mn-Cr Isochron 97

4.2 Brachinite Al-Mg Isochron 99

5.1 MSWD and Max Deviation vs Age 123

5.2 ln(^{26}Al/^{27}Al) vs Absolute Age 126

5.3 Achondrite Age Compoarison using Different Anchors 127

5.4 ln(^{53}Mn/^{55}Mn) vs Absolute Age 130

CHAPTER 1

INTRODUCTION

1.1 The Formation and Growth of Planetesimals in the Early Solar System

The formation of our Solar System likely marks a dynamic period in the evolution of its parent molecular cloud. Cloud collapse and accretion of infalling gas and dust led to the formation of a nebular disk around the young Sun. During this time the composition and ultimate structure of our Solar System was being defined by physiochemical forces. As the disk began to cool, the first (typically μm- to mm-sized) solids began condensing from the gas; subsequent processes in the nebula reheated and melted some these early-formed solids. Calcium-aluminum-rich inclusions (CAIs) found in primitive chondritic meteorites likely represent some of these first-formed solids in the solar nebula and are therefore considered to be cosmochemical markers of the start of our Solar System. This was followed quickly by the formation of larger planetesimal-sized objects, planetary embryos, and ultimately the rocky planets.

The accretion and early evolution of planetesimals was an important step in the formation history of the rocky planets. Planetesimals define a size range for objects whose sizes are great enough that their mass is held together by gravity (Johansen et al., 2014). This corresponds to minimum diameters of 10s – 1000s m (Benz et al., 2000) up to maximum diameters of 10s – 1000s km (Ida et al., 2008), where gravitational focusing leads to runaway growth. Astronomical observations as well as dynamical models suggest that planetesimal formation is a ubiquitous stage in the evolution of planetary systems.

There are several different hypotheses that have been discussed in the literature for the formation of planetesimals in the early Solar System (Windmark et al., 2012; Wurm et al., 2005). In their review, Johansen et al., (2014) explain that planetesimal formation likely proceeds at first un-aided by self-gravity as particles stick together forming pebbles until they reach Stokes numbers between 0.01 and 1, where self-gravity takes over as the growth mechanism. Astronomical observations of protoplanetary disks suggest that their lifetimes (i.e., the time period over which most of the mass is accreted into planetesimals and planetary bodies) are typically 1-10 Myr (e.g., Haisch, Jr. et al., 2001; Li & Xiao, 2016; Strom et al., 1989). Additionally, isotopic investigations of meteoritic materials indicate rapid formation of planetesimals and planets (Bizzarro et al., 2005; Kleine & Wadhwa, 2017; Kruijer et al., 2017). This work contributes to the growing knowledge base about the formation timescales of planetesimals in our Solar System. The following sections (1.2-1.4) provide a brief introduction to the types of meteoritic materials that have been investigated and the high-resolution chronometers that have been utilized as part of this work to obtain chronological constraints on planetesimal formation and differentiation processes in the early Solar System.

1.2 Achondrites

Achondrites are igneous meteorites which are remnants of the earliest stages of planetesimal formation and differentiation in the early Solar System. The short-lived radionuclide ^{26}Al ($t_{1/2}$ ~705,000 yrs) is thought to be the primary heat source for heating and melting of planetesimals. Depending on the accretion time (corresponding to different initial abundance of ^{26}Al) and initial mass, planetesimals underwent different

degrees of internal heating and melting. This variability in accretion time and initial mass resulted in a variety of different achondrite types, each recording its conditions of formation. The following sections describe the achondrite types that were investigated as part of this work.

1.2.1 Eucrites

Eucrites are basaltic rocks belonging to the Howardite-Eucrite-Diogenite (HED) clan of achondrites. The HED meteorites are among the most numerous achondrites and have been extensively studied (Mittlefehldt, 2015). These meteorites are thought to originate from the asteroid Vesta and are the only achondrite class (outside of lunar and martian meteorites) to have a known parent body (McSween et al., 2013). The surface composition of Vesta was mapped by NASA's Dawn spacecraft mission and was found to be similar to the bulk compositions of the HEDs (De Sanctis et al., 2012).

Eucrites have mineraologies dominated by fine- to medium-sized grains of pigeonite and plagioclase in sub-equal proportions. Most eucrites are brecciated and have experienced post-formation thermal metamorphism. The earliest model for eucrite formation was suggested by (Mason, 1967) and was developed in an attempt to explain HEDs as well as iron meteorites and pallasites (stony-iron meteorites) as the products of total melting on their parent body. The eucrites in Mason's model were the residual melts which formed during parent body crystallization. Stolper, (1977) carried out melting experiments and concluded that eucrites were primary partial melts of an ordinary chondrite parent body. Siderophile element abundances indicate that eucrite melts did not equilibrate with metal and do not support a partial melt model and instead support a

model where silicates and metal were completely molten (Righter & Drake, 1996). Subsequently, three studies (Righter & Drake, 1997; Ruzicka et al., 1997; Warren, 1997) laid out detailed petrogenesis models that involved major and trace element calculations that argued for, what would later be called, a magma ocean model for Vesta. Differences in the models centered on the sequence of crystallization from the magma ocean. In the model of (Righter & Drake, 1997) the early stages of crystallization formed harzburgites under equilibrium conditions and the residual liquid then underwent fractional crystallization to form the basaltic eucrites. The model by Ruzicka et al. (1997) had dunites and orthopyroxenite forming via fractional crystallization with the basaltic eucrites forming later under near-equilibrium conditions. The homogeneity of $\Delta^{17}O$ among bulk HEDs was used to argue for a magma ocean on Vesta arising from melting of a mixture of chondritic compositions (Greenwood et al., 2005); this uniformity necessitated vigorous convection within this magma ocean. The most recent model for the petrogenesis of Vesta involves early equilibrium crystallization which drives convective lock up leading to increasingly non-equilibrium fractional crystallization followed by basalt formation (Mandler & Elkins-Tanton, 2013).

Many chronologic investigations of Vesta have been conducted over the years. However, the chronology of eucrites is often inhibited by post-formation impact and thermal metamorphism. In an early landmark paper, the eucrite Juvinas was determined to have an ancient ^{87}Rb-^{87}Sr age of 4.5 Ga (Allégre et al., 1975). This was the first such report that indicated that igneous meteorites, and eucrites in particular, were forming in the earliest periods of Solar System history. Subsequently, Birck & Allègre, (1978) determined the ^{87}Rb-^{87}Sr age of two eucrites (Ibitira and Juvinas) which they used to infer

that differentiation of the HED parent body took place at ~4.5 Ga. Using ^{87}Rb-^{87}Sr and ^{143}Sm-^{147}Nd systematics, Nyquist et al., (1986) determined the ages of several clasts in the basaltic eucrite Yamato 75011 to be ~4.5 Ga. These ages were relatively low precision by today's standards and yet changed our understanding of the timeline of achondrite formation. With the advent of short-lived chronometers, Lugmair & Shukolyukov, (1998) reported high-precision ^{53}Mn-^{53}Cr relative ages for a number of achondrites. In particular, these authors reported a ^{53}Mn-^{53}Cr age of 4562.5 ± 1.0 Ma for the basaltic eucrite Juvinas and a model age of 4564.8 ± 0.9 Ma for the timing of silicate fractionation on the HED parent body (defined by whole rock analyses). This work demonstrated that the HED parent body formed, melted and began crystalizing basalts early in Solar System history. This result was supported by the results of thermal modelling of Vesta published the same year (Ghosh & McSween, 1998). The bulk ^{26}Al-^{26}Mg systematics were reported for several eucrites and diogenites by Bizzarro et al. (2005) and Schiller et al. (2011). These studies indicated that silicate fractionation began on the HED parent body by ~1 Ma after CAI formation. These model ages were used by Schiller et al. (2011) to suggest that the HEDs did not originate on Vesta, but instead formed on a much smaller parent body. The duration of igneous activity on Vesta is presently unknown. Numerous zircons from HEDs were investigated for their Pb-Pb systematics and give a mean Pb-Pb age of 4554.5 ± 2.0 Ma (Iizuka et al., 2015). These zircon dates were interpreted by Iizuka et al., (2015) to give the timing of "global crustal" metamorphism on Vesta. The most recent and only high-precision ^{26}Al-^{26}Mg internal isochrons for eucrites were reported by Hublet et al. (2017). These authors report ages, relative to CAIs, of 3.04, 4.17 and 6.75 Ma, respectively, of the basaltic eucrites Camel

Donga, Yamato 793591 and Yamato 792510. In this work, we report for the first time concordant internal isochron ages based on three high-resolution chronometers (^{26}Al-^{26}Mg, ^{53}Mn-^{53}Cr and ^{207}Pb-^{206}Pb) for one of the most unequilibrated eucrites and discuss these results and their implications for the petrogenesis of Vesta.

1.2.2 Brachinites

Brachinites are ultramafic rocks with dunitic to wehrlitic bulk compositions (Mittlefehldt, 2015). These achondrites are a small, but critically important group with mineralogies dominated by olivine and clinopyroxene with minor amounts of orthopyroxene, plagioclase and other trace minerals. It has been suggested that brachinites are residues of low degrees of partial melting on chondritic parent bodies (Day et al., 2009; Day, et al., 2012; Gardner-vandy et al., 2013; Goodrich & Delaney, 2000; Nehru et al., 1992). These arguments are based on textural, isotopic and geochemical data. However, other authors have interpreted the textural and geochemical properties of brachinites as being more consistent with formation as igneous cumulate rocks (Mittlefehldt et al., 2003).

The chronology of brachinites is not well constrained. These achondrites were first suggested to be ancient rocks based on excesses of ^{129}Xe (the radiogenic daughter product of ^{129}I) in the brachinites Eagles Nest, ALH 84025 and Brachina (Bogard et al., 1983; Ott et al., 1985, 1987; Swindle et al., 1998). An ancient ^{53}Mn-^{53}Cr age for Brachina was reported by Wadhwa et al., (1998) who suggested that Brachina was ~ 4 Ma younger than CAIs. In this work, we report the ^{53}Mn-^{53}Cr internal isochron ages and ^{26}Al-^{26}Mg

model ages of two brachinites, Brachina and NWA 4882. Understanding the chronology of brachinite formation can place constraints on their petrogenesis and relationship to other achondrites.

1.2.3 Ungrouped Achondrites

Ungrouped achondrites are so named because they do not fit into the currently known achondrite group definitions based on their mineralogical, geochemical and/or isotopic characteristics. Many of these ungrouped achondrites have been recovered recently in Northwest Africa (NWA) region. There have been several previous chronologic investigations of ungrouped achondrites. One of the first ungrouped achondrites to be studied, Asuka 881394, is a basaltic meteorite that was found to have an ancient crystallization age of ~2.4 Ma after CAI formation (Hublet et al., 2017; Nyquist et al., 2003; Wadhwa et al., 2009; Wimpenny et al., 2019). The NWA 2976 meteorite is another basaltic ungrouped achondrite whose formation age is ~ 4.2 Ma younger than CAIs (Bouvier et al., 2011). Yet another basaltic ungrouped achondrite with unusual mineral compositions, NWA 7325, was found to have formation age of ~ 4 Ma younger than CAIs (Koefoed et al., 2016). Recently, another interesting basaltic achondrite, NWA 6704, was found to have a ^{207}Pb-^{206}Pb age of ~ 4.6 Ma after CAI formation (Amelin et al., 2019; Sanborn et al., 2019).

One particularly exciting ungrouped achondrite studied by us, NWA 11119, has an andesitic-dacitic bulk composition, and has a ^{26}Al-^{26}Mg age that is ~2.5 Ma younger than CAIs (Srinivasan et al., 2018). This was an important discovery as it demonstrated that evolved SiO_2-rich crustal compositions were possible on at least some asteroidal

bodies early in Solar System history. This ungrouped achondrite will be discussed further in Chapter 2. Ungrouped achondrites are often sole representatives of previously unknown parent bodies and are critical to understanding the compositional diversity among achondrite parent bodies.

1.3 High-Resolution Isotopic Chronometers

1.3.1 Relative Chronometers

Relative chronometers are particularly useful for determining high-resolution relative ages of objects that were forming in the earliest periods of Solar System history. Due to their short half-lives (which are significantly shorter than the lifetime of the Solar System), the parent isotopes have completely decayed, and it is no longer possible to directly measure their abundance. Due to significant advances in analytical capabilities in recent year, geochemists are able to measure the isotopic compositions of low-concentration elements with ever better precision. This has enabled the measurement of small variations in the daughter isotopes of the short-lived radionuclides that had originally been present. For the determination of high-resolution relative ages of meteoritic samples based on a short-lived chronometer certain conditions must be met. First, the abundance of the parent isotope must be demonstrated to be distributed homogeneously in the reservoir from these meteoritic samples originated. This is an assumption which has been debated extensively in the literature for ^{26}Al (half-life ~705,000 yrs) and is further discussed in the following section. Second, the parent-daughter isotope systematics must not have been disturbed following the last isotopic equilibration event (which is the event that is dated by this system). Finally, to map a

relative high-resolution age based on a short-lived chronometer to an absolute time scale, an age anchor must be used. This age anchor is a meteoritic sample in which the initial abundance of the short-lived radionuclide has been determined and for which has an absolute U-corrected Pb-Pb age has been determined.

1.3.2 The ^{26}Al-^{26}Mg Chronometer

Aluminum-26 is a short-lived radioactive isotope with a half-life of 705,000 yrs (Norris et al., 1983). Although the ^{26}Al has long since decayed, the effects on the daughter isotope ^{26}Mg can be measured as a ratio to the major isotope ^{24}Mg. Because these effects are often very small, we adopt the μ-notation (parts per million) in order to show the non-mass dependent effects on ^{26}Mg. This is done as follows:

$$\mu^{26}Mg^{*}\,(\text{ppm}) = \left[\frac{\left(\frac{^{26}Mg}{^{24}Mg}\right)_{\text{sample}}}{\left(\frac{^{26}Mg}{^{24}Mg}\right)_{\text{standard}}} - 1\right] \times 10^{6}$$

In order to determine the ^{26}Al-^{26}Mg ages of the achondrites included in this dissertation, improvements to our laboratory's analytical capabilities were needed. This involved further developments based on the work that began in the Isotope Cosmochemistry and Geochemistry Lab (ICGL) at ASU by Spivak-Birndorf et al., (2009) and Bouvier et al., (2011). From the onset of this work, the necessity to improve the precision with which we measured Mg isotopes drove changes in the chemistry and analytical procedures. Only minor changes were made to the chemical procedures to improve our column yield. The Mg purification chemistry uses Biorad® AG50-x8 200-

400 mesh cation resin. This chemistry uses increasing volumes of titrated 1N HNO_3 totaling 1.1 mL to strip the transition metals from the column, followed by ~5 mL of 1N HNO_3 to collect the Mg, and finally 7 mL of 4N HCl to strip the remaining elements off the column. This procedure was repeated in triplicate to obtain quantitative recovery of purified Mg.

The next improvements made were to the mass spectrometric methods. We tested different concentrations of Mg solutions for different measurement times to improve our measurement precision. We optimized a method that utilized ~10 µg total Mg per sample. This typically involved 5 measurements comprised of 3 blocks of 25 cycles with 8 seconds of integration time per cycle. We ran samples and standards (in 3% HNO_3 solution) at a concentration of 1.5 ppm. We ran samples and standards this way over a period of four years and accumulated statistics on our external reproducibility over this time period. Based on repeated measurements of natural and synthetic Mg standards we estimate our long-term external reproducibility to be ±7 ppm on $\mu^{26}Mg^*$. In the final 1.5 years of this project and with the addition of a new Aridus II desolvating nebulizer, we were able to lower our measurement concentration to 250 ppb and achieve similar reproducibility while consuming only ~ 1 µg total Mg. Magnesium isotopes are measured in medium resolution mode with a typical Mass-Resolving Power (MRP = M/ΔM) >8000.

1.3.3 The ^{53}Mn-^{53}Cr Chronometer

Chromium-53 is another short-lived radioisotope with a half-life of 3.7 Ma (Honda & Imamura, 1971a). As was the case for ^{26}Al, the parent isotope has completely

decayed, and we measure the effects of this decay on the abundance of the daughter isotope ^{53}Cr. Since these are small deviations in isotope composition, we represent these non-mass dependent effects on ^{53}Cr in μ-notation (ppm) and occasionally in ε-notation (parts per 10,000) as follows:

$$\mu^{53}Cr^{*}\,(\text{ppm}) = \left[\frac{\left(\frac{^{53}Cr}{^{52}Cr}\right)_{\text{sample}}}{\left(\frac{^{53}CR}{^{52}Cr}\right)_{\text{standard}}} - 1\right] \times 10^{6}$$

In addition to its utility as a chronometer, chromium has the neutron-rich isotope ^{54}Cr which is associated with nucleosynthetic anomalies. Characterization of these anomalies among planetary materials has shown that ^{54}Cr can be used as a tracer of genetic relationships among meteoritic materials (e.g., Sanborn et al., 2019; Trinquier et al., 2007; Warren, 2011).

Purification of chromium is a complicated and time-consuming process. Development of the Cr chemistry began in the ICGL with work by graduate student Cameron Mercer and Lab Manager Dr. Steve Romaniello in 2014 in an attempt to separate Cr from CAIs. The chemical procedure has been modified several times to achieve higher Cr yields and better purification. The current Cr purification protocol in the ICGL is noted below.

Chromium was purified using a chemistry procedure modified after a previously published protocol by Yamakawa et al. (2009). This procedure requires four columns to separate Cr cleanly from other elements (specifically other transition metals such as Fe). The first column, using 1 mL of BioRad AG1-x8 200-400 mesh anion resin loaded onto a BioRad polypropylene column, separates Fe from other major elements. The sample is

loaded onto the column in 6M HCl and the Cr elutes off the column immediately in 5 mL of 6M HCl along with nickel (Ni), sodium (Na), titanium (Ti), vanadium (V), magnesium (Mg), calcium (Ca), and aluminum (Al). The Cr yield from this column is routinely > 95%. The second column, using 1 mL of Biorad AG50-x8 200-400 mesh anion resin loaded onto a BioRad polypropylene column, is designed to separate Cr from Ni and other REEs. As detailed in the work of Larsen et al. (2016), the exact speciation of Cr in chloride form must be controlled in order to elute Cr effectively. Our samples are fluxed on the hotplate in concentrated HCl for 5 hrs at 120 ºC. This ensures complete transformation of Cr species into the $CrCl_2^+$ form. This solution is removed from the hotplate, diluted with MQ H_2O to make 2.4 mL of 1M HCl, and immediately loaded onto the 2nd column. The Cr is eluted off the column in 7 mL of 1M HCl. The 3rd column uses AG50-x8 200-400 mesh resin loaded onto a custom-made Teflon column (with dimensions of h = 23.3 mm and d = 4.05 mm) and is designed to separate Cr from Na and the interfering elements Ti and V. As before, the speciation of Cr in HNO_3 must be carefully controlled such that Cr is in the form CrO_3 to ensure effective elution. The sample is heated in 1.5 mL of 1M HNO_3 in a sealed Savillex Teflon vial in an oven at 50 ºC for 24 hrs. The sample is then diluted with MQ H_2O in order to make 3 mL of 0.5M HNO_3 and immediately loaded onto the third column. After eluting Na, Ti, and V (among other elements) in 0.5M HNO_3, 0.5M HF, and 1M HCl, the Cr is eluted in 5 mL of 6M HCl.

These procedures were designed to address two specific issues: 1) effectively separate Cr from other elements, specifically those with isotopes that create interferences during measurement; and 2) promote high Cr yields. To prevent measurable isotopic

fractionation effects due to incomplete elution of Cr, total chemistry Cr yields need to be > 80% (typical in the literature) or even as high as >95% (Larsen et al., 2016). Larsen et al., (2016) performed a detailed study of the speciation of Cr in the acids of interest, and the effects that low yields produce on the measured Cr isotope ratios. These authors warn that high recovery (>95%) Cr chemistry is necessary to measure Cr isotopes accurately. In response to these findings, a series of tests were carried out to evaluate the impact of Cr recovery on the measured isotope ratios. These procedural tests demonstrated that at our current level of precision we do not see measurable isotopic effects at total Cr yields > 80% and our chemistry protocol is successfully and reproducibly producing total chemistry yields >> 80%. A more serious issue facing the successful measurement of Cr by Multi Collector Inductively Coupled Plasma Mass Spectrometer (MC-ICPMS), specifically measurement of the $^{54}Cr/^{52}Cr$ ratios, is the effective total separation of Fe from Cr. Iron-54 (^{54}Fe) is a direct isobaric interference on ^{54}Cr. As such, near complete separation of Cr from Fe (i.e. $Fe/Cr < 1x10^{-5}$) is needed to reduce the interference of ^{54}Fe on ^{54}Cr to a level that does not produce any measurable artifacts. Additionally, if the Fe is not completely separated during chemistry, then the Fe that remains in the sample solution is likely fractionated (Anbar et al., 2000). This complicates any means of correcting the isotopic interference from ^{54}Fe on ^{54}Cr and can produce erroneous measured $^{54}Cr/^{52}Cr$ ratios. We developed methods to remove any remaining Fe after our chemical procedures in a final clean-up step using BioRad AG1-x8 20-50 mesh resin. This resin is added (~10 beads) to the Cr cut from the 3rd column, after being evaporated and brought up in 10N HCl. The sample container is agitated on an orbital shaker to promote bead interaction with the acid, and then the solution is pipetted away from the

beads. This method is capable of removing >99% of the remaining Fe which ensures Fe/Cr $<1x10^{-5}$.

Chromium isotopes are measured in the ICGL at ASU on our dedicated Thermo *Neptune* MC-ICPMS. Chromium is measured in high-resolution mode (mass resolving power, $M/\Delta M >> 8000$) with instrumental setup as shown in Fig. 1.1. The cups are positioned such that measurements are made on the low mass shoulder of the peak in order to avoid interferences on ^{56}Fe from argon oxide (ArO), as Ar is the sample carrier gas. A typical peak shape and analysis position are shown in Fig. 1.1. The radiogenic excesses on ^{53}Cr from the decay of ^{53}Mn are given as $\mu^{53}Cr^*$ and the nucleosynthetic effects on ^{54}Cr are shown as $\mu^{54}Cr$. Based on repeat analyses of the terrestrial rock standard DTS-2, Allende WR, and NBS and SPEX pure Cr solutions, we currently estimate our external reproducibility for $\mu^{53}Cr^*$ to be ±10 ppm and for $\mu^{54}Cr$ to be ±22 ppm (Fig. S3). The analyses were optimized for ~1 µg of total Cr. Running at a concentration of 800 ppb, this typically allows for 4 – 5 analyses (each comprised of 50 individual cycles). All samples and standards are run in an identical fashion, where one data point represents an average of the 4 -5 individual analyses. Our uncertainties are reported as either the internal 2 standard error (2SE) or the external reproducibility (2SD), whichever is larger.

1.3.4 The Pb-Pb and Uranium Isotope Systematics

The U-Pb system is uniquely powerful high-resolution absolute chronometer. Includes the decay of two U isotopes: ^{238}U which decays to ^{206}Pb with a half-life of 4.5 Ga and ^{235}U which decays to ^{207}Pb with a half-life of 0.7 Ga. The work reported here on

this chronometer was conducted in collaboration with colleagues at Australian National Laboratory who have previously published their analytical techniques (Amelin et al., 2009; Koefoed et al., 2016). Purification of Pb begins with a serial leaching procedure using different acids with different concentrations to separate the different Pb components. The Pb isotopic composition of any meteoritic material is typically comprised of three components: radiogenic Pb, primordial Pb and modern terrestrial Pb. The radiogenic Pb is from the decay of the U isotopes and is used to determine the age of the sample. Primordial Pb (Tatsumoto et al., 1973) is the composition inherent to the Solar System while the modern terrestrial Pb (Stacey & Kramers, 1975) is the result of alteration during a meteorite's residence on Earth. This three-component mixture of Pb isotopic compositions inhibits accurate age determination and must be reduced to a two-component mixture with one component being radiogenic Pb and the other component ideally being the primordial composition. This is achieved during the progressive leaching procedure such that the data can be regressed using an isochron to determine an age. Unlike the relative chronometers, an absolute age of a meteorite can be determined using the Pb isotope systematics.

Until 2010 it was believed that the $^{238}U/^{235}U$ ratio was invariant among all natural samples. However, Brennecka et al. (2010) unambiguously demonstrated that there was significant variability in the $^{238}U/^{235}U$ ratio in CAIs. It has since been shown that there is variability in the $^{238}U/^{235}U$ ratio in bulk meteorites, including achondrites (Goldmann et al., 2015; Tissot et al., 2017). The $^{238}U/^{235}U$ ratio is used in the age calculation and an inaccuracy in this ratio can lead to inaccurate ages. It is, therefore, necessary to measure

the $^{238}U/^{235}U$ ratio in samples for which a Pb-Pb age is to be determined. For our U isotope measurements, we have employed the U chemistry and analytical procedures similar to those reported in Goldmann et al. (2015).

1.4 Chronology of the Early Solar System

In 1955, Wasserburg and Hayden reported the ^{40}K-^{40}Ar ages of chondritic meteorites to be 4.7×10^9 - 4.8×10^9 yrs. One year later, in 1956, Claire Patterson reported the age of meteorites and the Earth (based on Pb-Pb analyses of ordinary chondrites, a eucrite and iron meteorites) as $(4.55 \pm 0.07) \times 10^9$ yrs (Patterson, 1956). This pioneering work by Patterson has survived the test of time as our current best estimate for the age of the Solar System is $(4.5673 \pm 0.0003) \times 10^9$ yrs (Connelly et al., 2012). Dating techniques using the Pb-Pb method have seen great advancements through the years and now routinely achieve age uncertainties <0.5 Ma.

Chronometers that rely on the decay of short-lived radionuclides such as the ^{26}Al-^{26}Mg and ^{53}Mn-^{53}Cr systems have also been successfully applied to a variety of meteoritic materials. In 1976, Lee et al., (1976) demonstrated that excesses in ^{26}Mg were correlated with Al/Mg ratios in separates from CAIs and were definitively the result of *in situ* decay of ^{26}Al. These findings in Allende CAIs proved that ^{26}Al was live during the formation of CAIs. The following year, Lee et al., (1977) reported a $^{26}Al/^{27}Al$ ratio based on mineral separates from an Allende CAI of $\sim 5 \times 10^{-5}$. This ratio has been repeatedly shown to be the best estimate of the Solar System initial $^{26}Al/^{27}Al$ ratio (Kita et al., 2013; Macpherson et al., 1995) and is commonly referred to as the "canonical value".

Birck & Allègre (1985) first resolved anomalies in ^{53}Cr that were correlated with Mn/Cr ratios in minerals from an Allende CAI. Lugmair & Galer (1992) and Lugmair & Shukolyukov (1998) were the first to report Pb-Pb and Mn-Cr systematics, respectively, for the angrite LEW 86010. This angrite has since been used as an age anchor for other meteorites for which the Mn-Cr systematics have been determined. Lugmair & Shukolyukov (1998) additionally reported the relative ^{53}Mn-^{53}Cr ages of several eucrites (as well as other achondrites) and defined the timing of global differentiation of Vesta based on a whole rock isochron defined by the HED meteorites. Srinivasan et al. (1999) were the first to report excesses in ^{26}Mg in plagioclase from a eucrite (Piplia Kalan), although their plagioclase data did not show a good correlation of $^{26}Mg^*$ with Al/Mg ratios. The first concordant ages for both the ^{26}Al-^{26}Mg and ^{53}Mn-^{53}Cr chronometers were reported for the achondrite Asuka 881394 by Nyquist et al., (2003). At the time it was thought to be a eucrite but was later determined to be an ungrouped achondrite. Since then, three achondrites - the volcanic angrite D'Orbigny, and two ungrouped achondrites NWA 2976 and NWA 6704 - have reported concordant ages among the short-lived and U-corrected Pb-Pb systems. This dissertation expands on that work by adding high-resolution chronological constraints for a new ungrouped achondrite NWA 11119 (chapter 2) and the unequilibrated basaltic eucrite NWA 8661 (chapter 3).

CHAPTER 2

CHRONOLOGY OF UNGROUPED ACHONDRITES NORTHWEST AFRICA 11119 AND NORTHWEST AFRICA 7325/8486: DIFFERENTIATION HISTORY OF A PLANETESIMAL WITH A HETEROGENEOUSLY EVOLVED CRUST

2.1 Introduction

Achondrites are remnants of parent bodies which experienced varying degrees of internal heating and are the earliest examples of igneous processes which are prevalent among rocky bodies in the early Solar System. Relationships between achondrites, and their parent bodies, can be investigated using a variety of petrologic, geochemical and isotopic characteristics. When a direct relationship between an achondrite sample and previously characterized materials cannot be determined, such achondrites are classified as 'ungrouped', and often represent sampling of previously unknown parent bodies. Ungrouped achondrites expand our understanding of the types of parent bodies present and the diversity of processes acting in the early Solar System. Each new ungrouped achondrite that is recovered and studied allows us to obtain better constraints on the geologic diversity represented among planetesimals and their timescales of formation. Two such ungrouped achondrites, Northwest Africa (NWA) 11119 and NWA 8486 (paired stone to NWA 7325), which may have originated on a common parent body, are the focus of this study.

Northwest Africa 11119 is a porphyritic extrusive igneous rock with a silica-rich (andesitic-dacitic) bulk composition. The major mineralogy consists of phenocrysts of

magnesium (Mg)-rich pyroxene, calcium (Ca)-rich plagioclase, and free silica (i.e. tridymite). Texturally, NWA 11119 is composed of phenocrysts surrounded by quench melt, with the frequent occurrence of millimeter (mm)-sized vesicles/cavities, strong evidence of extrusive volcanism. At 30 vol% SiO_2, NWA 11119 contains the highest amount of free silica in any known achondrite (Srinivasan et al., 2018). Based on the Fe/Mn elemental ratio, NWA 11119 is also quite reduced compared to many achondrites and likely formed in a low oxygen fugacity (fO_2) environment below the Iron-Wustite (IW) buffer, but above the Mn-MnO buffer similar to winonaites (Bennedix et al., 1998).

The majority of known achondrites have basaltic to ultramafic compositions and are the results of low to high degrees of melting on their parent bodies, such that their bulk compositions can be approximated using heating experiments performed on known chondritic compositions. Srinivasan et al., (2018) discussed the petrologic pathways towards creating an andesitic/dacitic composition and found that it is difficult to produce high silicon dioxide (SiO_2) abundances in materials with low bulk alkali elements (< 1.5 wt%), and maintain low iron oxide (FeO) abundance by partial melting of L6 or H ordinary or R4 rumuruti chondrite-like compositions (Feldsteing et a., 2001; Gardner-vandy et al., 2013; Usui et al., 2015). A partial melting experiment of an EH4 enstatite chondrite-like composition produced andesitic-dacitic silicate melts with low alkali element contents, but the FeO was even lower than that of NWA 11119 due to the extremely reduced nature of the enstatite chondrites (McCoy et al., 1999). However, these partial melting experiments prove that driving to high SiO_2 is possible while maintaining low bulk alkalis if the fO_2 was intermediate between those tested in the H (IW-1) and EH4 (IW-5) studies. Regardless of the starting composition or melting

pathway, NWA 11119 represents the first unambiguous example of evolved volcanism on a planetesimal. Srinivasan et al. (2018) reported the ^{26}Al-^{26}Mg age of NWA 11119 to be 4564.8 ± 0.3 million years (Ma) establishing it as one of the oldest known achondrites.

The NWA 8486 achondrite, and the paired stones NWA 7325 and NWA 8014, are another example of unique ungrouped achondrites. The NWA 7325 stone was first described by Irving et al. (2013), who suggested that it may have originated from the planet Mercury based on its bulk composition. While this argument was not further substantiated, this work fueled interest in the stone. Barrat et al. (2015) subsequently published a detailed petrologic investigation of NWA 7325, concluding that it represents a fragment from a new, and previously unsampled achondrite parent body. Koefoed et al. (2016b) combined high precision U-Pb and ^{26}Al-^{26}Mg chronometers to determine the crystallization age of NWA 7325. They reported a Pb-Pb age of 4563.4 ± 2.4 Ma and an ^{26}Al-^{26}Mg age of 4563.09 ± 0.26 Ma, which indicates that NWA 7325 crystallized ~4 Ma after calcium-aluminum-rich inclusions (CAIs) the earliest-formed solids in our Solar System (Connelly et al., 2012). Goodrich et al. (2016) developed a detailed petrologic, trace element, and isotopic argument that while NWA 7325 shares some similarities to ureilites and the Acapulco meteorite, it is a unique and ungrouped achondrite. The ε^{54}Cr and ε^{50}Ti values of NWA 7325 show deficits relative to the terrestrial composition and while the ε^{54}Cr value is distinct from that of ureilites, it does overlap with that of acapulcoites (Goodrich et al., 2017). As pointed out by Barrat et al., (2015) and reaffirmed by Goodrich et al. (2016), the oxygen isotope composition of NWA 7325 plots with ureilites along the Carbonaceous Chondrite Anhydrous Mineral (CCAM) line, and is an extension of a mass dependent fractionation trend from the acapulcoites.

Goodrich et al., (2016) concluded that NWA 7325 is from a parent body previously unsampled by any meteorite.

The dynamics in the early Solar System likely promoted rapid accretion (Johansen & Lambrechts, 2017) and internal heating of achondrite parent bodies (Hevey & Sanders, 2006). Early internal heating was possible, primarily, by the energetic decay of the short-lived isotope ^{26}Al (Urey, 1955). To reach temperatures necessary for melting of a bulk chondritic composition, objects in the early Solar System needed to accrete early (<1.5 Ma after CAI formation), and efficiently to sizes >10 km (Hevey & Sanders, 2006). The chronologies of ungrouped achondrites (Amelin et al., 2018; Bouvier et al., 2011; Koefoed et al., 2016a; Sanborn et al., 2018; Srinivasan et al., 2018) have revealed that igneous activity was widespread among many different achondrite types in the early Solar System.

The accretion, differentiation, and cooling timescales of achondrite parent bodies can be interrogated using a variety of high precision isotopic chronometers. Several chronometers are capable of the necessary resolution to probe the timescales of early Solar System processes. The short-lived systems ^{26}Al-^{26}Mg ($t_{1/2}$ = 0.705 Ma) and ^{53}Mn-^{53}Cr ($t_{1/2}$ = 3.7 Ma) have been used to determine the high-resolution relative ages of achondrites, while the Pb-Pb chronometer, the highest resolution absolute chronometer with application to the early Solar System, has been used to determine their absolute ages. Recent studies of a variety of planetary materials have demonstrated variability in the ^{238}U/^{235}U ratio (Goldmann et al., 2015; Tissot et al., 2017). Therefore, it is necessary to measure the ^{238}U/^{235}U ratio in achondrites and other meteoritic materials to obtain accurate and robust Pb-Pb ages.

In this study we report the Pb-Pb ages of the ungrouped achondrites NWA 11119 and NWA 8486 (a sample thought to be paired with NWA 7325). We have additionally measured the $^{238}U/^{235}U$ ratio in a bulk sample of NWA 11119. We recently reported the chronological constraints based on the ^{26}Al-^{26}Mg systematics of NWA 11119 (Srinivasan et al., 2018). Here we additionally report the ^{26}Al-^{26}Mg age for NWA 7325. Moreover, we report here the ^{53}Mn-^{53}Cr age and bulk $\varepsilon^{54}Cr$ value for NWA 11119. The chronology of these ungrouped achondrites is discussed in the context of other achondrites. We also discuss the implications of the possibility of the formation of these two achondrites on the same parent body (but distinct from those of other known achondrites) in the early Solar System.

2.2 Methods

All sample preparation and chemical procedures were performed in under clean laboratory conditions at the Isotope Cosmochemistry and Geochronology Lab (ICGL) at Arizona State University (ASU) and the Sensitive and Precise Isotopic Dating of Earth's and Extraterrestrial Rocks (SPIDE^{2}R) lab at the Australian National University (ANU). All tools used for the dry sample preparation were cleaned thoroughly in isopropyl alcohol before use and Savilex Teflon vials and centrifuge tubes were rigorously cleaned using clean acids and Millipore Sigma "Milli-Q" (MQ) H_2O (with resistivity of 18.6 MΩ.cm). All acids used during dissolution (with the exceptions of HF and $HClO_4$ which were purchased at high purity grade) and chemistry were distilled in house and blanks were carefully monitored.

2.2.1 Sample Preparation and Methods for Pb-Pb Analyses of NWA 11119 and NWA 8486

A ~1.6 g bulk interior fragment of NWA 11119 was acquired from the Institute of Meteoritics (IOM) at the University of New Mexico (UNM). The bulk fragment was first rinsed in MQ H_2O in an ultrasonic bath before being dry-crushed under clean-laboratory conditions in the ICGL at ASU by hand using an agate pestle and mortar. Resulting powdered material was sieved to yield size fractions of >188 μm, 188-150 μm, 150-106 μm, 106-75 μm, 75-53 μm, and <53 μm. The different size fractions were treated with heavy liquids (bromoform and lithium polytungstate) to perform density separations. These density separates were then handpicked under a binocular microscope to obtain pure mineral separates of pyroxene, plagioclase and silica. Ultimately, four pyroxene fractions, one plagioclase fractions, one silica fractions and six WR fractions were processed through procedures described in the supplementary materials.

A ~ 2 g bulk interior fragment of NWA 8486 was acquired from the Center for Meteorite Studies (CMS) at Arizona State University (ASU). The bulk fragment was dry-crushed under clean-laboratory conditions in the ICGL at ASU by hand using an agate pestle and mortar. Resulting fractions, fragments and materials were sieved to yield size fractions of >250 μm, 125-250 μm, 60-125 μm and <60μm. A Frantz magnetic separator was used on all the size fractions to obtain pyroxene- and feldspar-rich fractions. From these, we selected one pyroxene-enriched fraction (~ 33 mg). We additionally performed hand picking under a binocular microscope to produce purer pyroxene separates. We thus obtained 4 pyroxene fractions ranging in size from ~20 to ~35 mg. These mineral fractions for NWA 8486 were about three times larger than those previously analyzed for

NWA 7325 (Koefoed et al., 2016). The details of the chemical procedures and mass spectrometry methods for the Pb-Pb analyses are provided in the supplementary materials sections 2.6.1 and 2.6.2 for NWA 11119 and NWA 8486, respectively.

2.2.2 Sample Preparation and Methods for $^{238}U/^{235}U$ Analyses of NWA 11119

An interior whole rock chip of ~ 2 g of NWA 11119 was obtained from the IOM. This fragment was cleaned with a dental tool to manually remove the small amount of terrestrial weathering that was evident on the surface. Next, the samples were ultrasonicated using MQ water to remove any remaining surface contamination. The whole rock fragment were then carefully crushed using an agate mortar and pestle, weighed, and prepared for dissolution. To ensure complete dissolution the following steps were taken. First, the powdered sample was divided into ~200 mg aliquots. Each powdered aliquot was treated with concentrated nitric acid (HNO_3): hydrofluoric acid (HF) on a hotplate at temperatures > 110 ºC and dried down; this was repeated twice. Subsequently, 400 µL of concentrated $HClO_4$ was added to each dried aliquot and was this was fluxed on a hotplate at ~ 225 ºC for 3 days and then dried down in order to help dissolve fluorides created during the digestion. Each aliquot was then repeatedly refluxed with concentrated HCl on the hotplate at 120 ºC to ensure complete dissolution. The aliquots were then brought up in 3M HNO_3, combined, and a small fraction was taken for analysis on the Thermo iCAP-Q in order to determine the U concentration. Based on this U concentration data, the solution was spiked with IRMM-3636 (4 ng of spike was added for every 250 ng of U in the sample). After spiking, the U was purified using the UTEVA resin and chemical procedures detailed in Brennecka et al. (2010). Uranium isotopes were

measured on the Neptune multiple collector inductively coupled plasma mass spectrometer (MC-ICPMS) at ASU in low resolution mode. The Neptune is equipped with 9 faraday cups using a combination of 10^{11} and 10^{12} Ω resistors. The 10^{11} Ω resistors were used for measuring the ^{238}U, ^{235}U and ^{234}U isotopes while 10^{12} Ω resistors were used on the ^{233}U and ^{236}U isotopes. The aliquots were introduced to the plasma using an APEX® desolvating nebulizer at a flow rate of 100 µL/min. This setup allowed for a sensitivity of ~0.8 x 10^{-11} A (i.e. ~800 mV with a 10^{11} Ω resistor) per ng/g U in solution. Standards and samples were run at concentrations of 50 ppb. During the course of several months, a variety of tests were run on pure U solutions (CRM-145a, CRM-129a, and Ricca), all spiked in a similar way to the sample aliquots. We use an IRMM ^{233}U:^{236}U double spike typically spiking samples and standards at a spike/sample ratio of 2.5. The NWA 11119 solution was inadvertently over spiked (spike/sample = 11) and therefore was run with a CRM-145 bracketing standard that was similarly spiked. Rock standards BCR-2 and AGV-2 (from USGS) were processed in a similar manner to the sample and were analyzed alongside the sample to ensure the accuracy and reproducibility of our measurements. Total procedural blank for U was <6 pg.

2.2.3 Sample Preparation and Methods for ^{53}Mn-^{53}Cr and $\varepsilon^{54}Cr$ Analyses of NWA 11119

The mineral separates and WR fraction used for determination of the ^{53}Mn-^{53}Cr and $\varepsilon^{54}Cr$ systematics for NWA 11119 were the same fractions whose ^{26}Al-^{26}Mg systematics were reported in (Srinivasan et al., 2018). These included one WR, one pyroxene (Px A), three plagioclase (Plag A, B, C), and one silica (SiO_2) fractions which were prepared as follows. The bulk sample (~200 mg) was ultrasonicated in MQ H_2O to

remove any terrestrial contamination. The bulk sample was then carefully crushed using an agate mortar and pestle, sieved, and minerals of interest were hand-picked under a binocular microscope in the ICGL at ASU. The mineral separates were dissolved on a hotplate using concentrated HNO_3:HF with a subsequent concentrated HCl step to remove fluorides. A WR fraction (62 mg) was crushed with an agate mortar and pestle and was digested on a hotplate for 2 days in 2:1 HNO_3:HF, then evaporated to dryness, brought up in fresh 2:1 HF:HNO_3 and then digested in a parr bomb at 190 ºC for 96 hrs. The WR fraction was then evaporated to dryness, fluxed with concentrated HCl to remove the fluorides. A 10% aliquot was taken from the WR and mineral separates to measure bulk chemical composition, including rare earth elements (REE) and other trace elements, as well as the $^{55}Mn/^{52}Cr$ ratios. Details of our Cr chemistry and mass spectrometry procedures can be found in the supplementary materials section 2.6.3.

Radiogenic excesses in ^{53}Cr ($\mu^{53}Cr^*$) from the decay of ^{53}Mn were calculated using sample-standard bracketing and internal normalization of samples and bracketing standards (using the exponential fractionation law) to a $^{50}Cr/^{52}Cr$ ratio of 0.15886 (Shields & Murphy, 1966). The slope and intercept of the internal isochron for NWA 11119 were calculated using software isoplotR (Vermeesch, 2018). This regression was checked against the regression made using software Isoplot (Ludwig, 2012) and was found to be consistent.

2.2.4 Sample Preparation and Methods for ^{26}Al-^{26}Mg Analyses of NWA 7325

An interior piece of NWA 7325 (~500 mg, free of any fusion crust), was obtained from the CMS at ASU. A ~85 mg fraction from this sample was kept for WR analysis.

This aliquot was crushed and treated with 2: 1 HNO_3:HF on a hotplate before being dissolved using a high-pressure Parr bomb. The remaining material was crushed and sieved prior to mineral separation. Procedures and protocols for dissolution and purification of Mg were similar to those described previously (Bouvier et al., 2011; Spivak-Birndorf et al., 2009) with only minor modifications as described below. Prior to any chemical separations, ~10 % aliquot of each sample solution was reserved for the determination of $^{27}Al/^{24}Mg$ ratios. Magnesium concentrations and $^{27}Al/^{24}Mg$ ratios were determined on a Thermo iCAP-Q mass spectrometer in the Keck Laboratory at ASU. Magnesium isotopes were analyzed using the *Neptune* MC-ICPMS in ICGL at ASU, using protocols similar to those described previously (Bouvier et al., 2011b; Spivak-Birndorf et al., 2009). Instrumental mass fractionation was corrected using a sample-standard bracketing technique. Radiogenic excesses in ^{26}Mg from the decay of ^{26}Al ($\mu^{26}Mg^*$) were calculated using sample-standard bracketing and internal normalization of samples and bracketing standards (using the exponential fractionation law) to a $^{26}Mg/^{24}Mg$ ratio of 0.12663 (Catanzaro et al., 1966). The slopes and intercepts of the internal isochron for NWA 7325 were calculated using software isoplotR (Vermeesch, 2018).

2.3 Results

2.3.1 Pb-Pb Systematics of NWA 11119 and NWA 8486

The isotopic data for the fifty-one NWA 11119 aliquots and the twenty NWA 8486 aliquots (which include all washes and residues from these samples) are shown in tables 2.1 and 2.2 respectively, along with calculated $^{207}Pb^*/^{206}Pb^*$ dates. The concentrations reported here relate to the aliquot weights prior to the onset of acid-leaching. We have also calculated total concentrations by combining wash and residue values. It is important to note that the acid-leaching process can extract elements from primary, secondary and interstitial phases within geological materials – we consider the reported values for the residue fractions to represent the minimum abundances for the primary phases, while the combined washes represent the maximum abundances.

We employ an acid-leaching process prior to column chemistry to separate various Pb components that may be present. Our aim is to remove non-radiogenic Pb from our samples such that the residues contain the highest concentration of radiogenic Pb. All residues for NWA 8486 display $^{206}Pb/^{204}Pb$ ratios of ~ 37-81, compared to the washes which display $^{206}Pb/^{204}Pb$ ratios of ~17-19 (Table 2.2). Two of our aliquot residues A113-04 (WR) and A113-34 (Pyroxene) displayed $^{206}Pb/^{204}Pb$ ratios that were < 50, which likely relates to residual common Pb within these fractions.

For NWA 11119, residues have $^{206}Pb/^{204}Pb$ ratios of ~ 18-386, while the second washes have $^{206}Pb/^{204}Pb$ of ~17-620, and first washes display $^{206}Pb/^{204}Pb$ ratios of ~ 19-99 and (Table 2.1). In each leaching step, the washes for the WR fractions were more radiogenic than those for the Px fractions, indicating the presence of U-enriched phase(s)

in the WR. As observed for NWA 7325 (Koefoed et al., 2016), the NWA 8486 and NWA 11119 residues are relatively un-radiogenic, and likely relate to low U abundances within this material.

2.3.2 U-Corrected Pb-Pb Age of NWA 11119

The Pb-Pb ages of the WR and mineral separates washes and residues are given in Table 2.1. A regression with all washes and residues from WR and mineral separates from NWA 11119 is plotted in Figure 2.1 as $^{207}Pb/^{206}$ vs. $^{204}Pb/^{206}Pb$ with primordial Pb (Tatsumoto et al., 1973) and terrestrial Pb (Stacey & Kramers, 1975) components. This regression shows a slope that does not go through the primordial Pb composition, likely caused by the inclusion of a common Pb component in some of these data (particularly in the least radiogenic fractions). The most robust age interpretations come from excluding those data with the highest amounts of contaminant Pb. In light of this, a regression including only the most radiogenic ($^{206}Pb/^{204}Pb > 250$) residues and washes is shown in Figure 2.2. The measured $^{238}U/^{235}U$ ratio of NWA 11119 is 137.811 ± 0.011 (Table S2.1). For this measurement, we estimate the uncertainty on our $^{238}U/^{235}U$ ratio to be ± 0.011 (2SD) based on repeat analyses of CRM-145 taken over the duration of our analysis period comprising 4 analytical sessions over the course of a month. This uncertainty is larger than the internal 2SE for this particular measurement. The corrected Pb-Pb age of NWA 11119 using our measured $^{238}U/^{235}U$ ratio is 4565.42 ± 0.77 Ma. Model Pb ages ($^{207}Pb^*/^{206}Pb^*$) are listed in Table 2.1 and shown in Figure 2.3. The error weighted mean

of all $^{207}Pb^*/^{206}Pb^*$ ages from those most radiogenic washes and residues is 4565.03 ± 0.34 Ma. A plot showing the $^{206}Pb/^{204}Pb$ vs $^{207}Pb^*/^{206}Pb^*$ model ages is shown in Figure 2.4.

Table 2.1 Pb isotopic data for all washes and residues of NWA 11119 whole rocks and mineral separates.

Sample	Pb	Pb	$^{206}Pb/^{204}Pb$		$^{207}Pb/^{206}Pb$		Error Corr.	$^{207}Pb^*/^{206}Pb^*$ &	
	ppb	pg	(Total)	%Err	(Total)	%Err	4/6-7/6	Age (Ma)	Error (Ma)
A142- Pyroxene 1, (4 mg)									
Wash 1b	12.9	56.8	21.4685	0.1080	0.8254	0.0345	0.0140	4532.66	1.54
Wash 2a	1.8	7.9	75.1755	3.0900	0.6812	0.2290	0.9771	4557.60	1.26
Wash 2b	0.5	2.4	85.9003	11.7000	0.6737	0.7610	0.9942	4557.57	3.12
Residue	2.7	11.8	64.6404	11.8000	0.6936	0.9500	0.9952	4564.80	4.74
A142- Pyroxene 2, (10 mg)									
Wash 1b	7.4	73.8	19.4349	0.1050	0.8505	0.0350	-0.0030	4544.76	1.75
Wash 2a	0.7	7.3	67.1240	2.9200	0.6870	0.2390	0.9793	4553.75	1.33
Wash 2b	0.2	2.3	86.3946	12.6000	0.6747	0.8070	0.9943	4560.88	3.38
Residue	1.1	10.6	169.1667	40.6000	0.6534	1.3700	0.9972	4571.11	4.65
A142- Whole Rock 1, (9 mg)									
Wash 1a	36.5	315.7	31.9989	0.1070	0.7628	0.0341	0.0160	4559.59	0.98
Wash 1b	6.0	51.6	98.8181	0.6720	0.6673	0.0520	0.7103	4558.83	0.65
Wash 2a	18.4	159.3	317.0637	0.6990	0.6373	0.0362	0.3550	4562.06	0.52
Wash 2b	5.1	44.3	293.1898	2.4700	0.6397	0.0609	0.8185	4565.10	0.55
Residue	12.2	104.9	386.2301	9.5600	0.6356	0.1530	0.9731	4564.06	0.66
A146- Whole Rock 2, (10 mg)									
Wash 1a	32.3	308.9	23.7184	0.1140	0.8060	0.0338	0.0520	4536.41	1.33
Wash 1b	12.3	117.9	53.1870	0.6420	0.7017	0.0699	0.8198	4545.28	0.91
Wash 2a	26.0	248.2	158.7040	0.9870	0.6508	0.0498	0.7196	4560.50	0.57
Wash 2b	4.8	46.0	190.1285	6.9000	0.6475	0.2150	0.9852	4563.86	0.85
Residue	12.9	123.0	124.3651	1.6100	0.6588	0.0817	0.9032	4560.85	0.63
A146- Whole Rock 3, (11 mg)									
Wash 1a	40.3	455.5	28.1864	0.1160	0.7744	0.0344	0.0910	4533.50	1.11
Wash 1b	12.8	144.5	64.0324	0.6700	0.6881	0.0646	0.8156	4547.92	0.77
Wash 2a	33.2	375.1	224.5364	0.9460	0.6429	0.0421	0.5813	4561.49	0.54
Wash 2b	7.5	85.2	289.1210	5.7600	0.6397	0.1240	0.9550	4564.56	0.65
Residue	22.6	255.2	70.6414	0.4120	0.6858	0.0456	0.6329	4559.58	0.67
A146- Silica, (11 mg)									
Wash 1b	16.3	177.5	19.5277	0.1540	0.8537	0.0362	-0.0120	4564.18	2.10
Wash 2a	1.2	13.4	53.2365	5.0300	0.7092	0.4690	0.9914	4566.77	2.90
Wash 2b	0.2	2.6	54.2773	28.4000	0.7106	2.5300	0.9947	4575.23	15.78
Residue	2.1	22.9	52.4483	2.9600	0.7098	0.2820	0.9862	4564.93	1.83
A146- Pyroxene 3, (11 mg)									
Wash 1b	19.3	203.6	19.0313	0.1180	0.8548	0.0350	-0.0040	4541.42	1.91
Wash 2a	1.2	12.6	47.5559	4.9200	0.7163	0.5120	0.9912	4558.15	3.30
Wash 2b	0.1	1.4	313.5661	205.0000	0.6429	3.7900	0.9979	4575.10	11.74
Residue	4.6	49.0	27.5746	0.4350	0.7836	0.0658	0.7904	4553.35	1.55
A146- Plagioclase, (4 mg)									
Wash 1b	58.8	235.6	22.4366	0.1260	0.8163	0.0353	0.0370	4533.44	1.54
Wash 2a	10.4	41.9	78.5885	2.9400	0.6789	0.2080	0.9821	4558.29	1.06
Wash 2b	33.6	134.6	19.6719	0.1300	0.8542	0.0369	-0.0300	4573.46	1.91
Residue	9.4	37.8	72.4176	2.9400	0.6837	0.2230	0.9830	4558.16	1.17
A146- "Desert Sand", (11 mg)									
Wash 1b	209.4	4.2	18.5711	0.4730	0.8493	0.3130	0.3228	4486.25	12.52
Wash 2a	173.9	1.7	17.9699	1.4400	0.8549	0.9240	0.7604	4470.74	28.68
Wash 2b	148.4	1.5	17.3621	2.6200	0.8872	2.2800	0.9145	4587.81	71.05

Residue	290.7	5.8	18.3407	0.3820	0.8493	0.2250	0.4867	4469.67	8.46
A158- Whole Rock 4, (8 mg)									
Wash 2a	28.6	223.2	182.5290	1.3800	0.6482	0.0559	0.7842	4563.26	0.57
Wash 2b	16.3	126.8	450.6717	7.6200	0.6343	0.1080	0.9441	4565.02	0.60
Residue	21.7	169.4	287.2243	3.9000	0.6398	0.0878	0.9187	4564.68	0.58
W2b + Residue	19.0	148.1	341.0758	5.3500	0.6376	0.0999	0.9364	4565.20	0.59
A158- Whole Rock 5, (14 mg)									
Wash 2a	20.0	274.1	428.5849	2.7400	0.6349	0.0515	0.7431	4565.09	0.53
Wash 2b	13.9	190.9	619.9551	6.9400	0.6319	0.0760	0.8903	4565.78	0.54
Residue	22.2	304.1	203.4907	1.5100	0.6466	0.0555	0.7762	4565.57	0.57
W2b + Residue	18.0	247.4	276.6152	2.5600	0.6405	0.0649	0.8441	4564.88	0.56
A158- Whole Rock 6, (11 mg)									
Wash 2a	29.6	334.9	363.3061	1.8700	0.6365	0.0457	0.6712	4564.57	0.52
Wash 2b	16.3	184.1	469.1686	5.3900	0.6340	0.0772	0.8955	4565.24	0.55
Residue	25.6	289.5	214.4841	1.6600	0.6416	0.0573	0.8066	4556.13	0.55
W2b + Residue	20.9	236.8	272.7724	2.6100	0.6389	0.0667	0.8598	4560.56	0.55

Radiogenic Pb (^{206}Pb and ^{207}Pb*) have been corrected for common Pb using the measured ^{204}Pb and the primordial isotopic composition (Tatsumoto et al., 1973).
&Ages are calculated using the measured ^{238}U/^{235}U = 137.811.

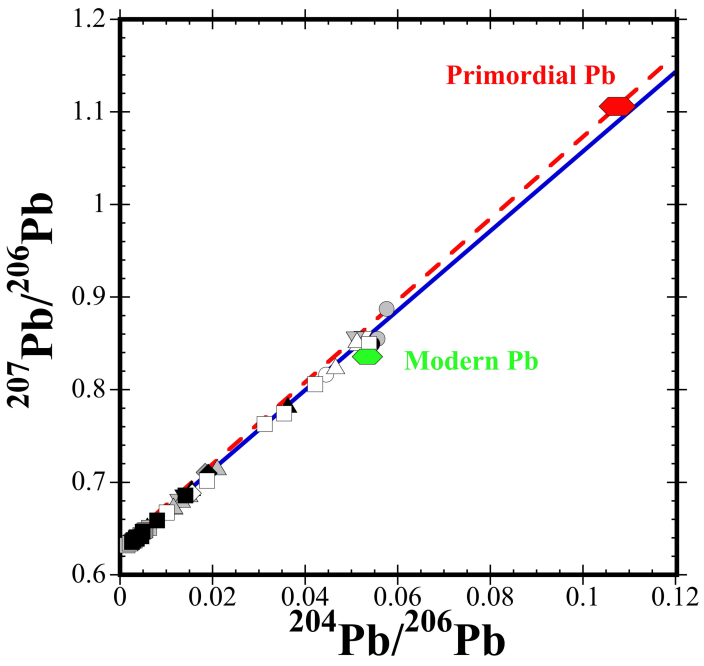


Figure 2.1 Plot showing ^{207}Pb/^{206}Pb vs. ^{204}Pb/^{206}Pb for all NWA 11119 residues and washes. Also plotted for comparison is the ratio for Modern Pb (Stacey and Kramers, 1975) and Primordial Pb (Tatsumoto et al., 1973). Successful removal of most non-radiogenic Pb from the residues by acid leaching is indicated by the spread of data along the isochron.

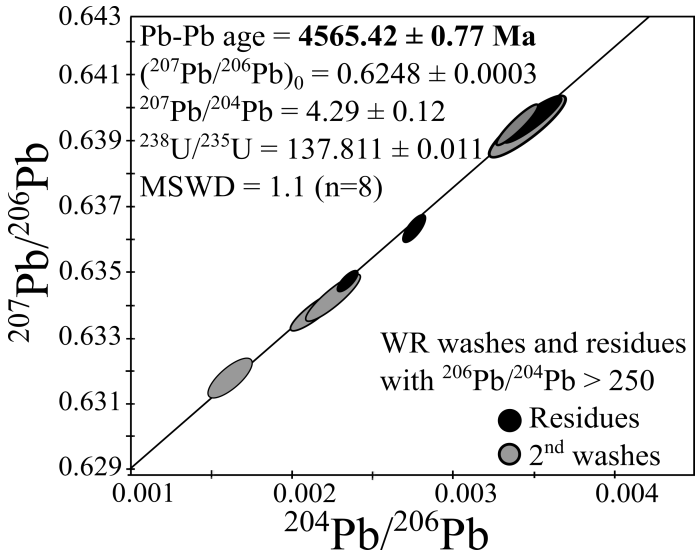


Figure 2.2 Plot showing the most radiogenic $^{207}Pb/^{206}Pb$ vs. $^{204}Pb/^{206}Pb$ for NWA 11119 WR residues and 2nd washes. This isochron regression gives our preferred U-corrected Pb-Pb for NWA 11119. The error envelopes are 2x the standard deviation.

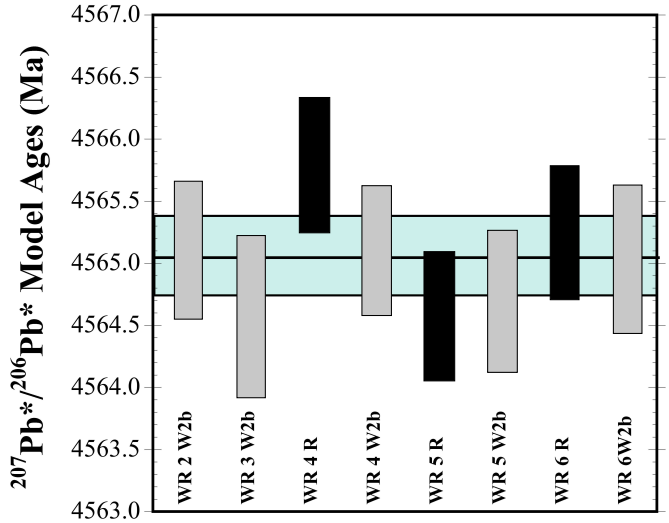


Figure 2.3 A plot of the $^{207}Pb^*/^{206}Pb^*$ mean model ages for NWA 11119. The solid black line represents the weighted mean value of 4565.03 ± 0.34 Ma. Error bars are 2SD.

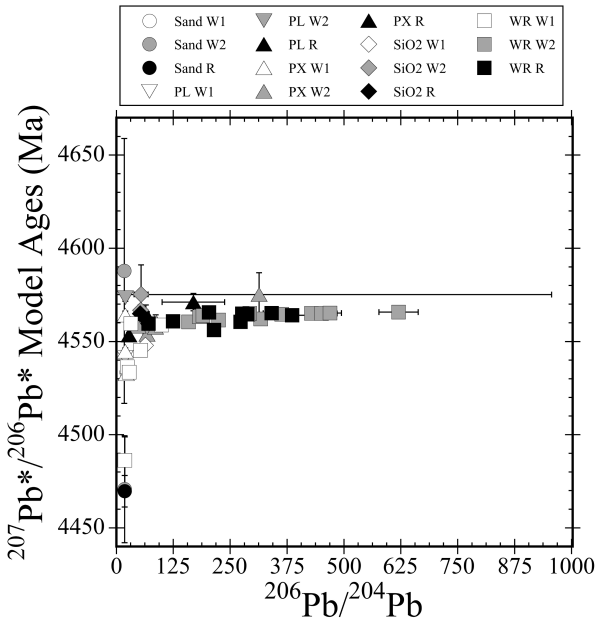


Figure 2.4 This figure shows the $^{207}Pb^*/^{206}Pb^*$ model ages vs the $^{206}Pb/^{204}Pb$ for NWA 11119 mineral separates and WR washes and residues. This plot shows the effectiveness of the acid washing procedure in separating the non-radiogenic Pb (low $^{206}Pb/^{204}Pb$) into the early washes. For the isochron regression, only those second washes and residues with $^{206}Pb/^{204}Pb$ >250 were used.

2.3.3 Pb-Pb Age of NWA 8486

A plot of $^{207}Pb/^{206}$ vs. $^{204}Pb/^{206}Pb$ for the full data set (washes and residues) is shown in Figure 2.5. The isochron defined on this plot has been regressed using only the residue data, yielding an isochron age of 4562 ± 40 Ma (MSWD = 79). As observed for NWA 7325 (Koefoed et al., 2016) the regression line calculated from the residue data passes close to the primordial Pb composition (Tatsumoto et al., 1973) (which represents the initial Pb isotopic composition), and the ratios from the washes are similar to the modern Pb value determined from the terrestrial upper crust (Stacey & Kramers, 1975) (which is indicative of the presence of terrestrial contaminant Pb).

The Pb-Pb isochron ages discussed below were calculated using a $^{238}U/^{235}U$ ratio of 137.794 (Goldmann et al., 2015) which represents the current best-estimate of the U isotopic composition of the Solar System. To calculate an accurate isochron age, it is important to select data that contain a high proportion of radiogenic Pb. As such, we excluded two residue samples – A113-04 (WR) and A113-34 (pyroxene), which displayed $^{206}Pb/^{204}Pb$ ratios of < 50 (Table 2.2). The remaining three residues A113-31, -32, -33, displayed $^{206}Pb/^{204}Pb$ ratios of > 50, which yield an isochron date of 4565.5 ± 5.8 Ma (MSWD = 0.56) (Figure 2.6); the error is relatively large given the limited spread in the data. To improve the precision of the Pb-Pb age for this meteorite, we combined our three pyroxene residues A113-31, -32, -33, with the six most radiogenic residues selected by Koefoed et al., (2016) for the paired stone NWA 7325 (which previously yielded an age of 4563.4 ± 2.6 Ma; MSWD = 1.7). The resulting isochron, shown in Figure 2.7, yields an age of 4563.9 ± 1.7 Ma (MSWD = 1.1), which is somewhat more precise than that obtained previously for this sample by Koefoed et al., (2016). Unfortunately, given the extremely U-depleted nature of NWA 8486, we did not have enough material to make a sufficiently precise measurement of its U isotope composition. In light of this, we calculated its age using $^{238}U/^{235}U$ 137.794 ± 0.027 from Goldmann et al., (2015) as well as our measured $^{238}U/^{235}U$ for NWA 11119 of 137.811 ± 0.011 (Table 2.2). Regardless of which $^{238}U/^{235}U$ is used, the Pb-Pb age of NWA 8486 is in complete agreement with the ^{26}Al-^{26}Mg age from Koefoed et al., (2016) and this study.

Model Pb ages ($^{207}Pb^*/^{206}Pb^*$) displayed in Table 2.2 for NWA 8486 have been calculated using two $^{238}U/^{235}U$ ratios: 1) 137.811, which is the value reported here for

NWA 11119; and 2) 137.794 (Goldmann et al., 2015). It is assumed that all ^{204}Pb remaining after blank correction represents initial Pb with a composition of primordial Pb (Tatsumoto et al., 1973).

Table 2.2 Pb isotopic data for all washes and residues of NWA 8486 whole rock and pyroxene separates.

Sample	Pb	Pb	^{206}Pb/^{204}Pb		^{207}Pb/^{206}Pb		Error Corr.	^{207}Pb*/^{206}Pb* §		^{207}Pb*/^{206}Pb* £	
	ppb	pg	(Total)	%Err	(Total)	%Err	4/6-7/6	Age (Ma)	Error	Age (Ma)	Error
A113-04, Whole rock enriched pyroxene, (33 mg)											
Wash 1	64.0	2112.7	18.6090	0.1200	0.8394	0.0960	0.0000	4439.84	4.42	4438.93	4.42
Wash 2a	6.0	196.4	17.9768	0.1430	0.8447	0.0967	0.0060	4418.25	4.88	4417.34	4.88
Wash 2b	0.6	19.8	17.1356	0.2960	0.8636	0.1620	0.6354	4446.80	6.01	4445.89	6.01
Residue	1.4	47.6	38.7233	1.3000	0.7320	0.1900	0.8454	4540.62	2.57	4539.71	2.57
A113-31, Pyroxene, (21 mg)											
Wash 1	44.3	930.4	18.5538	0.1210	0.8421	0.0960	0.0001	4449.71	4.42	4448.80	4.42
Wash 2a	2.0	42.7	18.3337	0.1480	0.8457	0.1040	0.0740	4451.93	4.81	4451.02	4.81
Wash 2b	0.1	2.8	17.6635	1.4300	0.8703	1.0900	0.8362	4526.55	33.53	4525.64	33.53
Residue	1.8	37.7	74.3805	4.0800	0.6829	0.3130	0.9441	4561.10	2.23	4560.20	2.23
A113-32, Pyroxene, (31 mg)											
Wash 1	50.3	1563.5	18.5635	0.1200	0.8418	0.0960	0.0001	4448.75	4.40	4447.84	4.40
Wash 2a	6.0	186.4	18.3947	0.2940	0.8368	0.0983	0.0020	4410.39	6.07	4409.48	6.07
Wash 2b	0.2	7.5	18.2109	0.4210	0.8462	0.2230	0.4732	4445.01	8.72	4444.10	8.72
Residue	2.0	60.9	54.4390	1.7000	0.7039	0.1880	0.8415	4557.74	2.17	4556.84	2.17
A113-33, Pyroxene, (20 mg)											
Wash 1	12.2	249.4	18.6353	0.3510	0.8413	0.1110	0.0005	4451.58	6.62	4450.67	6.62
Wash 2a	1.1	23.3	18.2746	0.1730	0.8413	0.1140	0.1840	4424.22	5.19	4423.31	5.19
Wash 2b	1.1	22.6	18.2491	0.1700	0.8523	0.1280	0.2521	4479.33	5.41	4478.42	5.41
Residue	1.7	35.3	80.7881	4.8200	0.6779	0.3420	0.9539	4560.55	2.22	4559.65	2.22
A113-34, Pyroxene, (34 mg)											
Wash 1	52.3	1805.9	18.6231	0.1210	0.8389	0.0960	0.0000	4438.57	4.42	4437.66	4.42
Wash 2a	3.9	135.0	18.6163	0.2000	0.8341	0.0984	0.0040	4413.28	5.11	4412.37	5.11
Wash 2b	0.9	32.3	18.5669	0.1520	0.8405	0.1070	0.0780	4442.58	4.90	4441.67	4.90
Residue	2.7	92.6	36.8888	0.6220	0.7461	0.1210	0.5755	4566.39	2.40	4565.49	2.40

Radiogenic Pb (^{206}Pb and ^{207}Pb*) have been corrected for common Pb using the measured ^{204}Pb and the primordial isotopic composition (Tatsumoto et al., 1973).
§ Ages are calculated using ^{238}U/^{235}U = 137.811 (reported here for NWA 11119).
£ Ages are calculated using ^{238}U/^{235}U = 137.794 (Goldmann et al., 2015).

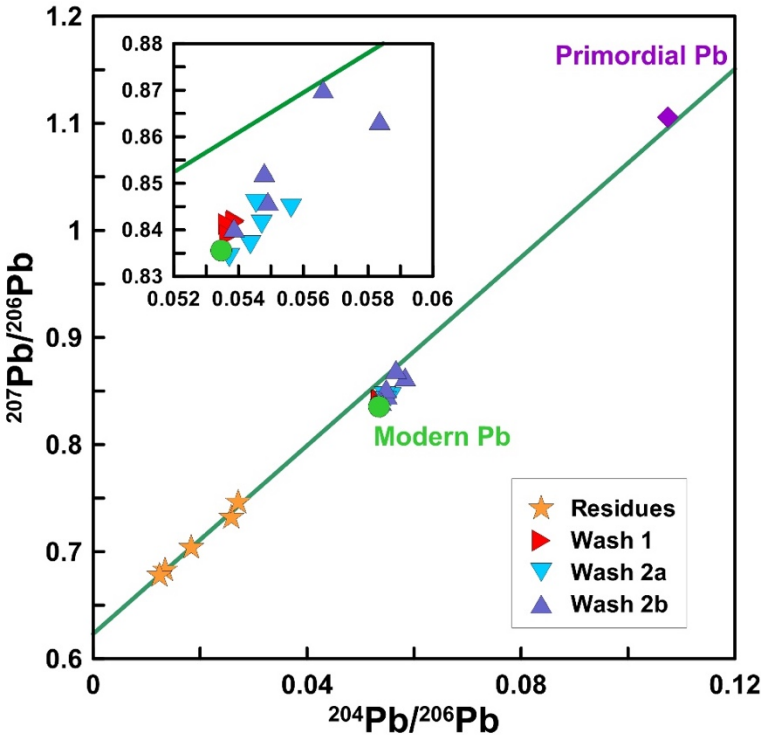


Figure 2.5 Plot showing $^{207}Pb/^{206}Pb$ vs. $^{204}Pb/^{206}Pb$ for all NWA 8486 residues and washes. Also plotted for comparison is the ratio for Modern Pb (Stacey & Kramers, 1975) and Primordial Pb (Tatsumoto et al., 1973). Successful removal of most non-radiogenic Pb from the residues by acid leaching is indicated by the spread of data along the regression.

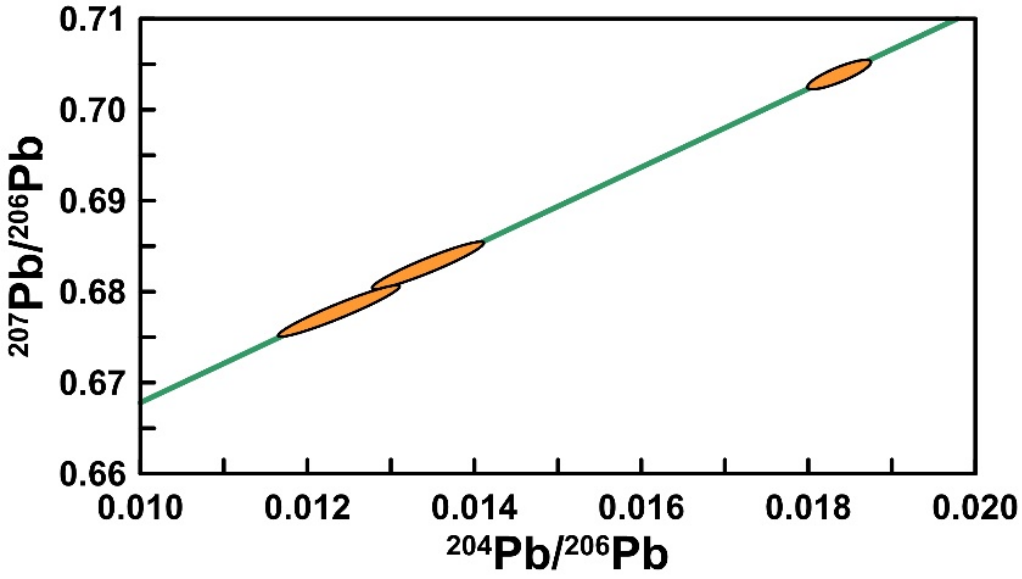


Figure 2.6 Plot of $^{207}Pb/^{206}Pb$ vs. $^{204}Pb/^{206}Pb$ for three pyroxene residues from NWA 8486 that display $^{206}Pb/^{204}Pb > 50$. Error ellipses are 2SD.

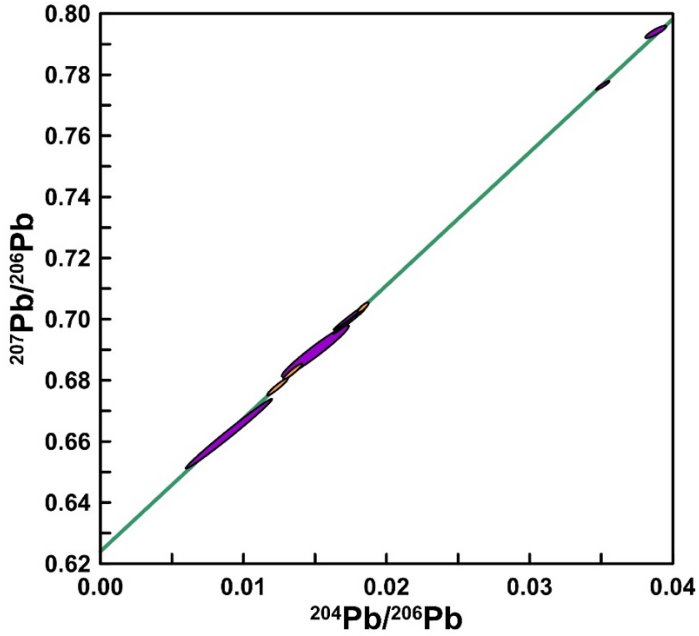


Figure 2.7 Plot of $^{207}Pb/^{206}Pb$ vs. $^{204}Pb/^{206}Pb$ including the previous six aliquots selected from NWA 7325 (orange) (Koefoed et al., 2016) and the three pyroxene NWA 8486 aliquots (purple) with $^{206}Pb/^{204}Pb > 50$. Error ellipses are 2SD

2.3.4 ^{53}Mn-^{53}Cr and ε ^{54}Cr Systematics of NWA 11119

The results of the Mn-Cr systematics for WR and mineral separates of NWA 11119 are shown in Table 2.3. The ^{53}Mn-^{53}Cr internal isochron for NWA 11119 (Figure 2.8) is comprised of one whole rock (WR), one pyroxene (Px A), one silica (SiO_2) and three plagioclase (Plag A, B, C) fractions and gives a ^{53}Mn/^{55}Mn ratio of (3.50 ± 1.12) x 10^{-6} with an initial $\mu^{53}Cr^*_0$ = 15 ± 18 ppm (MSWD = 0.71; n = 6). Relative to the D'Orbigny angrite age anchor with ^{53}Mn/^{55}Mn = (3.24 ± 0.04) x 10^{-6} (Glavin et al., 2004) and U-corrected Pb-Pb age = 4563.37 ± 0.25 Ma (Amelin, 2008; Brennecka & Wadhwa, 2012), we calculate a ^{53}Mn-^{53}Cr age for NWA 11119 of 4563.78 ± 1.73 Ma. NWA 11119 has an $\varepsilon^{54}Cr$ = -0.79 ± 0.10 which is a weighted mean value for the WR and all mineral separates.

Table 2.3. NWA 11119 ^{53}Mn-^{53}Cr and μ^{54}Cr systematics

Sample	^{55}Mn/^{52}Cr	2SD	$\mu^{53}Cr^*$	2SD	$\mu^{54}Cr$	2SD	n
NWA 11119							
Whole Rock (WR)	1.64	0.08	68.40	11.62	-81.49	17.76	10
Tridymite (SiO_2)	2.10	0.11	79.54	2.73	-62.08	5.60	2
Plagioclase 1 (Plag 1)	2.13	0.11	86.97	6.33	-76.35	16.96	4
Plagioclase 2 (Plag 2)	1.66	0.08	65.34	11.06	-83.85	10.87	7
Plagioclase 3 (Plag 3)	3.01	0.15	65.68	63.70	-131.03	74.54	1
Pyroxene (Px)	1.20	0.06	47.37	7.38	-87.87	10.04	8
Standards							
NBS-979			0.09	7.01	-0.40	15.32	152
SPEX Cr			-3.54	13.32	-4.70	22.02	23
DTS			13.00	19.49	5.56	33.79	50
Allende			8.35	6.58	91.74	16.74	11

This table shows the mineral separates and whole rock as well as synthetic Cr standards and rock standards. The uncertainty on our ^{55}Mn/^{52}Cr is ± 5% while the uncertainties on the Cr isotope ratios are 2x the standard deviation (see text).

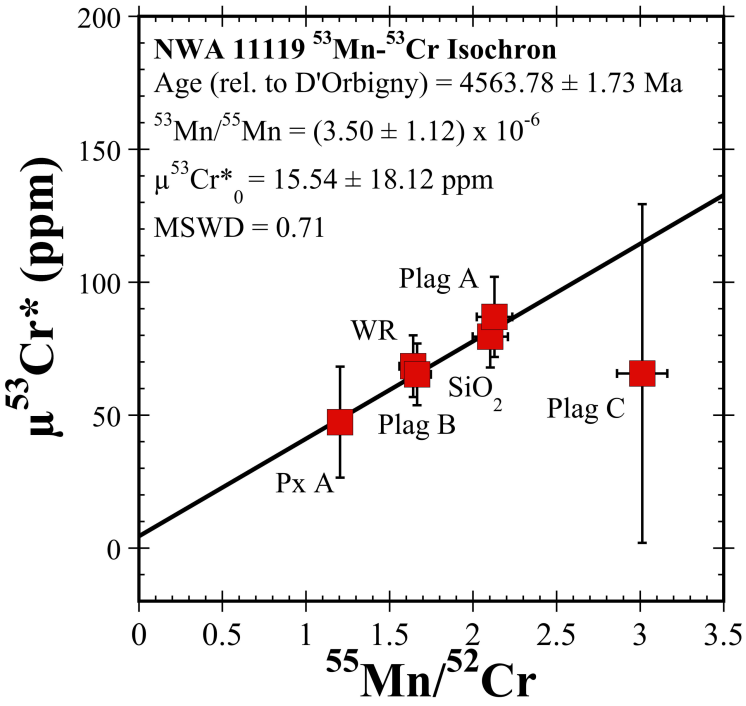


Figure 2.8 The internal ^{53}Mn-^{53}Cr isochron for NWA 11119. This includes mineral separates of pyroxene, plagioclase, SiO_2, and WR data. The age is relative to D'Orbigny (Amelin, 2008; Glavin et al., 2004; Goldmann et al., 2015).

2.3.5 ^{26}Al-^{26}Mg Systematics of NWA 7325

The results of our Al-Mg analyses of NWA 7325 whole rock and mineral separates are shown in Table 2.4. The ^{26}Al-^{26}Mg internal isochron for NWA 7325 (comprising of one WR, two olivine-rich fractions, two pyroxene, and three plagioclase separates) corresponds to $^{26}Al/^{27}Al = (2.96 \pm 0.35) \times 10^{-7}$ and an initial $\mu^{26}Mg^*_0 = 86 \pm 6$ ppm (MSWD = 1.1; n = 8) (Figure 2.9). Relative to the D'Orbigny angrite age anchor with $^{26}Al/^{27}Al = (3.98 \pm 0.21) \times 10^{-7}$ (Kleine & Wadhwa, 2017) and U-corrected Pb-Pb age = 4563.37 ± 0.25 Ma (Amelin, 2008; Brennecka & Wadhwa, 2012), we calculate an Al-Mg age for NWA 7325 of 4563.06 ± 0.26 Ma. This age is in agreement with the Al-Mg age reported by (Koefoed et al., 2016).

Table 2.4 NWA 7325 ^{26}Al-^{26}Mg systematics

Sample	^{27}Al/^{24}Mg	±5%	μ^{26}Mg*	2SE	n
NWA 7325					
Plagioclase 1 (Plag 1)	76.87	3.84	238.02	22.28	8
Plagioclase 2 (Plag 2)	46.00	2.30	200.80	17.82	7
Plagioclase 3 (plag 3)	33.51	1.68	147.50	17.17	4
Pyroxene 1 (Px 1)	0.18	0.01	82.50	9.25	4
Pyroxene 2 (Px 2)	5.13	0.26	101.21	14.75	8
Olivine-rich 1 (OL 1)	0.17	0.01	86.24	50.36	8
Olivine-rich 2 (OL 2)	0.20	0.01	88.75	11.02	8
Whole Rock (WR)	0.63	0.03	87.05	13.81	8
Standards					
DSM-3			-0.19	14.36	205
Allende			4.61	4.08	21
BCR-2			-11.67	7.32	13
Juvinas			18.48	6.91	8

This table contains the Al-Mg data for mineral separates and whole rock fom NWA 7325 as well as synthetic Mg standards and rock standards. The uncertainty on our ^{27}Al/^{24}Mg is ± 5% while the uncertainties on the Mg isotope ratios are 2x the standard error (SE). For the regression, the μ^{26}Mg* uncertainties were either the internal 2SE or the external 2SD (see text), whichever is larger.

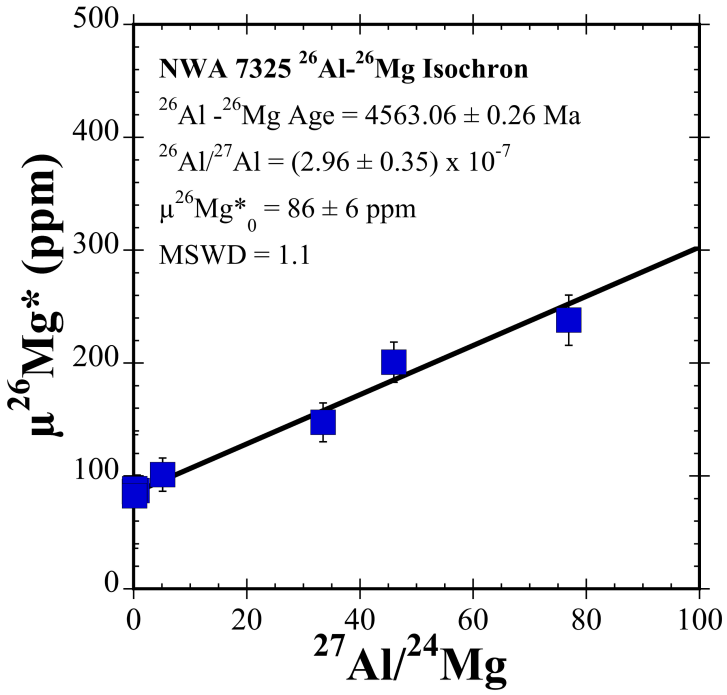


Figure 2.9 The internal ^{26}Al-^{26}Mg isochron for NWA 7325. This includes two pyroxene, three plagioclase, two olivine-rich separates and a WR fraction. The age is relative to the D'Orbigny angrite (Amelin, 2008; Brennecka & Wadhwa, 2012a; Kleine & Wadhwa, 2017).

2.4 Discussion

2.4.1 High-Resolution Chronology of NWA 11119 and NWA 7325/8486

The chronology of the ungrouped achondrites NWA 11119, NWA 7325/8486 (paired) is reported here using three different chronometers: Al-Mg, Mn-Cr, and Pb-Pb. While each chronometer has limitations (discussed below), when considered together, they allow for robust age interpretations. Furthermore, as the samples are ungrouped achondrites that sample previously unknown parent body(ies), constraining their age systematics provides new insights into the timeline of igneous activity on planetesimals in the early Solar System.

Meteoritic samples contain three sources of Pb, which must be accounted for in order to accurately determine the age of the sample: 1) radiogenic Pb produced by the decay of ^{238}U and ^{235}U; 2) primordial Pb considered to be the starting Pb isotopic composition of Solar System materials (Tatsumuto et al., 1973); and 3) terrestrial Pb, which results from contamination during the residence time on Earth (Stacey and Kramer, 1975). The effects of these other sources of Pb can be seen in the Pb isotope composition of washes and residues (Table 2.1 and 2.2) and the plot showing the $^{206}Pb/^{204}Pb$ vs the $^{207}Pb^*/^{206}Pb^*$ model ages (Figure 2.4) This shows that the leaching procedure was effective at separating the terrestrial Pb from the radiogenic and primordial components. In light of this, we have chosen to use only those most radiogenic ($^{206}Pb/^{204}Pb > 250$) washes and residues in our age determinations. The effectiveness of this procedure is further evidenced by the agreement between the Pb-Pb isochron age of 4565.42 ± 0.77 Ma (Figure 2.2) and the weighted mean of the $^{207}Pb^*/^{206}Pb^*$ model ages of 4565.03 ± 0.34 Ma (Figure 2.3) of NWA 11119.

The preferred Pb-Pb ages of NWA 11119 and NWA 8486 are based on the most radiogenic fractions for these samples and are 4565.42 ± 0.77 Ma (Fig. 2.2) and 4563.9 ± 1.7 Ma (Fig. 2.7), respectively. Although these ages suggest that NWA 11119 may be somewhat older than NWA 8486, they actually agree within the relatively large uncertainties. The relatively large uncertainties result from the low U concentrations in both NWA 11119 (20 ppb U) and NWA 8486 (13 ppb), which complicate the data in two ways: 1) The low U concentration results in low abundances of the radiogenic Pb, which make the Pb isotopic analyses challenging; and 2) The low U concentrations make it

challenging to measure the $^{238}U/^{235}U$ ratio of the bulk sample which is required for accurate determination of the Pb-Pb age (Brennecka & Wadhwa, 2012; Tissot & Dauphas, 2015).

The measured $^{238}U/^{235}U$ ratio for NWA 11119 (137.811 ± 0.11) is within uncertainty of the Solar System average (137.794) and the achondrite average (137.791) defined by (Goldmann et al., 2015). Interestingly, in their recent high-precision study of the U isotope compositions of angrites, Tissot et al., (2017) found that there is resolvable variation in the $^{238}U/^{235}U$ ratio between the plutonic and quenched angrites. The quenched angrites D'Orbigny and Sahara 99555 both have $^{238}U/^{235}U$ ratios with an average $\delta^{238}U = -0.29 \pm 0.07$ (Tissot et al., 2017) similar to chondrites ($\delta^{238}U = -0.31 \pm 0.04$; Goldmann et al., 2015). The plutonic angrites Angra dos Reis, NWA 6291, NWA 4801 and NWA 4590, on the other hand, have a lighter U isotope composition with an average $\delta^{238}U = -0.46 \pm 0.03$ (Tissot et al., 2017). This isotopic variation is explained not by terrestrial weathering or decay from live ^{247}Cm in the early Solar System, but as the result of U stable isotope fractionation during magmatic processes. This finding stresses the need to measure the $^{238}U/^{235}U$ ratio, whenever possible, of any meteoritic sample for which a Pb-Pb age is to be determined.

In this study, we were able to determine the U isotope composition of NWA 11119 ($^{238}U/^{235}U = 137.811 \pm 0.011$). However, we did not have sufficient sample to determine the U isotope composition of NWA 8486. In light of this and the recent work of (Tissot et al., 2017), we are left with the problem of how to appropriately account for the $^{238}U/^{235}U$ ratio for NWA 8486. In Table 2.2, we report the Pb-Pb model age of NWA 8486 using the average Solar System and average achondrite data from (Goldmann et al.,

2015) and the $^{238}U/^{235}U$ ratio reported here for NWA 11119. These ages are the same within the errors.

NWA 11119 has a ^{53}Mn-^{53}Cr age of 4563.78 ± 1.73 Ma relative to the D'Orbigny angrite (Amelin, 2008; Brennecka & Wadhwa, 2012; Glavin et al., 2004). Recent chronological investigations of another ungrouped achondrite NWA 6704 have determined a $^{53}Mn/^{55}Mn$ ratio of (2.59 ± 0.34) x 10^{-6} and U-corrected Pb-Pb age of 4562.76 ± 0.30 Ma for this sample (Amelin et al., 2018; Sanborn et al., 2018). As such, this new ungrouped achondrite might also serve as an additional age anchor. By anchoring NWA 11119 to the ungrouped achondrite NWA 6704, we calculate a ^{53}Mn-^{53}Cr age of 4563.78 ± 1.73 Ma, which is in agreement with the ^{53}Mn-^{53}Cr age using D'Orbigny as the ange anchor. Nevertheless, these ^{53}Mn-^{53}Cr ages for NWA 11119 have large uncertainties which are the result of limited spread in the $^{55}Mn/^{52}Cr$ ratios of the mineral separates and WR for NWA 11119 as well as large analytical uncertainties in the plag C data point that has the highest $^{55}Mn/^{52}Cr$ ratio (Fig. 2.8).

An error weighted mean of the Pb-Pb, ^{26}Al-^{26}Mg and ^{53}Mn-^{53}Cr ages can be calculated to determine a single age for NWA 11119, which requires that all age uncertainties incorporate the uncertainties associated with their respective decay constants. For ^{26}Al-^{26}Mg and ^{53}Mn-^{53}Cr, these uncertainties are relatively small and do not contribute significantly to the overall age uncertainties calculated. For the Pb-Pb system, the decay constant uncertainties for ^{238}U and ^{235}U are large enough to make a significant increase in the age uncertainty. As discussed by Amelin, (2006), the decay constant uncertainties to the Pb-Pb system need only be included when comparing ages across different isotopic systems. When calculating an error weighted mean the

individual uncertainties for each age are given weights (Wi = 1/(age uncertainty^2). These weights are used to account for the effect each individual age uncertainty has on the calculated mean. If all weights were equal, the error weighted mean and arithmetic mean would be identical. When considering the ^{53}Mn-^{53}Cr and Pb-Pb age reported here, the age uncertainties (taking into account the decay constant error) are 1.73 – 7 Ma, while the ^{26}Al-^{26}Mg age uncertainty reported by Srinivasan et al., (2018) for this sample is 0.3 Ma. This means that the error weighted mean is being strongly influenced by the high precision ^{26}Al-^{26}Mg age. The calculated error weighted mean age for NWA 11119 is 4564.8 ± 0.3 Ma. This is our preferred formation age for this sample.

The ^{26}Al-^{26}Mg internal isochron for NWA 7325 (Fig. 2.9), defined by WR and mineral separates, yields a ^{26}Al/^{27}Al = (2.92 ± 0.15) × 10^{-7} and an initial μ^{26}Mg*$_0$ = 87 ± 3 ppm (MSWD = 1.4; n = 8). These values are in agreement with those that reported by (Koefoed et al., 2016) of ^{26}Al/^{27}Al = (3.03 ± 0.14) × 10^{-7} and an initial μ^{26}Mg*$_0$ = 93 ± 4 ppm. A noteworthy feature of the NWA 7325 Al-Mg internal isochron is that it lies well above the bulk chondritic value of ^{27}Al/^{24}Mg ~0.1 and μ^{26}Mg* ~0 (Larsen et al., 2011; Lodders, 2003) and has a well-resolved positive intercept of μ^{26}Mg*$_0$ = 87 ± 3 ppm. Such a high μ^{26}Mg$_0$* has not been previously reported for any other achondrite with the possible exception of the ungrouped GRA 06128/06129, which is characterized by a μ^{26}Mg$_0$* = 80 ± 9 ppm (Shearer et al., 2010). However, in contrast to NWA 7325, GRA 06128/06129 does not show any evidence for the incorporation of live ^{26}Al at the time of its last Al-Mg equilibration. The high positive initial μ^{26}Mg$_0$* for NWA 7325 could imply a distinct, non-chondritic initial Mg isotope composition for its parent body, implying gross heterogeneities in the initial Mg isotope composition in the early Solar

System. Alternatively, the source reservoir for this achondrite may have evolved with a highly superchondritic Al/Mg ratio early in the history of the Solar System prior to the partial melting event that formed the NWA 7325 parent melt. In this case, an ^{26}Al-^{26}Mg model age of 4566.4 Ma can determined by assuming that NWA 7325 originally formed from a bulk chondrite-like composition and may be interpreted as the timing of silicate fractionation in the source region. For such silicate fractionation to be occurring on the NWA 7325 parent body a mere ~0.9 Ma after CAIs (Connelly et al., 2012) would require efficient accretion almost contemporaneously with CAI formation. In either of the cases considered above, the ^{26}Al-^{26}Mg systematics of NWA 7325 further support that this meteorite originated on a parent body distinct from that of other known achondrites. The ^{26}Al-^{26}Mg internal isochron age for NWA 7325 (relative to the D'Orbigny angrite) of 4563.06 ± 0.26 Ma agrees with its Pb-Pb age. The calculated error weighted mean age based on the Pb-Pb and Al-Mg ages presented here for NWA 7325/8476 is 4563.1 ± 0.3 Ma. This is our preferred formation age for this sample. This age is ~1.7 Ma younger than the preferred formation age for NWA 11119.

Finally, we note that the formation age of NWA 7325/8486 agrees with the ages reported for several of the quenched angrites (Amelin, 2006; Brennecka & Wadhwa, 2012) and other ungrouped achondrites such as NWA 2976 and NWA 6704 (Amelin et al., 2018; Bouvier et al., 2011; Sanborn et al., 2018). This suggest that there was active contemporaneous igneous activity on several distinct planetesimals in the early Solar System.

2.4.2 Petrogenesis of the Silica-Rich Ungrouped Achondrite NWA 11119

To form an achondrite with the evolved mineralogy of NWA 11119 requires special consideration (Srinivasan et al., 2018). NWA 11119 has bulk composition that is andesitic to dacitic, with low total alkali contents and low bulk FeO. There are problems in considering terrestrial andesites as an example of how to produce a lithology like that of NWA 11119. Terrestrial andesites make up a significant portion of the continental crust on Earth and yet research is ongoing to explain how and when continental crusts were emplaced (Campbell & Taylor, 1983; Rudnick, 1995). A few prevailing hypotheses involve andesites forming by melting oceanic basalts. Often these oceanic basalts are relatively volatile and water rich and are partially melted during subduction to produce andesites. Alternatively, terrestrial andesite production might involve partial melting of a basaltic crust where magma ascends from the mantle, stagnates in the crust, interacts with the country rock, and can even be recharged by fresh magma (Gomez-Tuena et al., 2013). It is unlikely that NWA 11119 formed as the result of plate tectonics. However, formation via partial melting of a basalt composition remains an interesting possibility.

Another potential scenario is partial melting of a chondrite-like precursor material, which would correlate with the unfractionated REE pattern for NWA 11119 (Srinivasan et al., 2018). At present, there are no experimental studies involving partial melting of chondritic compositions in the fO_2 range that might be expected for NWA 11119 (i.e. ~IW -4) as described in Srinivasan et al. (2018). However, there are studies using H and EH4 meteorite starting compositions (McCoy et al., 1999; Usui et al., 2015) that can create high SiO_2 melts. Nevertheless, an H chondrite starting composition is unlikely based on the high alkali element abundances in the partial melts, while an EH4

composition is unlikely since the FeO is too low in the partial melts. The equilibrium partial melting experiments of (McCoy et al., 1999; Usui et al., 2015) show that while no direct relationship exists between chondrite-like compositions and NWA 11119, there is evidence that at fO_2 intermediate to that of H and EH4 chondrites at low degrees of partial melting can produce a high SiO_2 melt.

Previous literature highlights a few achondrites and lithologies within achondrites that have similarities to NWA 11119. Ungrouped achondrites GRA 06128/06129 have trachyandesitic bulk compositions described by (Day et al., 2009a; Shearer et al., 2010) and were the first such achondrites that show that evolved, high SiO_2 melts were possible on differentiated asteroidal bodies. These achondrites have similar oxygen isotope compositions, bulk rock REE pattern, and high SiO_2 contents to NWA 11119, but differ significantly in their total alkali content, mineralogy, and bulk FeO contents (Day et al., 2009; Shearer et al., 2010; Srinivasan et al., 2018). They are thought to have formed as the result of low degrees (<13%) of partial melting of a volatile rich chondritic source, perhaps L6 type ordinary chondrite like composition (Day et al., 2009; Shearer et al., 2010). The Almahata Sitta ureilite fragments contain one stone (42.2 g), ALM-A, that has a trachyandesitic composition, with similar bulk rock REE pattern, high SiO_2, and oxygen isotope composition with NWA 11119 (Bischoff et al., 2014). The formation of ALM-A was modelled as the result of low degrees of disequilibrium partial melting (<5%) of an R chondrite like composition (Bischoff et al., 2014). Recently, a dacite clast was described in the Dominion Range 2010 Howardite (Hahn Jr. et al., 2017). In this study, the dacite clast was modelled as forming from a 10-20% partial melt of a Juvinas-like starting composition. While volumetrically small, this clast indicates that remelting

of basaltic compositions was occurring on Vesta and represents the first identification of a re-melted crustal sample on an asteroidal body.

Recently, a paper by Collinet & Grove, (2020) carried out a series of melting experiments using carbonaceous and ordinary chondrite starting compositions at low pressure under varying fO_2 conditions. The results from Collinet & Grove, (2020) indicate that all planetesimals not depleted in moderately volatile elements relative to the Sun's photosphere would produce low-degree melts enriched in SiO_2, Al_2O_3 and alkali elements. Additionally, these early forming low-degree melts, once cooled, could produce rocks with up to 80 vol% plagioclase (An_{10-30}). This is compositionally similar to the trachyandesite GRA 06128/9 (Day et al., 2009; Shearer et al., 2010) and the ALM-A clast from the Almahata Sitta ureilite strewn field (Bischoff et al., 2014). These compositions differ significantly from NWA 11119 which has low bulk alkali elements, Ca-rich plagioclase (An_{87}) and abundant free silica. These examples demonstrate that evolved, high silica melts are possible. However, the exact petrogenesis of NWA 11119 remains unclear and will require further geochemical modelling.

2.4.3 NWA 11119 and NWA 7325/8486: Arguments for and against a Shared Parent Body

In this section, arguments will be presented for and against a shared parent body for NWA 11119 and NWA 7325/8486. The first observation is that physically, these two meteorites share an uncanny resemblance in hand sample. This is due to the presence of bright green, Cr-bearing high-Ca pyroxene and grey "frosty" Ca-plagioclase found in both achondrites. NWA 11119 has a truly unique characteristic that distinguishes it from

NWA 7325 and all other known achondrites in that it contains 30 vol% free silica. Oxygen isotopes have long been used as a tool to classify meteorites (Clayton, 1993). The mass independent $\Delta^{17}O$ isotope anomalies are distinctive among different meteorite classes and while the origin of these variations is not yet fully understood, the data are a useful tool in determining genetic relationships among Solar System objects. In addition to $\Delta^{17}O$, mass-independent anomalies in ^{54}Cr, ^{50}Ti, and $^{95\text{-}96}Mo$ have also been cultivated as isotopic tools useful in the determination of genetic relationships between object in the Solar System. The nucleosynthetic isotope anomalies in ^{54}Cr, ^{50}Ti, and $^{95\text{-}96}Mo$ all point towards a dichotomy in the Solar System between objects that may have formed relatively close to the Sun versus those that likely formed further out (Kruijer et al., 2017; Sanborn et al., 2018; Trinquier et al., 2009; Warren, 2011). This dichotomy has been attributed to a physical separation caused by rapid early accretion of Jupiter (Kruijer et al., 2017). Whatever the mechanism, the isotopic dichotomy appears real and provides valuable insights into processes in the early Solar System. In light of this, we can look for points of comparison in the isotopic data for NWA 11119 and NWA 7325/8486. Goodrich et al., 2017 reported Cr and Ti isotopic data for NWA 7325 by (Goodrich et al., 2017) which showed that the mass-independent anomalies in ^{54}Cr and ^{50}Ti isotopic resemble those in other materials in the non-carbonaceous (NC) reservoir which is characterized by deficits in both ^{54}Cr and ^{50}Ti relative to terrestrial composition. At present, only the $\Delta^{17}O$ and ^{54}Cr data exist for NWA 11119. The $\Delta^{17}O$ composition of NWA 11119 is found to be identical to that of NWA 7325 and other NC achondrites (Srinivasan et al., 2018). For NWA 11119, we report the $\varepsilon^{54}Cr$ value of -0.79 ± 0.10 which agrees within uncertainty with that of NWA 7325 ($\varepsilon^{54}Cr = -0.61 \pm 0.22$). Taken

together, the $\Delta^{17}O$ and ^{54}Cr isotopic data indicate a genetic relationship between these two achondrites. Whether this is simply the consequence of formation of distinct parent bodies in the same isotopic nebular reservoir or of formation on a shared parent body cannot be confirmed with the current constraints.

Srinivasan et al., (2018) have argued against a shared parent body for NWA 11119 and NWA 7325/8486 based on the Fe/Mn ratios of their pyroxenes. NWA 7325 has subchondritic Mn/Mg ratio (Goodrich et al., 2017) and is thought to be a cumulate, while NWA 11119 has a spread in values from chondritic to superchondritic (Srinivasan et al., 2018) that indicate fractional crystallization took place. Comparison of the Fe/Mg vs Fe/Mn ratios reveals that NWA 11119 has comparatively more bulk Mn and Fe with less bulk Mg, which might be expected given the evolved composition. NWA 7325 has comparatively less bulk Mn and Fe with more bulk Mg. These trends can be seen in supplementary Figure 5 from (Srinivasan et al., 2018). The question remains whether these differences in bulk composition preclude formation on a common parent body. NWA 7325 is a cumulate with an extremely low Mn/Mg ratio compared to all other achondrites. This could result through loss of Mn during formation or as a result of removal of an early forming melt (taking with it the Fe and potentially Mn). As has been suggested by previous authors (Goodrich et al., 2017; Koefoed et al., 2016; Weber et al., 2016), NWA 7325/8486 might have experience a multi-stage igneous evolution where the parental melt formed with depleted incompatible elements by remelting of an earlier lithology. Another distinguishing feature of NWA 7325/8486 is the highly elevated initial $\mu^{26}Mg^*$. One means of creating such an elevated $\mu^{26}Mg^*$ would involve the source

lithology of NWA 7325/8486 having superchondritic Al/Mg which could be achieved through a multi-stage igneous history.

Plagioclase compositions can be used to discriminate between different achondrite types. Goodrich et al. (2017) show that the plagioclase in NWA 7325 is enriched in Mg and Sr, while depleted in K, Fe, Ti, and Ba compared to other achondrites. It would be difficult to produce this type of composition through a single-stage melting of a chondritic precursor since K, Ba, and Sr are all hosted in plagioclase. There is also a clear difference when comparing the plagioclase An number vs Mg# in olivine or pyroxene of NWA 11119 (~An_{87}; Mg# = 90) and NWA 7325/8486 (~An_{98}; Mg# ~ 98) with all other achondrites. This combination of high Ca-plagioclase and high Mg-olivine/pyroxene is not seen in other achondrites with the exception of the Mg-An clasts in polymict ureilites as discussed in (Goodrich et al., 2017). This is further evidence not only for the ungrouped nature of NWA 11119 and NWA 7325/8486, but also for the possibility of a shared parent body.

In light of evidence discussed above, we suggest that NWA 7325/8486 and NWA 11119 most likely originated on a common parent body. Here, we describe a petrogenetic scenario that may account for all the distinctive geochemical and isotopic features of these unique achondrites. The ^{54}Cr vs ^{50}Ti vs $\Delta^{17}O$ isotope systematics allow us to place their parent body in the inner Solar System due to the similarity of these characteristics to other (non-carbonaceous) meteoritic materials thought to originated on parent bodies in the inner Solar System (Goodrich et al., 2017; Sanborn et al., 2019). This parent body evolved under reduced oxygen fugacity conditions (i.e. IW~ -3 to -4) (Goodrich et al., 2017; Srinivasan et al., 2018). It accreted, melted, and differentiated early with major

silicate fractionation initially occurring within ~1 Ma after CAIs to produce at least some regions in the mantle with superchondritic Al/Mg ratios (based on the Al-Mg model age for NWA 7325 reported here). An initial crust was formed on this parent body which may have been produced simply by partial melting of a chondritic source or by remelting of an originally basaltic precursor material. These partial melts would be enriched in REEs (~ 10x CI chondrites), alkali depleted and initially silica-saturated. These melts would erupt and form NWA 11119 at ~ 4565 Ma (or ~2 Ma after CAI formation). Subsequently, partial melting of a source with a superchondritic Al/Mg ratio resulted in the parent melt of NWA 7325/8486, which formed at ~4563 Ma (or ~4 Ma after CAI formation).

2.4.4 Concordance Between Chronometers and Implications for the Initial Distribution of ^{26}Al in the Early Solar System

Concordance between multiple isotope chronometers indicates that the system cooled through the closure temperatures of the relevant isotopes in the minerals of interest over a period of time that is smaller than the time resolution of these chronometers. To preserve this concordance, the rocks dated with these chronometers must not have experienced disturbance to the isotopic systems by secondary processes such as thermal and/or shock metamorphism. With respect to the chronometers discussed here, only the angrite D'Orbigny (Amelin, 2008; Brennecka & Wadhwa, 2012; Glavin et al., 2004; Spivak-Birndorf et al., 2009) and the ungrouped achondrite NWA 6704/6693 (Amelin et al., 2018; Sanborn et al., 2018) have been reported showing concordance between U-corrected Pb-Pb, ^{53}Mn-^{53}Cr and ^{26}Al-^{26}Mg chronometers. The CAI 22E from the Efremovka CV3 has a U-corrected Pb age and has been investigated for its ^{26}Al-^{26}Mg

systematics (Connelly et al., 2012; Larsen et al., 2011), but lacks ^{53}Mn-^{53}Cr data. This allows D'Orbigny, the CAI 22E and now NWA 6704 to be used as age anchors for the ^{26}Al-^{26}Mg system. For anchoring ^{53}Mn-^{53}Cr, only NWA 6704 and D'Orbigny are available. The data reported here for the U-corrected Pb-Pb age as well as the ^{53}Mn-^{53}Cr and ^{26}Al-^{26}Mg systematics makes NWA 11119 another candidate for age anchor in the early Solar System (note that the ^{26}Al-^{26}Mg systematics in NWA 11119 have been reported by us previously in Srinivasan et al., 2018).

Concordance between the absolute Pb-Pb chronometer and other short-lived chronometric systems in meteoritic materials is typically taken to be evidence that the distribution of the relevant short-lived radionuclide was homogenous in the formation reservoirs of these materials. Each of these potential age anchors discussed above represent distinct regions in the Solar System: CAIs are thought to have formed well within 1 AU (Desch et al., 2018), while D'Orbigny originated on the angrite parent body likely in the inner Solar System, and NWA 6704 (which is an ungrouped achondrite related to the carbonaceous chondrites) formed presumably beyond Jupiter (Sanborn et al., 2019; Warren, 2011). This is particularly important for the distribution of ^{26}Al in the early Solar System and the utility of the ^{26}Al-^{26}Mg system as a chronometer. While there are arguments against the homogenous distribution of ^{26}Al (Larsen et al., 2011; Schiller et al., 2015), the overwhelming majority of available data indicates that ^{26}Al was homogenously distributed in the early Solar System (Kita et al., 2013; Macpherson et al., 1995; Wasserburg et al., 2012). This study, as well as the recent work of

(Amelin et al., 2019; Sanborn et al., 2018), provide confidence in the utility of the ^{26}Al-^{26}Mg chronometer and provide further evidence for the homogenous distribution of ^{26}Al in the early Solar System.

2.5 Conclusions

The ungrouped achondrites NWA 11119 and NWA 7325/8486 have distinctive compositions, mineralogies, and isotopic characteristics . The chronology of such ungrouped achondrites places important constraints on the timing and diversity of igneous activity in the early Solar System. In this study, we report the U-corrected Pb-Pb age of NWA 11119 to be 4565.42 ± 0.77 Ma. Additionally, we report the ^{53}Mn-^{53}Cr age of NWA 11119 to be 4563.78 ± 1.73 Ma. These ages are in complete agreement with our previously published ^{26}Al-^{26}Mg age of 4564.8 ± 0.3 from (Srinivasan et al., 2018). Incorporating the U-corrected Pb-Pb age, the ^{53}Mn-^{53}Cr age, and the ^{26}Al-^{26}Mg age (both rel. to D'Orbigny) the error weighted mean age for NWA 11119 is 4564.8 ± 0.3 Ma. This concordance between three high-resolution chronometric systems indicates that the cooling history of the volcanic NWA 11119 was undisturbed by subsequent thermal metamorphism. NWA 11119 is one of the oldest known achondrites and has arguably one of the most unique compositions in being the most silica-enriched achondrite. Taken together, the chronology and petrology of this sample have implications for the types and timescales of igneous processes on planetesimals in the early Solar System.

The Pb-Pb age and ^{26}Al-^{26}Mg age of NWA 7325/8486 are also reported here to be 4563.9 ± 1.7 Ma and 4563.06 ± 0.26, respectively. The error weighted mean age from both these ages is 4563.1 ± 0.3 Ma, which is ~1.7 Ma younger than NWA 11119. A case

can be made for these ungrouped achondrites originating on a shared parent body based on similarities in mineralogy, geochemistry, and isotopic composition. This parent body then demonstrates a previously unrecognized complexity in possibly crustal compositions. Regardless of whether these achondrites indeed shared a common parent body, the chronological results reported here indicate that igneous activity on planetesimals was capable of producing complex and evolved compositions very early in Solar System history.

2.6 Supplementary Materials

2.6.1 Pb Methods for NWA 11119

Chemical processing of the mineral separates and WR was performed in the SPIDE^{2}R laboratories located at ANU using procedures similar to those developed by Amelin (2008) and Koefoed et al. (2016). These aliquots were first washed in ethanol for 30 minutes and subjected to an ultrasonic bath. They were then rinsed three times using distilled acetone to remove surface contamination (i.e. dust) and clean the samples prior to acid leaching and subsequent digestion. The samples were leached using a procedure designed to promote separation of the contaminant Pb (terrestrial) component from the Pb inherent in the sample (radiogenic and primordial) with progressive acid washes before a final digestion of the residue. The leaching stage was separated into two separate washes. The first leaching step (wash 1a and 1b) consisted of two washes of 0.3 M hydrogen bromide (HBr) followed by four washes of 0.5 M nitric acid (HNO_3) with 5 minutes of ultrasonic agitation followed by centrifuging between each washing step. The second leaching step consisted of two 7M HNO_3 washes (wash 2a) followed by two 6M

hydrochloric acid (HCl) washes (wash 2b) which were interspersed with periods on a hot plate at 110 ºC for one hour and centrifuging. The remaining residue for each aliquot was dissolved in a 2:1 25M hydrofluoric acid (HF), 12M HNO_3 solution.

All washes and residues were spiked with the mixed ^{202}Pb-^{205}Pb-^{229}Th-^{232}U-^{236}U 'double spike' tracer "DD2" (Amelin et al., 2010). Chemical purification of Pb and U was performed following previously described procedures (Koefoed et al., 2016). The Pb purification chemistry protocol employs reusable, purpose-made Teflon columns that were packed with ~0.05 mL of Eichrom AG1-X8 200-400 mesh anion exchange resin. Following column conditioning, each aliquot was loaded onto the column in a 1 M HCl and 9 M HBr solution. Matrix elements within the washes and residues were eluted in 0.3 M HBr with a final pass of 2.5 M HCl, while Pb was eluted using 0.5 M HNO_3. Each wash and residue per aliquot were taken through columns twice to ensure a high yield of chemical separation of elements. Following Pb separation, additional separation of U and Th was accomplished using the same Teflon columns loaded with ~0.05 ml of Eichrom UTEVA resin (Koefoed et al., 2016). Following column chemistry, the washes, residues, and blanks were loaded onto double refined rhenium (Re) filaments using an Aldrich colloidal silica gel ($SiO_2Al_2O_3$ 0.5%) for subsequent analysis using Thermal Ionization Mass Spectrometry (TIMS) following (Huyskens et al., 2012).

Pb isotopes within our NWA 11119 aliquot washes (1a, 1b, 2a, 2b) and residues were measured using a Thermo *Triton Plus* TIMS instrument at ANU. The intensity of the ion beam produced from the filament correlates to the Pb abundance within the aliquot. As such, Pb isotopes were analyzed either in static mode using multiple Faraday cup detectors, or by using 'peak-jumping' on the secondary electron multiplier (SEM)

detector. To monitor the reproducibility of the TIMS analysis, we ran a filament loaded with the NIST SRM 981 standard, spiked with the same DD2 tracer as the sample aliquots. We also ran three filaments loaded with the Early Time A, B and X solutions as additional standards. Four column blanks, and blanks collected from column washes 1, 2a, 2b and the residue were analyzed for Pb using the modified Finnigan MAT 261 TIMS instrument at ANU. While the procedural column blanks ranged from 0.52 to 5.47 pg Pb, we used a median value of 0.36 pg Pb to account for our analyses and those collected for the previous three experiments run on the MAT 261. The residue blank for these experiments was ranged from 0.14 to 0.33 pg Pb, which yielded a combined blank of 0.84 pg Pb. Isotopic data collected by both the Triton and MAT 261 were reduced using the PBDAT reduction software (Ludwig, 1980) and were compared to the Anyspike reduction method (Schmitz & Schoene, 2007).

2.6.2 Pb Methods for NWA 8486

Chemical processing of these fractions was performed in the SPIDE^{2}R laboratories located at ANU during two separate visits, using procedures similar to those developed by Amelin et al., (2008) and Koefoed et al., (2016). Prior to Pb chemical separation, the aliquots were first acid-leached or washed. The five NWA 8486 aliquots were washed in ethanol for 30 minutes and subjected to an ultrasonic bath. They were then rinsed three times using distilled acetone to remove surface contamination (i.e. dust) and clean the samples prior to acid leaching and subsequent digestion. The samples were leached using a procedure designed to remove the contaminant Pb (non-radiogenic) component with progressive acid washes before a final hotplate digestion of the residue.

The leaching stage was separated into two separate washes. The first leaching step (wash 1) consisted of four washes of 0.5 M nitric acid (HNO_3) with 15 minutes of ultrasonic agitation followed by centrifuging. The second leaching step consisted of two 7M HNO_3 washes (wash 2a) followed by two 6M hydrochloric acid (HCl) washes (wash 2b) which were interspersed with periods on a hot plate at 110 ºC for one hour and centrifuging. The remaining residue for each aliquot was dissolved in a mixed 25M hydrofluoric acid (HF), 12M HNO_3 solution.

All washes and residues were spiked with a ^{202}Pb-^{205}Pb-^{229}Th-^{233}U-^{236}U 'double spike' tracer (DD2) prior to column chemistry (Amelin et al., 2010). Chemical purification of Pb and U was performed following previously described procedures (Koefoed et al., 2016). The Pb purification chemistry protocol employs reusable, purpose-made Teflon columns that were packed with ~0.05 mL of Eichrom AG1-X8 200-400 mesh anion exchange resin. Following column conditioning, each aliquot was loaded onto the column in a 0.5 M HCl and 9M HBr solution. Matrix elements within the washes and residues were eluted in 0.3 M HBr with a final pass of 2.5 M HCl, while Pb was eluted using 0.5 M HNO_3. Each wash and residue per aliquot were taken through columns twice to ensure a high yield of chemical separation of elements. Following Pb separation, additional separation of U and Th was accomplished using the same Teflon columns loaded with ~0.05 ml of Eichrom UTEVA resin (Koefoed et al., 2016). Following column chemistry, the washes, residues, and blanks were loaded onto double refined rhenium (Re) filaments using an Aldrich colloidal silica gel ($SiO_2Al_2O_3$ 0.5%) for subsequent analysis using Thermal Ionization Mass Spectrometry (TIMS) following (Huyskens et al., 2012).

For Pb analysis of NWA 8486, Pb isotopes within our NWA 8486 aliquot washes (1, 2a, 2b) and residues were measured using a Thermo *Triton Plus* TIMS instrument at ANU. The intensity of the ion beam produced from the filament correlates to the Pb abundance within the aliquot. As such, Pb isotopes were analyzed either in static mode using multiple Faraday cup detectors, or by using 'peak-jumping' on the secondary electron multiplier (SEM) detector. To monitor the reproducibility of the TIMS analysis, we ran a filament loaded with the NIST SRM 981 standard, spiked with the same DD2 tracer as the sample aliquots. We also ran three filaments loaded with the Early Time A, B and X solutions as additional standards. Four column blanks, and blanks collected from column washes 1, 2a, 2b and the residue were analyzed for Pb isotopes using the modified Finnigan MAT 261 TIMS instrument at ANU. While the procedural column blanks ranged from 0.23 to 0.96 pg Pb, we used a median value of 0.36 pg Pb to account for our analyses and those collected for the previous three experiments run on the MAT 261. The procedural blank for wash 1 was lost during filament loading, while washes 2a and 2b were 0.37 pg and 0.43 pg Pb, respectively. We used a median value for previous wash 1 blanks to compensate for this loss, which, combined with the median column blank yielded a combined blank wash value of 0.73 pg Pb. The residue blank for these experiments was 0.48 pg Pb, which yielded a combined blank of 0.84 pg Pb. Isotopic data collected by both the Triton and MAT 261 were reduced using the PBDAT reduction software (Ludwig, 1980) and were compared to the Anyspike reduction method (Schmitz & Schoene, 2007).

2.6.3 Cr Methods

Chromium was purified using a chemistry procedure modified after previously published Cr chemistry protocols (Yamakawa et al., 2009). This chemistry procedure requires four columns to separate Cr cleanly from other elements (specifically other transition metals such as Fe). The first column, using of 1 mL of BioRad AG1-x8 200-400 mesh anion resin loaded onto a BioRad polypropylene column, separates Fe from other major elements. The sample is loaded onto the column in 6M HCl and the Cr elutes off the column immediately in 5 mLs of 6M HCl along with nickel (Ni), sodium (Na), titanium (Ti), vanadium (V), magnesium (Mg), calcium (Ca), and aluminum (Al). The Cr yield from this column is always > 95%. The second column, using of 1 mL of Biorad AG50-x8 200-400 mesh anion resin loaded onto a BioRad polypropylene column, is designed to separate Cr from Ni and other REEs. As detailed in a recent paper by Larsen et al., (2016), the exact speciation of Cr in chloride form must be controlled in order to elute Cr as desired. As a result of this, our samples are fluxed on the hotplate in concentrated HCl for 5 hrs at 120 ºC. This ensures complete transformation of Cr species into the $CrCl_2^+$ form. This solution is removed from the hotplate, diluted with MQ H_2O to make 2.4 mLs of 1M HCl, and immediately loaded onto the 2nd column. The Cr elutes off the column in 7 mLs of 1M HCl. The 3rd column uses AG50-x8 200-400 mesh resin loaded onto a purpose made Teflon column with dimensions of h = 23.3 mm and d = 4.05 mm and is designed to separate Cr from Na and interference elements Ti and V. As before, the speciation of Cr in HNO_3 must be carefully controlled such that Cr is in the form CrO_3 to ensure effective elution. The sample is heated in 1.5 mLs of 1M HNO_3 in a sealed Savilex Teflon vial in an oven at 50 ºC for 24 hrs. The sample is then diluted with

MQ H_2O in order to make 3 mLs of 0.5M HNO_3 and immediately loaded onto the third column. After eluting Na, Ti, and V (among other elements) in 0.5M HNO_3, 0.5M HF, and 1M HCl the Cr elutes in 5 mLs of 6M HCl.

These procedures were designed to address two specific issues: 1) effectively separate Cr from other elements, specifically those with isotopes that create interferences during measurement; and 2) promote high Cr yields through the chemistry. To prevent measurable isotopic effects due to incomplete elution of Cr, total chemistry Cr yields need to be > 80% (typical in the literature) or even as high as >95% (Larsen et al., 2016). Larsen et al. (2016) performed a detailed study of the speciation of Cr in the acids of interest, and the effects that low yields would produce on the measured Cr isotope ratios. Larsen et al. (2016) warn that high recovery (>95%) Cr chemistry is necessary to measure Cr isotopes accurately. In response to these findings, we designed an experimental approach in which we tested our chemistry using NBS 979 pure Cr solution. Our procedural testing shows that at our current level of precision we do not see measurable isotopic effects at total Cr yields >80% and our chemistry protocol is successfully and repeatedly producing total chemistry yields >>80%. A more serious issue facing the successful measurement of Cr by MC-ICPMS (specifically the $^{54}Cr/^{52}Cr$ ratios) is the effective total separation of Fe from Cr. Iron-54 (^{54}Fe) is a direct isobaric interference on ^{54}Cr and, unlike measurement with TIMS techniques, we cannot control the ionization of Cr vs Fe using MC-ICPMS techniques. Instead, we must act to produce an eluent through column chemistry that has near complete separation of Cr from Fe (i.e. $Fe/Cr < 1x10^{-5}$) in order to confidently account for the interference of ^{54}Fe on ^{54}Cr. Additionally, if the Fe is residual and inherent to the sample (i.e. not completely

separated during chemistry) then the Fe that remains is likely fractionated (Anbar et al., 2000). This complicates any means of accounting successfully for the isotopic interference from ^{54}Fe on ^{54}Cr and can produce erroneously light ^{54}Cr/^{52}Cr ratios. Our developed methods remove any Fe remaining through the chemistry in a final Fe clean-up step using BioRad AG1-x8 20 - 50 mesh resin. This resin is added (~10 beads) to the Cr cut from the 3rd column, after being evaporated and brought up in 10N HCl, The sample container is agitated on an orbital shaker to promote bead interaction with the acid, and then the solution is pipetted away from the beads. This method is capable of removing >99% of the remaining Fe which ensures Fe/Cr <1x10^{-5}.

Chromium isotopes are measured in the ICGL at ASU on our dedicated Thermo *Neptune* MC-ICPMS. Chromium is measured in high resolution mode (mass resolving power, M/ΔM >> 8000). The cups are positioned such that measurements are made on the low mass shoulder of the peak in order to avoid interferences on ^{56}Fe from argon oxide (ArO), as Ar is the sample carrier gas. A typical peak shape and analysis position are shown in Figure S2.1. Chromium isotopes are reported in μ-notation as follows:

$$\mu\,{}^{x}Cr = \left[\frac{\left(\frac{{}^{x}Cr}{{}^{52}Cr}\right)_{sample}}{\left(\frac{{}^{x}Cr}{{}^{52}Cr}\right)_{standard}} - 1\right] x\ 10^{9}$$

where x = 53 or 54. The radiogenic excesses on ^{53}Cr from the decay of ^{53}Mn are given as μ^{53}Cr* and the nucleosynthetic effects on ^{54}Cr are shown as μ^{54}Cr. Based on repeat analyses of the terrestrial rock standard DTS-2, Allende WR, and NBS and SPEX pure Cr solutions, we currently estimate our external reproducibility for μ^{53}Cr* ± 10 ppm and μ^{54}Cr ± 22 ppm (Fig. S2.2). The analyses were optimized for a typical mass of Cr of ~1

μg. Running at a concentration of 800 ppb, this typically allows for between 4 – 5 analyses per 1 μg Cr. All samples and standards are run in an identical fashion, where one data point represents 4 -5 individual analyses (each comprised of 50 individual cycles). Our uncertainties are reported as either the internal 2 standard error (2SE = 2 x standard deviation/ sqrt(n)) or the external reproducibility, whichever is larger.

2.6.4 Supplementary Figures

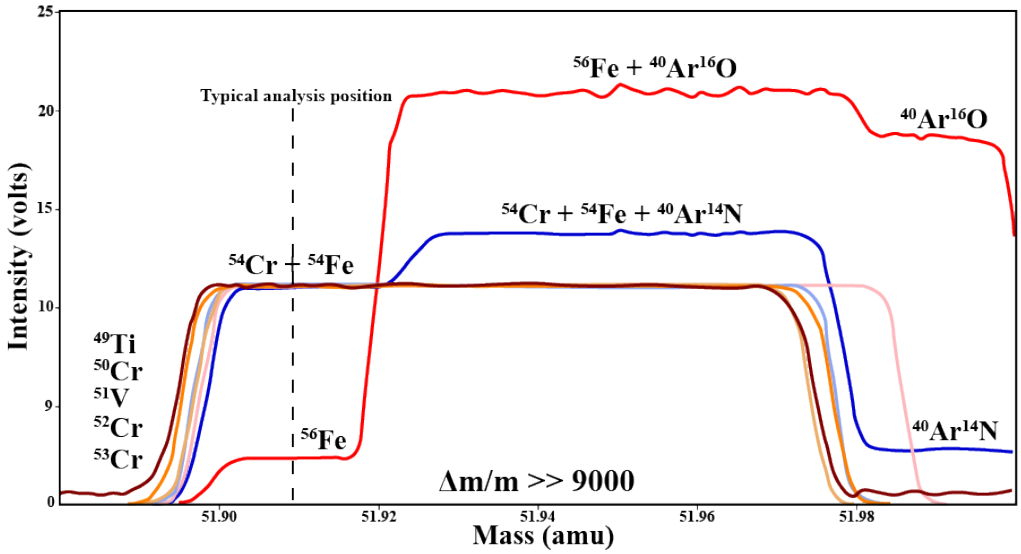


Figure S2.1. Typical peak positions during Cr isotope analyses in high resolution mode with mass resolving power (Δm/m) >> 9000 conducted on the Thermo MC-ICPMS instrument in the ICGL at ASU. A typical analysis position is shown demonstrating the avoidance of direct isobaric interferences.

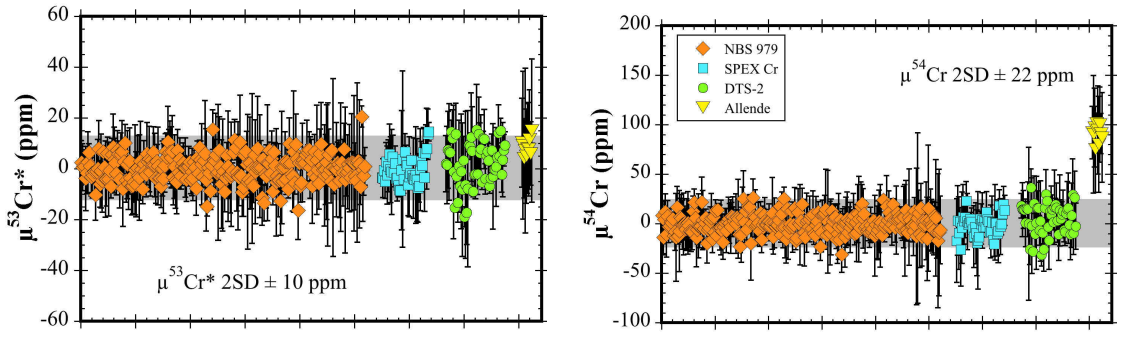


Figure S2.2 The external reproducibility of our $\mu^{53}Cr^*$ (ppm) and $\mu^{54}Cr$ (ppm) measurements in the ICGL to date. Each data point represents ~1μg of total Cr consumed and is plotted with its internal 2SE. The external reproducibility is reported as the 2SD of repeat analyses of NBS 979 (orange diamonds), SPEX Cr (blue squares), and DTS-2 (green circles) and is shown as the horizontal grey band in each plot. Our external reproducibility for $\mu^{53}Cr^*$ is ± 12 ppm and for $\mu^{54}Cr$ is ± 22 ppm. Samples are treated in an identical way with the uncertainties on individual samples given as the internal 2SE based on repeat analyses of that sample or the external 2SD shown here, whichever is larger.

2.6.5 Supplementary Tables

Table S2.1 Uranium Isotope Systematics of NWA 11119

Sample			Double-spike data reduction				Sample-standard bracketing data reduction						
		Spike/ Sample	$\delta[^{234}U/^{238}U]$	2SD	$\delta^{238}U/^{235}U$	2SD	$\delta[^{234}U/^{238}U]$	2SD	$\delta^{238}U/^{235}U$	2SD	$^{238}U/^{235}U$	2SD	n
Standards													
CRM-145	ICP solution	2.35	-33.50	22.87	-0.60	0.43	-34.28	6.09	0.00	0.08	137.837	0.011	144
CRM-129	ICP solution	2.55	-19.63	24.62	-2.45	0.24	-22.72	4.00	-1.70	0.07	137.602	0.009	20
Ricca*	ICP solution	2.50	4.21	26.37	-0.96	0.28	1.11	3.43	-0.21	0.09	137.809	0.012	20
AGV	Andesite	2.51	0.15	19.93	-0.94	0.19	-0.14	1.92	-0.17	0.06	137.814	0.009	28
BCR	Basalt	2.51	12.09	26.22	-0.93	0.25	4.94	2.57	-0.25	0.08	137.803	0.011	9
Ungrouped Achondrite													
NWA 11119	Andesite -Dacite	11.55	50.32	2.76	-1.01	0.08	30.92	0.43	-0.19	<0.01	137.811	0.011	1

The uranium isotope composition of samples and standards run during the same analytical session. Sample-standard bracketing uses CRM-145 as the bracketing standard. The $^{238}U/^{235}U$ ratio is reported relative to CRM-112 from Richter et al. (2010). NWA 11119 was bracketed against CRM-145 with a spike/sample ratio = 11. Uncertainty on the $^{238}U/^{235}U$ for NWA 11119 is the 2SD of repeat CRM-145 as it is larger than the internal 2SE.
*Ricca Chemical Company PU1KN-100 Uranium ICP Standard.

CHAPTER 3

HIGH RESOLUTION CHRONOLOGY OF THE UNEQUILIBRATED EUCRITE NORTHWEST AFRICA 8661: TIMING OF BASALTIC CRUST FORMATION ON VESTA

3.1 Introduction

The Howardite-Eucrite-Diogenite (HED) group represents the most common types of achondrites and are the only meteorites (with the exception of meteorites thought to originate from Mars and the Moon) with a known parent body, i.e., the asteroid 4Vesta, which is the second largest asteroid in the asteroid belt . The exact petrogenesis of eucrites is still a matter of some debate. A partial melt scenario was first put forward by Stolper, (1977) who experimentally determined that eucrites could form as the result of partial melting of a chondritic source reservoir. Since then, a number of papers have suggested that eucrites and diogenites are best explained as resulting from the crystallization of high degrees of melting on an asteroidal body (i.e., from a "magma ocean"). The arguments for a magma ocean have been made based on major and trace element compositions as well as oxygen isotope compositions (Greenwood et al., 2005; Righter & Drake, 1997; Ruzicka et al., 1997). Recent work by Mandler & Elkins-Tanton, (2013) offers a petrogenetic model which explains eucrites are forming from residual liquids following diogenite crystallization from a magma ocean.

One aspect of eucrite formation which remains unclear is the timing of original formation in the crust of their parent body. Lugmair & Shukolyukov, (1998) used the

^{53}Mn-^{53}Cr chronometer to investigate the internal mineral and whole rock isochrons of various HED meteorite to reveal ancient ages of basalt formation and silicate differentiation on their parent body. The first evidence for live ^{26}Al was discovered in plagioclase separates from the eucrite Piplia Kalan by Srinivasan et al., (1999). Subsequent work also shows that basalt formation and silicate fractionation was likely occurring very early on Vesta (Bizzarro et al., 2005; Schiller et al., 2010, 2011) . Recently, Hublet et al., (2017) reported ^{26}Al-^{26}Mg systematics for several basaltic eucrites and diogenites. Internal isochrons were reported for three basaltic eucrites Camel Donga, Y-792510 and Y-793591 whose ^{26}Al-^{26}Mg ages are suggested to be ~3 – 7 Ma younger than CAIs.

In this study, the chronology of the unequilibrated eucrite Northwest Africa (NWA) 8661 is investigated in high precision using three independent isotope systems including the short-lived ^{26}Al-^{26}Mg and ^{53}Mn-^{53}Cr chronometers and the absolute Pb-Pb chronometer. The ε^{54}Cr isotope systematics are also reported which, in combination with the previously determined Δ^{17}O composition, can be used to constrain the genetic relationship between NWA 8661 and other achondrites.

3.2 Petrography of NWA 8661

NWA 8661 is a pristine, unequilibrated, unbrecciated basaltic eucrite. Macroscopically, this 763–gram meteorite's texture is typical of unbrecciated noncumulate eucrites: medium-grained subophitic, with equant pyroxenes up to 3 mm across and lathy plagioclases up to 3 mm long. Most of the rock consists of grains about

1/3 to 1/2 of these maximum sizes. Irregular-shaped, interstitial vesicles, up to 1 mm across, occupy some 3 vol%. Saharan weathering is scarcely detectible. This eucrite is to an exquisite degree unaffected by thermal metamorphism. Pyroxenes lack any discernible exsolution features (optically or via SEM). Mesostasis areas retain their original igneous textures as extremely fine-grained intergrowths. “Cloudy” inclusions are rare in both pyroxene and plagioclase. The pyroxene zonation resembles that of other rare unequilibrated eucrites [e.g., Bluewing 001 (Warren & Gessler, 2001)] (Fig. S3.1). The mesostasis contains, inter alia, minor pyroxferroite and olivine, which locally mantles amoeboid pure-Fe metal.

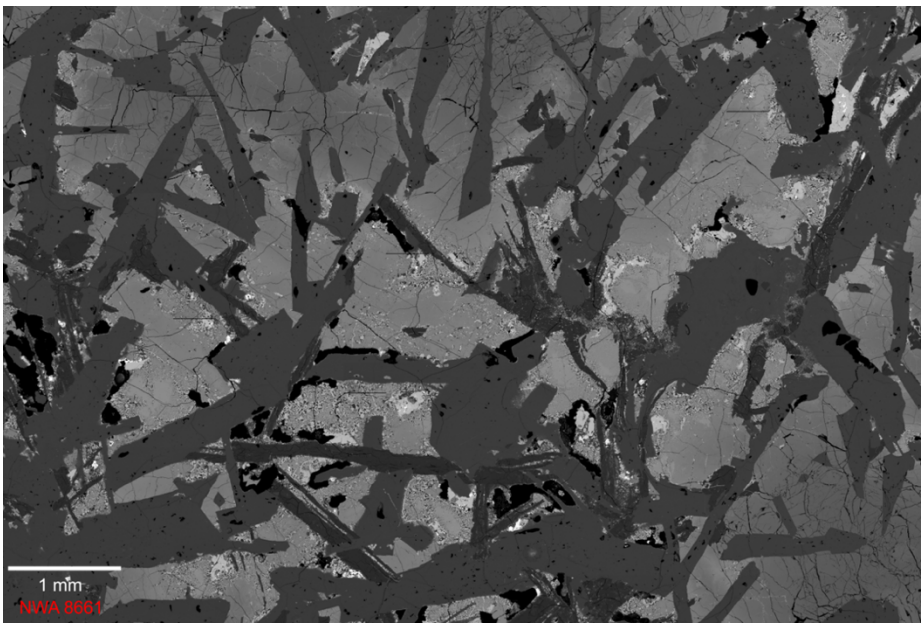


Figure 3.1. Back scattered electron image of NWA 8661. This image shows the large lathy dark gray plagioclase, light gray pyroxene with intact chemical zonation and clear lack of exsolution lamellae, regions of mesostasis as well as numerous vesicles (black). This BSE image was provided by Paul Warren (pers. comm.).

3.3 High-Precision Chronology of NWA 8661 and its Implications

The results of ^{26}Al-^{26}Mg analyses of whole rock and mineral separates of NWA 8661 are given in Table S3.1 and illustrated in Figure 3.2a. As can be seen in Fig. 3.2a, the ^{26}Al-^{26}Mg isochron for NWA 8661 is characterized by an elevated initial $\mu^{26}Mg^*_0$ = 17.2 ± 9.0 ppm, which is similar to that for other eucrites (Bizzarro et al., 2005; Hublet et al., 2017; Schiller et al., 2010). NWA 8661 has an $^{26}Al/^{27}Al = (4.3 \pm 0.5) \times 10^{7}$, which compared to the D'Orbigny angrite age anchor (Brennecka & Wadhwa, 2012; Kleine & Wadhwa, 2017) gives an ^{26}Al-^{26}Mg age = 4563.4 ± 0.3 Ma (Fig. 3.2a).

The ^{53}Mn-^{53}Cr systematics in the whole rock and mineral separates of NWA 8661 are given inTable S3.2 and shown in Fig. 3.2b. The ^{53}Mn-^{53}Cr isochron (Fig. 3.2b) has an initial $\mu^{53}Cr^*_0$ = 10.1 ± 19.5 ppm and a $^{53}Mn/^{55}Mn = (3.4 \pm 1.2) \times 10^{6}$ (MSWD = 0.9), which relative to D'Orbigny (Brennecka & Wadhwa, 2012; Glavin et al., 2004) gives a ^{53}Mn-^{53}Cr age = 4563.6 ± 1.6 Ma. Additionally, NWA 8661 has a weighted mean $\varepsilon^{54}Cr$ = -0.49 ± 0.11 which is in agreement with that reported for other HEDs (Sanborn et al., 2019; Wimpenny et al., 2019).

The Pb-Pb systematics of NWA 8661 pyroxene residues (Table S3.3) give a U-corrected, absolute age of 4565.4 ± 1.5 Ma (Figure 3.2c). The $^{207}Pb^*/^{206}Pb^*$ model ages of NWA 8661 (calculated assuming that all non-radiogenic Pb is primordial) have a weighted mean of 4563.9 ± 0.2 Ma (Figure 3.2d). See supplementary materials section 3.3.6 for details on isotopic analyses and further discussion of Pb-Pb ages.

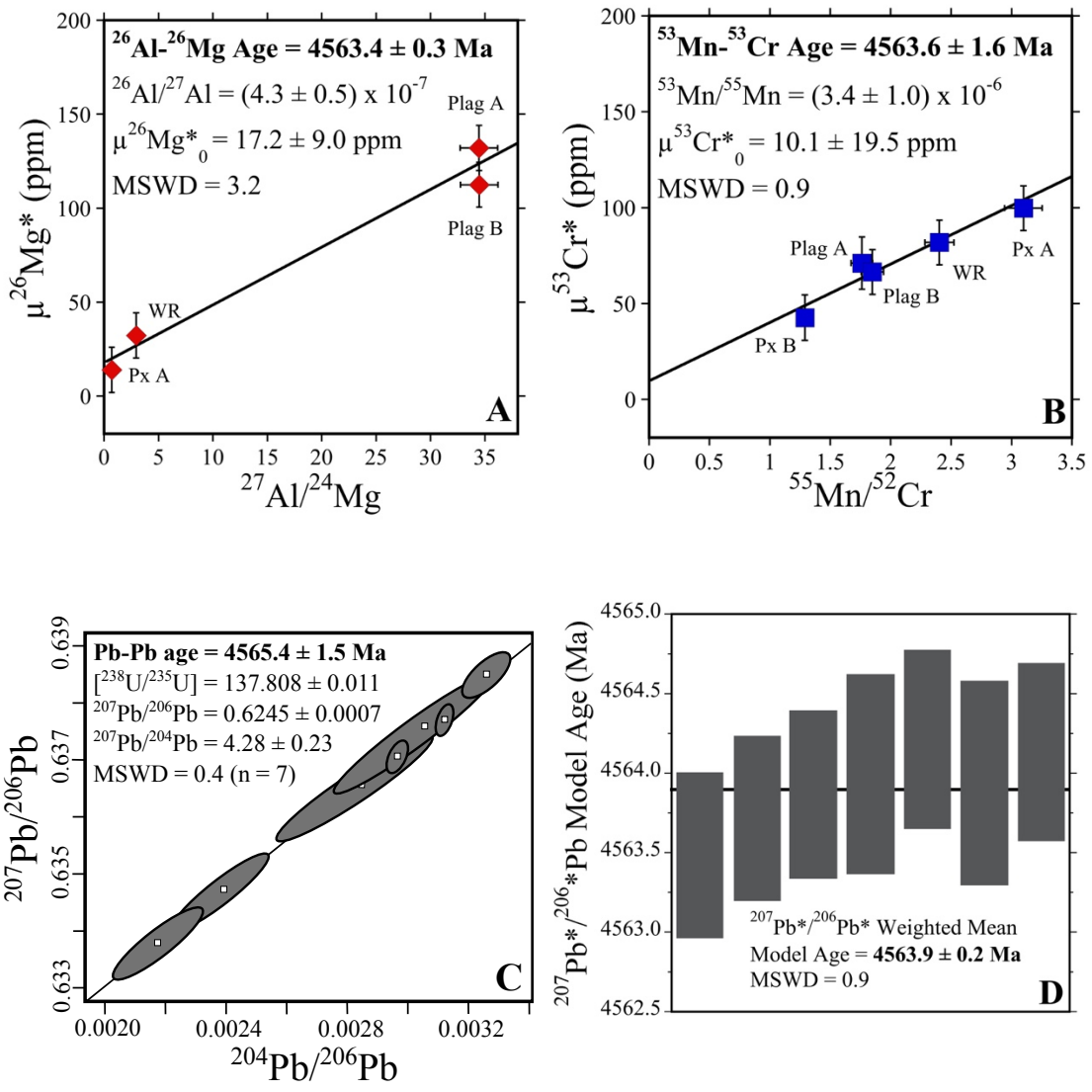


Figure 3.2 The ^{26}Al-^{26}Mg, ^{53}Mn-^{53}Cr, and Pb-Pb systematics in NWA 8661. A) The ^{26}Al-^{26}Mg internal isochron. B) The ^{53}Mn-^{53}Cr internal isochron. C) The Pb-Pb isochron comprised of the most radiogenic (^{206}Pb/^{204}Pb > 300) whole rock residues. D) The ^{207}Pb*/^{206}Pb* model ages for the same whole rock residues used in the isochron shown in Fig. 3.2C. WR = whole rock, OL = olivine, Px = pyroxene, Sil = silicate.

The ^{26}Al-^{26}Mg, ^{53}Mn-^{53}Cr, and Pb-Pb systematics presented here for the NWA 8661 eucrite yield concordant internal isochron ages for three different high-resolution isotopic chronometers, which is a first for any eucrite. This has several important implications not only for the petrogenesis of NWA 8661, but also more broadly for the timing of crust formation on the asteroid 4Vesta. Concordance between the three isotopic systems in this unequilibrated eucrite indicates that the rock cooled quickly through the closure temperatures of each system such that all three isotope systems record the same age. Basaltic eucrites are thought to have initially experienced rapid cooling rates (0.01 – 100°C/hr) followed by extended thermal metamorphism at subsolidus temperatures (Yamaguchi et al., 1997). The ancient ^{26}Al-^{26}Mg, ^{53}Mn-^{53}Cr, and Pb-Pb ages of this eucrite, the concordance between these chronometric systems, and the petrologic evidence indicate that this eucrite avoided the post formation alteration that effects nearly all basaltic eucrites.

Isotopic evidence suggests that the crust of Vesta records a thermal history that extended from as early as ~0.6 Ma up to at least ~35 Ma after CAIs (Roszjar et al., 2016; Schiller et al., 2010). Thermal modeling of Vesta agrees with the isotopic evidence in that Vesta heated rapidly (due to the decay of ^{26}Al) and then cooled over the next ~150 Ma (Ghosh & McSween, 1998; Neumann et al., 2014). Whether due to heating associated with internal magmatism or impact, Vesta's crust experienced extensive subsolidus thermal metamorphism. The ancient and concordant ages of NWA 8661 indicate that at least some portions of Vesta's crust escaped this metamorphism. It is possible that the magmatism on Vesta was punctuated by near surface sills and dykes as was suggested by Wilson & Keil, (2017). Alternatively, it is possible that NWA 8661 was removed from

the surface of Vesta (possibly by an impact) early in its history. If NWA 8661 was part of an early ejection of material from Vesta's surface then this material would have avoided the fate of so many other eucrites. As has been previously suggested, NWA 8661 could have originated from a "secondary" parent body (Greenwood et al., 2020) which might have been ejected early and survived in a stable orbit (~10 km to ensure survival), an argument used to explain the lack of impact resetting in other unbrecciated eucrites (Bogard & Garrison, 2003).

Another important aspect of concordance between chronometers relates to the assumptions inherent in using short-lived relative chronometers such as ^{26}Al-^{26}Mg and ^{53}Mn-^{53}Cr. Being able to determine a relative age between two objects requires that the distribution of the radioactive parent isotope was homogeneously distributed in the early Solar System. In this way, the only difference between the ratios of the unknown sample and the age anchor are the result of decay and are thereby directly related to time. While there has been recent evidence that would argue against a homogeneous distribution of ^{26}Al in the early Solar System (Bollard et al., 2017; Larsen et al., 2011; Schiller et al., 2015), the overwhelming majority of studies argue in favor of a homogeneous distribution (Amelin et al., 2019; Kita et al., 2013; Macpherson et al., 1995; Sanborn et al., 2019). In this study, the absolute U-corrected Pb-Pb age of NWA 8661 agrees within the uncertainties with the ^{26}Al-^{26}Mg and ^{53}Mn-^{53}Cr ages. This indicates that the assumption regarding ^{26}Al homogeneity is validated and that the difference in the ^{26}Al/^{27}Al ratios between NWA 8661 and the age anchor D'Orbigny is the result of the passage of time.

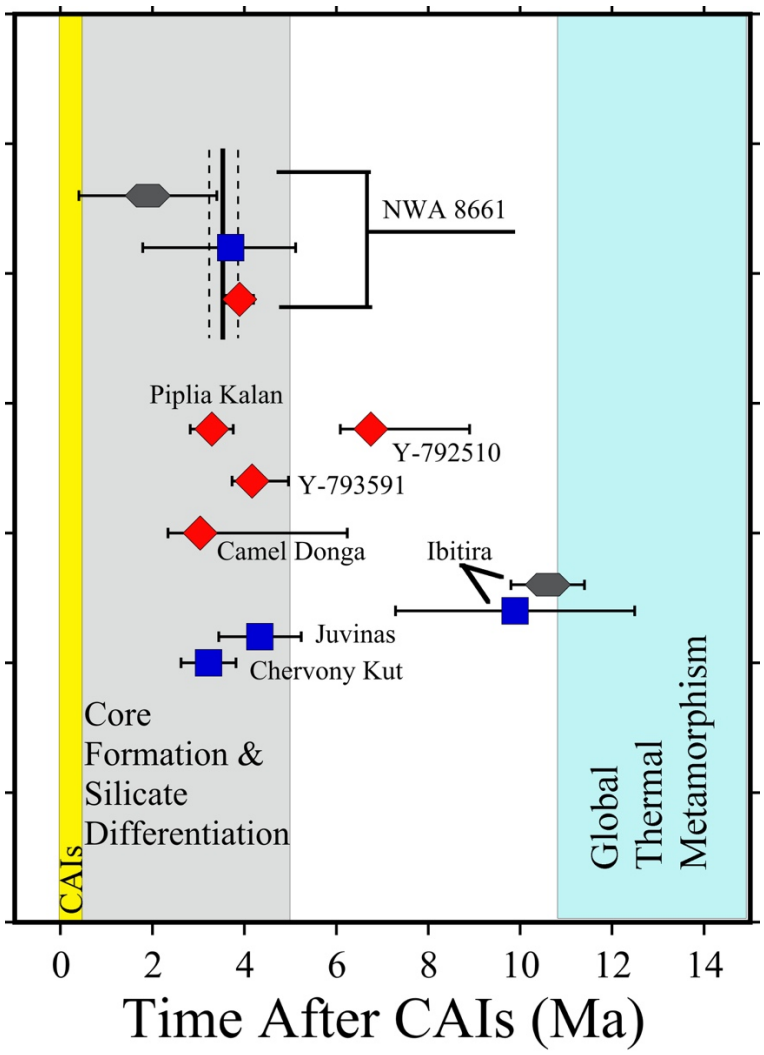


Figure 3.3 The ^{26}Al-^{26}Mg, ^{53}Mn-^{53}Cr, and Pb-Pb internal isochron ages of NWA 8661 compared to other previously determined internal isochron ages for other noncumulate basaltic eucrites. The gray hexagons are Pb-Pb isochron ages, blue squares are ^{53}Mn-^{53}Cr ages, and red diamonds are ^{26}Al-^{26}Mg ages. The data for NWA 8661 are shown at the top and illustrate the concordance between the ^{26}Al-^{26}Mg, ^{53}Mn-^{53}Cr and the Pb-Pb internal isochron age (calculated with the measured U isotope composition). The black solid and dashed lines represent the weighted mean age (and weighted 2SD) for NWA 8661 which is 4563.8 ± 0.3 Ma. The yellow vertical band indicates the timing of CAI formation (Connelly et al., 2012). The gray vertical band represents the time interval over which core formation and global silicate differentiation occurred on Vesta (~1 to 5 Ma after CAI formation) (Kleine et al., 2005; Kleine et al., 2004; Lugmair & Shukolyukov, 1998; Schiller et al., 2011; Touboul et al., 2015; Trinquier et al., 2008). The timing of global metamorphism of the crust of Vesta (light blue vertical band) is based on the Pb-Pb ages of zircons in a noncumulate eucrite (Iizuka et al., 2015). All ^{26}Al-^{26}Mg and ^{53}Mn-^{53}Cr ages shown here are relative to the D'Orbigny angrite (Amelin, 2008; Brennecka & Wadhwa, 2012; Glavin et al., 2004; Kleine & Wadhwa, 2017; Spivak-Birndorf et al.,

2009). The ^{26}Al-^{26}Mg data for Camel Donga, Y-793591, Y-792510, and Piplia Kalan are from Hublet et al., (2017) and (Srinivasan et al., 1999). The ^{53}Mn-^{53}Cr data for Chervony Kut, Juvinas and Ibitira are from Lugmair & Shukolyukov, (1998)The Pb-Pb age for Ibitira is from Iizuka et al., (2014).

Taking the weighted mean of the ^{26}Al-^{26}Mg, ^{53}Mn-^{53}Cr, and Pb-Pb ages reported here, we obtain a best estimate of the crystallization age of NWA 8661 of 4563.8 ± 0.3 Ma. Relative to the Pb-Pb age of CAIs (Connelly et al., 2012), this age is 3.5 ± 0.4 Ma younger. The ^{26}Al-^{26}Mg, ^{53}Mn-^{53}Cr, and Pb-Pb ages of NWA 8661 are shown in Fig. 3.3 in comparison to the only other high precision internal isochron ages for other noncumulate eucrites obtained previously. As can be seen in this figure, this is the first noncumulate eucrite for which three high-resolution chronometers (including the absolute Pb-Pb chronometer) yield concordant ancient ages. Our best estimate for the crystallization age of NWA 8661 (4563.8 ± 0.3 Ma) thus represents the timing of the earliest crust formation on Vesta at 3.5 ± 0.4 Ma after CAIs. While this is consistent with previous estimates based solely on either the relative ^{26}Al-^{26}Mg (Hublet et al., 2017) or the relative ^{53}Mn-^{53}Cr chronometer (Lugmair & Shukolyukov, 1998), it yields a more precisely defined time interval for the formation of the earliest basaltic crust on Vesta at ~ 3-4 Ma after CAIs.

Previously determined chronologic data for the HEDs allows us to constrain the timeline of accretion and differentiation of Vesta. Vesta's accretion must have been efficient and occurred early to acquire enough ^{26}Al to melt the body. Core formation began within the 4 Ma of CAI formation (Kleine et al., 2005). Silicate fractionation occurred ~1-3 Ma after CAI formation based on ^{26}Al-^{26}Mg model ages of both eucrites

and diogenites (Hublet et al., 2017; Schiller et al., 2010; Schiller et al., 2011). The duration of magmatism on Vesta is more difficult to constrain as thermal metamorphism and impacts obfuscate the record. Thermal modelling of Vesta indicates that conditions were favorable to maintain silicate melts for up to 150 Ma after CAI formation (Neumann et al., 2014). Iizuka et al. (2015) attribute a preponderance of U-Pb zircon ages at ~ 11 to ~15 Ma after CAI formation to the timing of global metamorphism on Vesta (Fig. 3.3). Another interpretation of the relatively young zircon ages is that these define instead the peak of magmatic activity in the crust of Vesta up to a few tens of millions of years after CAI formation (Roszjar et al., 2016).

Given the numerous HED meteorites in our meteorite collections, these samples represent our best opportunity to study igneous activity on a planetesimal (4Vesta) in the early Solar System. Recent advancements in analytical capabilities have allowed significant improvements in defining the chronology of HEDs and their parent asteroid 4 Vesta. Nevertheless, there are still some significant challenges in understanding the precise timescales of magmatic activity and crust formation on 4Vesta due to the overprinting of secondary processes resulting from impact-related shock and thermal metamorphism. It is rare to find a eucrite so pristinely preserved as NWA 8661. The weighted mean age (using ^{26}Al-^{26}Mg, ^{53}Mn-^{53}Cr, Pb-Pb and ^{207}Pb*/^{206}Pb* ages) of NWA 8661 is 4563.8 ± 0.3 Ma. This is the first such report of concordance between three high-resolution isotopic chronometers for any HED and unequivocally argues for basalt formation as early as 3.5 ± 0.4 Ma after CAIs. Hopefully, the recovery and investigation

of more unequilibrated eucrites will allow a more comprehensive understanding of the timeline of basaltic crust formation on one of the most prominent asteroidal bodies in the Solar System.

3.4 Supplementary Materials

3.4.1 NWA 8661 Sample Preparation

Approximately ~600 mg of interior fragments from NWA 8661 were obtained from P. Warren (UCLA). All sample preparations were conducted under clean laboratory conditions in the Isotope Cosmochemistry and Geochemistry Laboratory (ICGL) at ASU and the Sensitive and Precise Isotope Dating of Earth's and Extraterrestrial Rocks (SPIDE^{2}R) Lab at ANU. The bulk sample was first cleaned with MQ H_2O in an ultrasonic bath to remove any surface contamination. Of the ~600 mg, ~200 mg was used for bulk U isotope measurements. Of the remaining ~400 mg, ~60 mg was dissolved to obtain a whole rock (WR) fraction for ^{26}Al-^{26}Mg and ^{53}Mn-^{53}Cr analyses. Mineral separation for ^{26}Al-^{26}Mg and ^{53}Mn-^{53}Cr investigations required crushing, dry sieving, and density separation from a ~200 mg bulk sample. For Pb-Pb analyses, ~200 mg was processed by hand-picked for minerals of interest, with ~50 mg set aside for WR analyses. Details of the individual digestion and chemical separations are given below.

3.4.2 ^{26}Al-^{26}Mg Methods

The ~60mg WR aliquot for ^{26}Al-^{26}Mg was crushed and treated with HNO_3:HF on a hotplate before being dissolved in its entirety using a high pressure parr bomb set-up using 2:1 HF:HNO_3. Mineral separates were picked using a binocular microscope before

being digested on a hotplate in HNO_3:HF. These consisted of two plagioclase (Plag 1 and 2) two pyroxene (Px 1 and 2) aliquots. For the ^{26}Al-^{26}Mg system, only Px 1 was used. Procedures and protocols for dissolution and purification of Mg were similar to those described previously (Bouvier et al., 2011b; Spivak-Birndorf et al., 2009) with only minor modifications described below. Prior to any chemical separations, ~10 % aliquot of each sample solution was reserved for the determination of $^{27}Al/^{24}Mg$ ratios. Magnesium concentrations and $^{27}Al/^{24}Mg$ ratios were determined on a ThermoFisher iCAP-Q mass spectrometer in the Keck Laboratory at ASU. Magnesium isotopes were analyzed using the *Neptune* MC-ICPMS in ICGL at ASU, using protocols similar to those described earlier in (Bouvier et al., 2011b; Spivak-Birndorf et al., 2009). Instrumental mass fractionation was corrected using a sample-standard bracketing technique. Radiogenic excesses in ^{26}Mg from the decay of ^{26}Al ($\mu^{26}Mg^*$) were calculated using sample-standard bracketing and internal normalization of samples and bracketing standards (using the exponential fractionation law) to a $^{26}Mg/^{24}Mg$ ratio of 0.12663 (Catanzaro et al., 1966). The slopes and intercepts of the internal isochron for NWA 8661 were calculated using software isoplotR (Vermeesch, 2018). Magnesium isotopes are reported in μ-notation as follows:

$$\mu\,^{x}Mg = \left[\frac{\left(\frac{^{x}Mg}{^{24}Mg}\right)_{sample}}{\left(\frac{^{x}Mg}{^{24}Mg}\right)_{standard}} - 1\right] x\ 10^{9}$$

Based on repeat analyses of the terrestrial rock standard BCR-2, DTS-1, San Carlos Olivine (SCOL), JR-2 and DSM-3 and SPEX pure Mg solution, we currently estimate

our external reproducibility for $\mu^{26}Mg^*$ ± 12 ppm. Running at a concentration of 250 ppb typically allows for between ~ 5 analyses per 1 µg Mg. All samples and standards are run in an identical fashion, where one data point represents ~5 individual analyses (each comprised of 75 individual cycles). Our uncertainties are reported as either the internal 2 standard error (2SE = 2 x standard deviation/ sqrt(n)) or the external reproducibility, whichever is larger. The $^{27}Al/^{24}Mg$ and magnesium isotope results for both samples and standards are shown in Table S2.

The internal ^{26}Al-^{26}Mgisocrhon for NWA 8661 has a mean square weighted deviation of this regression (MSWD = 3.2) indicates the data points are over-dispersed about the regression. The tolerance of an MSWD for a regression made of 3 – 4 data points should result in an MSWD < 2.4 for the regression to be statistically significant. Since the ^{26}Al-^{26}Mg regression does not meet this criterion, the uncertainties on the slope can be expanded by the square root of the MSWD in order to produce a regression with an MSWD = 1. If this error expansion is performed on the ^{26}Al-^{26}Mg isochron it results in an initial $\mu^{26}Mg^*_0$ = 17.2 ± 34.4 ppm and a slope of $^{26}Al/^{27}Al = (4.3 \pm 2.1) \times 10^{7}$ (MSWD = 1) which results in an ^{26}Al-^{26}Mg age = 4563.4 ± 0.5 Ma where all uncertainties are at 95% confidence interval. For the purposes of this discussion, it does not matter which age uncertainty is used though we believe the 0.5 Ma uncertainty using the error expansion to be more conservative.

3.4.3 ^{53}Mn-^{53}Cr Methods

For the ^{53}Mn-^{53}Cr systematics, the same aliquots from the magnesium chemistry were used. The efficiency of the Mg chemistry (>99%) allowed for recombination of the

non-Mg cut from the chemistry to be recombined with the unaltered sample solution. Chromium was purified and analyzed in the same fashion described in Chapter 1 supplementary materials.

3.4.4 Pb-Pb Methods

Chemical processing of the mineral separates and WR was performed in the SPIDE^{2}R laboratories located at ANU using procedures similar to those developed by (Amelin, 2008) and (Koefoed et al., 2016). These aliquots were first washed in ethanol for 30 minutes and subjected to an ultrasonic bath. They were then rinsed three times using distilled acetone to remove surface contamination (i.e. dust) and clean the samples prior to acid leaching and subsequent digestion. The samples were leached using a procedure designed to promote separation of the contaminant Pb (terrestrial) component from the Pb inherent in the sample (radiogenic and primordial) with progressive acid washes before a final digestion of the residue. The leaching stage was separated into two separate washes. The first leaching step (wash 1a and 1b) consisted of two washes of 0.3 M hydrogen bromide (HBr) followed by four washes of 0.5 M nitric acid (HNO_3) with 5 minutes of ultrasonic agitation followed by centrifuging between each washing step. The second leaching step consisted of two 7M HNO_3 washes (wash 2a) followed by two 6M hydrochloric acid (HCl) washes (wash 2b) which were interspersed with periods on a hot plate at 110 ºC for one hour and centrifuging. The remaining residue for each aliquot was dissolved in a 2:1 25M hydrofluoric acid (HF), 12M HNO_3 solution.

All washes and residues were spiked with the mixed ^{202}Pb-^{205}Pb-^{229}Th-^{232}U-^{236}U ‘double spike’ tracer “DD2” (Amelin et al., 2010). Chemical purification of Pb and U

was performed following previously described procedures (Koefoed et al., 2016). The Pb purification chemistry protocol employs reusable, purpose-made Teflon columns that were packed with ~0.05 mL of Eichrom AG1-X8 200-400 mesh anion exchange resin. Following column conditioning, each aliquot was loaded onto the column in a 1 M HCl and 9 M HBr solution. Matrix elements within the washes and residues were eluted in 0.3 M HBr with a final pass of 2.5 M HCl, while Pb was eluted using 0.5 M HNO_3. Each wash and residue per aliquot were taken through columns twice to ensure a high yield of chemical separation of elements. Following Pb separation, additional separation of U and Th was accomplished using the same Teflon columns loaded with ~0.05 ml of Eichrom UTEVA resin (Koefoed et al., 2016). Following column chemistry, the washes, residues, and blanks were loaded onto double refined rhenium (Re) filaments using an Aldrich colloidal silica gel ($SiO_2Al_2O_3$ 0.5%) for subsequent analysis using Thermal Ionization Mass Spectrometry (TIMS) following (Huyskens et al., 2012).

Pb isotopes within our NWA 8661 aliquot washes (1a, 1b, 2a, 2b) and residues were measured using a Thermo Fisher *Triton Plus* TIMS instrument at ANU. The intensity of the ion beam produced from the filament correlates to the Pb abundance within the aliquot. As such, Pb isotopes were analyzed either in static mode using multiple Faraday cup detectors, or by using 'peak-jumping' on the secondary electron multiplier (SEM) detector. To monitor the reproducibility of the TIMS analysis, we ran a filament loaded with the NIST SRM 981 standard, spiked with the same DD2 tracer as the sample aliquots. We also ran three filaments loaded with the Early Time A, B and X solutions as additional standards. Four column blanks, and blanks collected from column washes 1, 2a, 2b and the residue were analyzed for Pb using the modified Finnigan MAT

261 TIMS instrument at ANU. While the procedural column blanks ranged from 0.52 to 5.47 pg Pb, we used a median value of 0.36 pg Pb to account for our analyses and those collected for the previous three experiments run on the MAT 261. The residue blank for these experiments was ranged from 0.14 to 0.33 pg Pb, which yielded a combined blank of 0.84 pg Pb. Isotopic data collected by both the Triton and MAT 261 were reduced using the PBDAT reduction software (Ludwig, 1980) and were compared to the Anyspike reduction method (Schmitz & Schoene, 2007).

3.4.5 Uranium Methods

In order to determine the bulk $^{238}U/^{235}U$ of NWA 8661, ~200mg was dissolved in bulk. This involved digestion on a hotplate in HNO_3:HF followed by high pressure digestion in a parr bomb set up using a 2:1 HF:HNO_3 mix. Following the parr bomb digestion, the sample was treated on a hotplate using $HClO_4$ in order to destroy all the fluorides created during the digestion process. Samples were then spiked with IRMM-3636 before being brought up in the load acid for the chemical separation of uranium. The uranium chemistry was taken from (Brennecka et al., 2010; Goldmann et al., 2015). Uranium isotopes were measure in the ICGL using our *Neptune* MC-ICPMS. The uranium isotope results are shown in Table S5.

3.4.6 Pb-Pb Systematics of NWA 8661

Figure S3.2 shows a regression that includes all the Pb data collected for all washes and residues from 18 aliquots dissolved along with the modern terrestrial composition (Stacey & Kramers, 1975) and the primordial Pb composition (Tatsumoto et

al., 1973). This regression has a high Mean Squared Weighted Deviation (MSWD) which indicates that the data is over dispersed about the regression. This is likely caused by mixing of multiple Pb isotope compositions including normal closed system radiogenic, primordial, terrestrial, and potentially a fourth which is a "parentless" radiogenic Pb, referred to as aborted high-μ Pb (Amelin, 2008). The data points which contain this anomalous Pb are all washes and residues of plagioclase aliquots. High-μ Pb has an isotopic composition dependent on the duration of radiogenic growth during the early Solar System when the $^{238}U/^{204}Pb$ was high. If this aborted high-μ Pb is then removed from the parent rock or somehow redistributed into an area with an otherwise primordial Pb isotopic composition the results are uncorrelated $^{207}Pb/^{206}Pb$ vs $^{204}Pb/^{206}Pb$ variation. As was described for the angrite Sahara 99555 (Amelin, 2008) and some eucrites (Sanders and Scott, 2007), this could result from early accretion and later remobilization of Pb during accretion. In light of this abnormal Pb isotopic composition, those washes and residues containing aborted high-μ Pb were not included in the age determination. These data can be seen plotting above the regression in Fig. S2.

In order to extract a meaningful age, we need to reduce the system from a four-component to a two-component mixture. One of these components must be the closed system radiogenic Pb and the other is (preferably) primordial Pb which has a well-defined isotopic composition. The purpose of the leaching procedure is to reduce the number of Pb components in the sample by allowing us to evaluate which components of Pb remain in each leaching step.

The best regression is given by the pyroxene residues which all have $^{206}Pb/^{204}Pb >$ 300. The regression for all seven such points yields an age of 4565.2 ± 1.5 Ma (MSWD =

0.4). This isochron passes marginally below primordial Pb. Using the same analyses, the weighted mean $^{207}Pb^*/^{206}Pb^*$ model age is 4563.9 ± 0.2 Ma (MSWD = 0.9; which includes the uncertainty of the measured $^{238}U/^{235}U$). The isochron and model age estimates agree within their 2SD uncertainties. Our preferred Pb-Pb age for NWA 8661 comes from this model date. Model ages are not preferable given the assumption that all non-radiogenic Pb must be primordial. However, given that a.) the Pb in NWA 8661 is not very radiogenic which leads to large uncertainties in the y-intercept of the isochron, b.) this ages agrees with the Pb isochron age within 2SD and c.) this model age is better representative of the ages defined by the short-lived system, confidence is bolstered in use of the model age.

3.5 Supplementary Figures

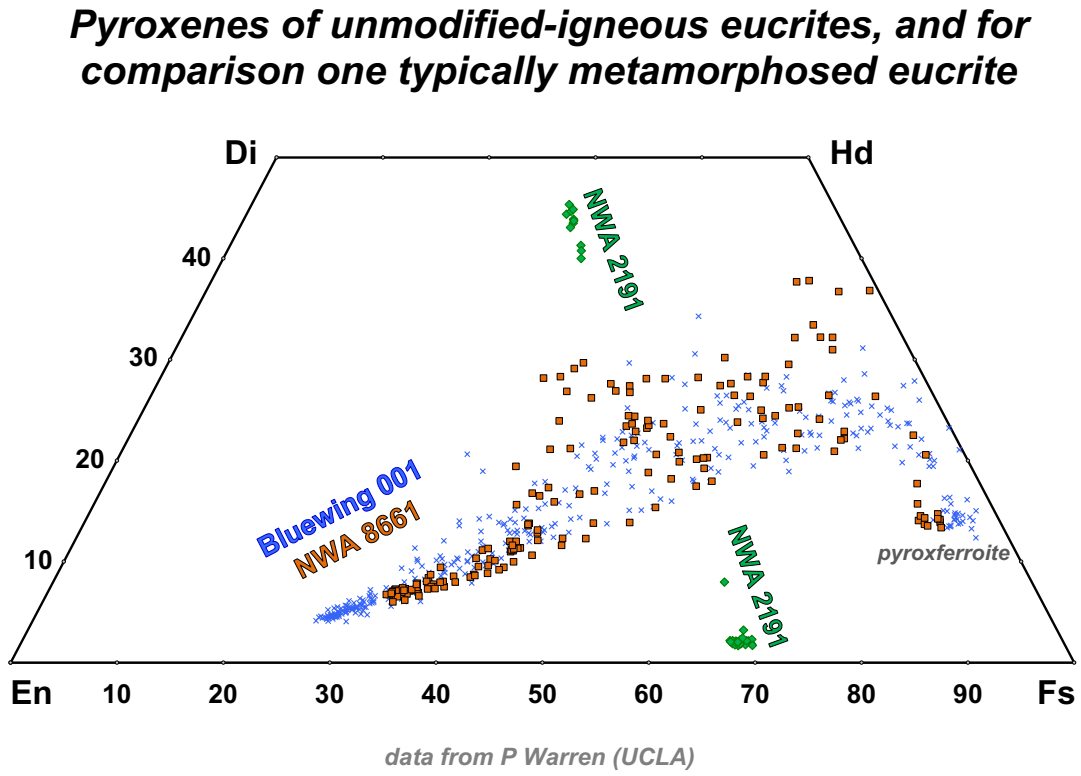


Figure S3.1 The pyroxene quadrilateral for NWA 8661, Bluewing 001, and NWA 2191 for reference (Warren, pers. comm.). This shows the chemical zonation trends in the pyroxene compositions illustrating the unequilibrated nature of NWA 8661. Bluewing 001 is another pristine eucrite showing similar pyroxene compositional trends. NWA 2191 is shown for comparison as a typical basaltic eucrite with equilibrated pyroxene compositions.

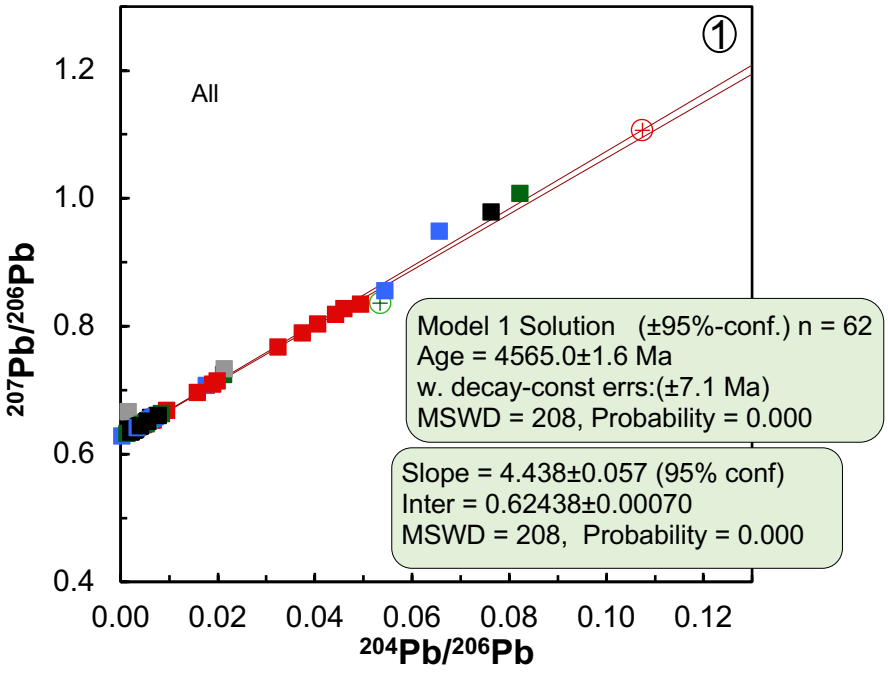


Figure S3.2 This figure shows a regression made using all available Pb data for NWA 8661 and also includes the modern terrestrial composition (green circle) (Stacey & Kramers, 1975) and the primordial composition (red circle) (Tatsumoto et al., 1973).

3.6 Supplementary Tables

Table S3.1 The ^{26}Al-^{26}Mg systematics for NWA 8661 as well as the Mg standards run during the same analytical sessions.

Sample	^{27}Al/^{24}Mg	2SD	μ^{26}Mg*	2SE	n
NWA 8661					
Whole Rock (WR)	2.95	0.15	32.31	5.12	5
Plagioclase 1 (Plag 1)	34.45	1.72	132.07	5.82	5
Plagioclase 2 (Plag 2)	34.47	1.72	112.48	7.20	5
Pyroxene 1 (Px 1)	0.71	0.04	13.94	6.54	5
Standards					
DSM-3			-0.53	5.39	272
JR-2			0.21	6.21	14
BCR-2			-6.49	8.80	31
DTS-1			-0.05	0.80	14

Magnesium isotopes for NWA 8661 are shown with their internal 2SE; however, in regressing the isochron the long-term reproducibility (2SD) of ±12ppm for μ^{26}Mg* was used since the internal 2SE values are always smaller.

Table S3.2 The ^{53}Mn-^{53}Cr systematics for NWA 8661 as well as the Cr standards run during the same analytical sessions.

Sample	^{55}Mn/^{52}Cr	±5%	μ^{53}Cr*	2SE	μ^{54}Cr	2SE	n
NWA 8661							
Whole Rock (WR)	2.40	0.12	81.87	5.63	-50.52	10.78	20
Plagioclase 1 (Plag 1)	1.76	0.09	71.14	13.60	-18.54	24.60	1
Plagioclase 2 (Plag 2)	1.85	0.09	66.49	11.43	-49.54	26.51	1
Pyroxene 1 (Px 1)	3.10	0.15	99.79	11.64	-56.02	23.82	12
Pyroxene 2 (Px 2)	1.29	0.06	42.85	7.96	-67.33	15.13	9
Standards							
NBS-979			0.09	7.01	-0.40	15.32	152
SPEX Cr			-3.54	13.32	-4.70	22.02	23
DTS			13.00	19.49	5.56	33.79	50
Allende			8.35	6.58	91.74	16.74	11

Chromium isotopes for NWA 8661 are shown with their internal 2SE for the isochron, the data is regressed using the internal 2SE or long-term reproducibility for the μ^{53}Cr* (±12ppm), whichever is larger.

Table S3.3 The Pb isotopic data for NWA 8661.

Sample	Pb ppb	Pb Pg	$^{206}Pb/^{204}Pb$ (Total)	%Err	$^{207}Pb/^{206}Pb$ (Total)	%Err	Error Corr. 4/6-7/6	$^{207}Pb^{*}/^{206}Pb^{*}$ Age (Ma)	Error (Ma)
A142- Pyroxene 1, (11.9mg)									
Wash 1	72.02	854.16	151.54	0.14	0.65	0.03	0.03	4560.22	0.55
Wash 2a	47.43	562.58	206.64	0.17	0.65	0.03	0.08	4564.26	0.53
Wash 2b	21.85	259.09	247.35	0.35	0.64	0.03	0.21	4565.33	0.52
Residue*	84.32	1000.04	321.14	0.78	0.64	0.04	0.39	4563.48	0.51
A142- Pyroxene 2, (10.2mg)									
Wash 1	90.68	921.34	146.81	0.15	0.65	0.03	0.02	4559.59	0.55
Wash 2a	46.02	467.56	227.23	0.22	0.64	0.03	0.10	4564.62	0.53
Wash 2b	20.85	211.84	253.23	0.43	0.64	0.04	0.26	4565.64	0.53
Residue*	84.47	858.24	337.37	0.96	0.64	0.04	0.45	4563.71	0.51
A142- Whole Rock 1, (10.0mg)									
Wash 1a	50.39	504.41	184.79	0.18	0.65	0.03	0.09	4558.14	0.55
Wash 1b	10.49	105.00	172.16	0.58	0.65	0.04	0.48	4565.13	0.55
Wash 2a	31.29	313.17	56.16	0.12	0.71	0.03	0.06	4570.89	0.70
Wash 2b	17.11	171.23	46.94	0.13	0.72	0.03	0.12	4573.91	0.76
Residue	42.42	424.66	132.12	0.73	0.66	0.05	0.66	4566.34	0.57
A143- Pyroxene 3, (2.2mg)									
Wash 1	76.89	171.46	20.19	0.16	0.83	0.04	0.04	4506.08	2.19
Wash 2a	1.01	2.25	597.15	2730.00	0.67	21.90	1.00	4641.62	101.45
Residue	13.53	30.18	445.69	48.10	0.64	0.65	1.00	4568.88	1.91
A143- Pyroxene 4, (1.7mg)									
Wash 1	37.64	62.49	22.51	0.57	0.82	0.07	0.65	4541.62	3.58
Wash 2a	1.27	2.11	46.69	72.60	0.73	6.57	0.99	4598.22	57.99
Residue	16.33	27.11	172.56	20.40	0.65	0.68	1.00	4568.11	2.30
A143- Pyroxene 5, (1.1mg)									
Wash 1	37.07	40.40	21.72	0.71	0.83	0.08	0.39	4548.90	5.65
Residue	11.15	12.15	460.38	125.00	0.64	1.59	1.00	4574.93	4.78
A143- Pyroxene 6, (1.3mg)									
Wash 1	26.55	34.78	24.62	1.49	0.80	0.19	0.90	4549.40	5.81
Wash 2a	3313.66	4340.89	18.33	0.11	0.85	0.05	0.14	4495.39	2.25
Residue	15.61	20.45	157.38	24.30	0.66	0.87	1.00	4574.13	3.10
A143- Pyroxene 7, (2.7mg)									
Wash 1	255.23	686.57	205.77	1.65	0.65	0.06	0.80	4562.67	0.57
Wash 2a	116.54	313.50	2825.88	650.00	0.63	1.40	1.00	4568.11	3.72
Wash 2b	46.19	124.24	701.27	41.90	0.63	0.37	0.99	4565.11	1.11
Residue*	182.79	491.71	307.02	2.01	0.64	0.05	0.76	4563.86	0.53
A143- Plagioclase 1, (8.0mg)									
Wash 1	18.04	143.40	26.64	0.50	0.79	0.07	0.76	4550.43	1.99
Wash 2a	16.70	132.75	15.20	6.87	0.95	4.61	0.99	4726.08	142.43
Wash 2b	19.64	156.10	12.15	0.60	1.01	0.30	0.97	4696.07	11.05
Residue	27.59	219.32	13.10	0.19	0.98	0.08	0.75	4648.32	4.11
A152- Pyroxene 8, (0.9mg)									
Wash 1b	180.25	169.44	104.18	3.53	0.67	0.19	0.98	4564.11	0.93
Wash 2a	89.67	84.29	148.78	5.41	0.66	0.21	0.98	4566.77	0.91
Wash 2b	43.73	41.10	116.91	4.85	0.66	0.24	0.99	4563.73	1.03
Wash 2b + Residue	95.83	90.08	249.81	7.81	0.64	0.19	0.98	4563.65	0.77
Residue*	148.35	139.45	354.16	7.24	0.64	0.13	0.96	4563.99	0.63
A152- Pyroxene 9, (2.2mg)									
Wash 1b	127.11	280.91	30.77	0.39	0.77	0.06	0.77	4554.20	1.22
Wash 2a	41.25	91.15	161.29	5.48	0.65	0.20	0.98	4567.18	0.85
Wash 2b	15.27	33.74	216.04	11.50	0.65	0.31	0.99	4566.03	1.11
Wash 2b + Residue	61.13	135.11	411.98	8.80	0.64	0.13	0.96	4564.89	0.64
Residue*	107.16	236.83	459.74	5.62	0.63	0.08	0.90	4564.21	0.56
A152- Pyroxene 10, (1.3mg)									
Wash 1b	133.21	170.51	50.16	1.43	0.71	0.14	0.96	4563.62	1.14
Wash 2a	46.03	58.92	220.67	11.70	0.64	0.32	0.99	4565.49	1.09
Wash 2b	23.64	30.25	250.26	14.90	0.64	0.35	0.99	4565.70	1.20
Wash 2b + Residue	63.47	81.24	320.54	11.20	0.64	0.21	0.98	4564.47	0.80

Residue*	103.59	132.59	331.16	7.06	0.64	0.13	0.96	4563.93	0.64
A152- Pyroxene 11, (2.4mg)									
Wash 1b	119.69	288.45	52.28	0.90	0.71	0.09	0.92	4559.17	0.88
Wash 2a	35.01	84.37	182.13	6.68	0.65	0.22	0.98	4565.57	0.87
Wash 2b	21.27	51.25	193.04	6.69	0.65	0.21	0.98	4565.73	0.84
Wash 2b + Residue	62.33	150.22	135.05	2.46	0.66	0.11	0.94	4564.22	0.69
Residue	103.54	249.54	126.15	1.38	0.66	0.07	0.86	4563.07	0.64
A152- Pyroxene 12, (2.2mg)									
Wash 1b	92.16	205.53	62.94	1.61	0.69	0.14	0.96	4563.26	0.96
Wash 2a	41.57	92.70	138.28	4.62	0.66	0.19	0.98	4566.16	0.86
Wash 2b	21.89	48.82	174.91	6.43	0.65	0.22	0.99	4566.41	0.87
Wash 2b + Residue	60.16	134.16	342.40	7.38	0.64	0.13	0.97	4563.97	0.63
Residue*	98.61	219.90	420.13	5.55	0.63	0.09	0.92	4564.13	0.56
A152- Pyroxene 13, (3.6mg)									
Wash 1b	111.76	401.23	242.54	3.72	0.64	0.10	0.93	4565.39	0.60
Wash 2a	52.79	189.53	254.14	4.23	0.64	0.10	0.94	4565.88	0.61
Wash 2b	28.29	101.58	270.72	4.68	0.64	0.11	0.95	4565.58	0.61
Wash 2b + Residue	60.17	216.01	259.04	3.34	0.64	0.08	0.91	4565.52	0.58
Residue	92.14	330.80	253.13	2.14	0.64	0.06	0.82	4564.89	0.55
A158- Pyroxene 14, (0.9mg)									
Wash 2a	149.43	141.95	287.70	3.54	0.64	0.08	0.90	4564.70	0.57
Wash 2b	73.53	69.85	182.32	5.00	0.65	0.16	0.97	4565.84	0.76
Wash 2b + Residue	129.41	122.94	221.80	3.81	0.64	0.11	0.94	4565.32	0.62
Residue	185.38	176.11	241.38	2.90	0.64	0.08	0.90	4565.11	0.58
A158- Pyroxene 15, (4.1mg)									
Wash 2a	86.55	353.14	185.51	0.92	0.65	0.05	0.63	4565.70	0.57
Wash 2b	31.14	127.06	183.20	2.76	0.65	0.09	0.93	4567.13	0.62
Wash 2b + Residue	71.90	293.35	178.29	1.29	0.65	0.05	0.77	4566.59	0.56
Residue	112.67	459.71	176.79	0.82	0.65	0.04	0.61	4566.47	0.55

Table S3.4 This table contains all pertinent U isotope measurement for NWA 8661 and U standards run during the same analytical session.

Sample			Double-spike data reduction				Sample-standard bracketing data reduction						
		Spike/ Sample	$\delta[^{234}U/^{238}U]$	2SD	$\delta^{238}U/^{235}U$	2SD	$\delta[^{234}U/^{238}U]$	2SD	$\delta^{238}U/^{235}U$	2SD	$^{238}U/^{235}U$	2SD	n
Standards													
CRM-145	ICP solution	2.35	-33.50	22.87	-0.60	0.43	-34.28	6.09	0.00	0.08	137.837	0.011	144
CRM-129	ICP solution	2.55	-19.63	24.62	-2.45	0.24	-22.72	4.00	-1.70	0.07	137.602	0.009	20
Ricca*	ICP solution	2.50	4.21	26.37	-0.96	0.28	1.11	3.43	-0.21	0.09	137.809	0.012	20
AGV	Andesite	2.51	0.15	19.93	-0.94	0.19	-0.14	1.92	-0.17	0.06	137.814	0.009	28
BCR	Basalt	2.51	12.09	26.22	-0.93	0.25	4.94	2.57	-0.25	0.08	137.803	0.011	9
Sample													
NWA 8661	Basaltic Eucrite	3.94	19.42	2.68	-1.07	0.07	20.64	0.62	-0.21	0.02	137.808	0.011	1

Sample-standard bracketing uses CRM-145 as bracketing standard. The $^{238}U/^{235}U$ ratio is reported relative to CRM-112 from (Richter et al., 2010). Uncertainty on $^{238}U/^{235}U$ uses the 2SD of repeat CRM-145 as it is larger than the internal 2SE. NWA 8661 was bracketed against CRM-145 with a spike/sample ratio = 4.
*Ricca Chemical Company PU1KN-100 Uranium ICP Standard

CHAPTER 4

THE TIMING OF BRACHINITE FORMATION BASED ON SHORT-LIVED ISOTOPE SYSTEMATICS OF BRACHINA AND NORTHWEST AFRICA 4882

4.1 Introduction

Brachinites are unbrecciated, ultramafic rocks with dunitic to wehrlitic bulk compositions. Though few members comprise this group of achondrites, they are crucial links to understanding the dynamic processes which built rocky bodies in the early Solar System. Brachina, the type specimen was first classified as a chassignite by Johnson et al., (1977) and was later determined to be a unique achondrite based on oxygen isotope, noble gas and geochemical data (Bogard et al., 1983; Crozaz & Pellas, 1984; Nehru et al., 1983, 1992). Since then, a number of papers have addressed the origins of the brachinites and brachinite-like achondrites. See Keil, (2014) for a detailed summary of pertinent literature.

The petrogenesis of brachinites have puzzled researchers, with current models for brachinite formation focusing on two main hypotheses. Brachinites could be primitive achondrites which formed as partial melt residues from a chondritic source (Nehru et al., 1983) or they could be igneous and/or cumulate rocks (Johnson et al., 1977). The argument for brachinites as primitive achondrites is based on textural, geochemical and isotopic lines of evidence. Brachinites have been modelled to originate as residues from low degrees of partial melting (~1-30%) of chondrite-, carbonaceous chondrite- and R chondrite-like compositions (Day et al., 2012; Goodrich et al., 1998; Gardner-Vandy et al., 2013). The melt produced must be capable of migration through the brachinite parent

body and away from the residues. This would require temperatures to reach the Fe-FeS eutectic (950C) and likely above the silicate solidus (1050C). Recently, (Day et al., 2012) described what the melt composition would look like and theorized that the felsic achondrites GRA 06128/06129 might well represent these melts. Arguments in favor of brachinites being igneous rocks are based upon their ultramafic mineralogies as well as many having igneous textures among other geochemical evidences (Mittlefehldt et al., 2003).

To complicate matters further, currently no high precision crystallization ages exist for brachinites. This is in part hampered by their olivine dominated mineralogies. Brachinites have been known to be ancient rocks based on excesses in ^{129}Xe as well as fission track dating using ^{244}Pu (Crozaz and Pellas 1984; Ott et al. 1987; Swindle et al. 1998). The first ^{53}Mn-^{53}Cr systematics for Brachina were reported in an abstract by (Wadhwa et al., 1998) who reported and age of 4563.7 ± 0.9 Ma relative to LEW 86010. Here we report high precision ^{53}Mn-^{53}Cr and ^{26}Al-^{26}Mg systematics for Brachina and NWA 4882.

4.2 Methods

4.2.1 ^{53}Mn-^{53}Cr Methods

All sample handling, mineral separation and ion exchange chromatography procedures were performed under clean laboratory conditions in the Isotope Cosmochemistry and Geochronology Lab (ICGL) at Arizona State University (ASU). An interior fragment, free of any fusion crust was ultrasonicated in methanol and ultra-pure H_2O before any further processing. For NWA 4882, a small chip (~50 mg) was broken off and digested

using HNO_3:HF treatment, followed by dissolution of residual chromites in a Parr bomb, to obtain a dissolved whole rock (WR) sample. Another larger chip (~106 mg) was broken off the main mass and processed through a differential dissolution protocol that results in an olivine-rich fraction (Ol), a pyroxene- and plagioclase-rich silicate fraction (Sil) and a chromite fraction (Chr). A ~10% aliquot of each fraction was reserved for Mn/Cr ratios, while aliquots of the remaining fractions (each containing 5-30 μg of Cr) were processed for Cr purification.

For Brachina, an interior fragment, free of any fusion crust, was selected from a piece of Brachina that was obtained from the South Australian Museum. The fragment was ultrasonicated in methanol before any further processing. A single large chromite grain (Chr-1) was handpicked from small fragment that was crushed. A small chip (~30 mg) was broken off and digested using HNO_3:HF treatment, followed by dissolution of residual chromites in a Parr bomb, to obtain a dissolved whole rock (WR) sample. Another larger chip (~101 mg) was also broken off the main piece and was processed through a differential dissolution protocol that resulted in an olivine-rich fraction (Ol), a pyroxene- and plagioclase-rich silicate fraction (Sil) and a second chromite fraction (Chr-2).

Chromium isotopes were measure on the Thermo Neptune Multi-collector Inductively Coupled Mass Spectrometer (MC-ICPMS) in the ICGL at ASU. The Cr isotopic data (Table 4.1) are reported relative to the NBS 979 standard after internal normalization to $^{50}Cr/^{52}Cr = 0.051859$ (Shields & Murphy, 1966). The radiogenic excess on ^{53}Cr are reported in μ-notation where $\mu^{53}Cr^* = [(^{53}Cr/^{52}Cr)_{sample}/(^{53}Cr/^{52}Cr)_{NBS\text{-}979} - 1] \times 10^6$. Our long-term reproducibility is ±11 ppm and ± 20 ppm (2SD) for $\mu^{53}Cr^*$ and $\mu^{54}Cr$,

respectively, based on repeat measurements of synthetic Cr standards and rocks standards (where each measurement utilized ~1 μg of Cr). The uncertainties on our sample data are reported as either the internal 2SE or the long-term 2SD, whichever is larger. Details about the chemical separation of Cr and analytical setup can be found in Chapter 1 of this dissertation. All ^{53}Mn-^{63}Cr isochron regressions were made using the freely available ISOPLOT and IsoplotR (Ludwig, 2012; Vermeesch, 2018).

4.2.2 ^{26}Al-^{26}Mg Methods

The same interior fragments which were digested for WR analyses of Cr isotopes were also used for WR analyses of Mg isotopes. Whole rock chips of NWA 4882 (~300mg) and Brachina (~100mg) were ultrasonicated in methanol and ultra-pure H_2O prior to further processing. In order to obtain clean minerals separates, the whole rock chips from Brachina and NWA 4882 were carefully crushed and sieved. This was followed by hand-picking clean olivine grains under a binocular microscope for both Brachina (Olivine 1 and 2 were ~5mg each) and NWA 4882 (Olivine ~5mg).

Prior to chemical purification of Mg, a ~1% aliquot of each of the dissolved samples was reserved for measuring Al and Mg concentrations using a Thermo ICAP-Q quadrupole mass spectrometer in the Keck Laboratory at ASU. Subsequently, Mg was purified from the remaining solutions following the procedure of (Spivak-Birndorf et al., 2009). Magnesium isotopes were measured on the ICGL's Thermofinnagan Neptune multi-collector inductively coupled plasma mass spectrometer (MC-ICPMS). An Aridus II desolvating nebulizer was used for sample introduction, with a flow rate of ~100 μl/min. The concentrations of the sample and standard solutions were typically ~1.5 ppm

(matched to within ~10%). The mass-independent effects on the $^{26}Mg/^{24}Mg$ ratio were determined using sample-standard bracketing and internal normalization of both samples and bracketing standard (DSM-3) to a $^{25}Mg/^{24}Mg = 0.12663$ (Catanzaro et al., 1966) using an exponential fractionation law. Radiogenic excesses in ^{26}Mg are reported in ppm notation where $\mu^{26}Mg^* = [(^{26}Mg/^{24}Mg)_{sample}/(^{26}Mg/^{24}Mg)_{DSM\text{-}3}\text{-}1] \times 10^6$. Based on repeated analyses of the DSM-3 Mg standard and the BCR rock standard over the course of the past year, our external reproducibility (2SD) on $\mu^{26}Mg^*$ is ± 7 ppm. For all Mg data, we report either the internal 2SE for repeat runs of the samples or the 2SD long-term reproducibility, whichever is larger. The ^{26}Al-^{26}Mg isochron regressions were calculated using the freely available ISOPLOT and IsoplotR (Ludwig, 2012; Vermeesch, 2018).

4.3 Results

4.3.1 ^{53}Mn-^{53}Cr Systematics of Brachina

The results from this high-precision investigation into the ^{53}Mn-^{53}Cr systematics of Brachina are shown in table 4.1 and figure 4.1. The $^{55}Mn/^{52}Cr$ ratio and $\mu^{53}Cr$ are strongly corelated among the mineral fractions and WR of Brachina with a well resolved positive slope. The slope of the internal isochron regression corresponds to a $^{53}Mn/^{55}Mn = (4.3 \pm 0.3) \times 10^{-6}$ (MSWD = 1.3) with the initial $\mu^{53}Cr_i = -7.9 \pm 7.4$ ppm. Taken relative to the D'Orbigny angrite, the ^{53}Mn-^{53}Cr internal isochron age of Brachina is 4564.9 ± 0.5 Ma. Relative to recently reported ungrouped achondrite NWA 6704, the age of Brachina is 4565.5 ± 0.9 Ma. Brachina WR has a $\mu^{54}Cr = -83 \pm 17$ ppm.

4.3.2 ^{53}Mn-^{53}Cr Systematics of NWA 4882

The results from this high-precision investigation into the ^{53}Mn-^{53}Cr systematics of NWA 4882 are shown in table 4.1 and figure 4.1. The ^{55}Mn/^{52}Cr ratios and μ^{53}Cr are corelated among the mineral fractions and WR of NWA 4882 with a resolved, albeit lower slope than Brachina. The slope of the internal isochron regression of NWA 4882 corresponds to a ^{53}Mn/^{55}Mn = $(2.4 \pm 0.8) \times 10^{-7}$ (MSWD = 1.0) with a positive initial $\mu^{53}Cr_i$ of 28.5 ± 7.6 ppm. Taken relative to the D'Orbigny angrite, the ^{53}Mn-^{53}Cr internal isochron age of NWA 4882 is 4549.4 ± 2.3 Ma. Relative to recently reported ungrouped achondrite NWA 6704, the ^{53}Mn-^{53}Cr internal isochron age of NWA 4882 is 4549.9 ± 2.3 Ma. Additionally, NWA 4882 has a μ^{54}Cr = -50 ± 6 ppm.

Table 4.1 ^{53}Mn-^{53}Cr systematics of Brachina and NWA 4882 as well as all standards run during the same analytical sessions.

Sample	**^{55}Mn/^{52}Cr**	**± 5%**	**μ^{53}Cr***	**2sd**	**μ^{54}Cr**	**2sd**	**n**
Brachina							
Whole Rock	0.843	0.04	9.43	16.32	-83.16	17.01	14
Olivine	6.511	0.33	241.22	7.75	-80.33	21.10	5
Silicates	0.262	0.01	3.64	12.95	-106.52	32.64	5
Chromite 1	0.007	3.27E-04	-5.98	21.20	-64.86	34.19	5
Chromite 2	0.006	3.13E-04	-3.18	8.57	-52.49	13.04	5
NWA 4882							
Whole Rock	0.464	0.02	28.61	5.82	-50.43	5.61	5
Olivine	21.556	1.08	71.58	10.20	102.61	23.75	6
Silicates	5.266	0.26	48.48	14.27	7.31	12.37	7
Chromite	0.018	8.79E-04	24.98	6.29	-18.00	9.88	4
Standards							
NBS-979			0.02	10.61	-1.16	19.20	57
SPEX			0.08	10.22	-0.74	28.97	10
Allende			9.71	11.25	92.42	24.94	8
DTS			8.85	9.01	14.64	12.75	7

4.3.3 ^{26}Al-^{26}Mg Systematics of Brachina and NWA 4882

The ^{26}Al-^{26}Mg systematics of Brachina and NWA 4882 were investigated to determine whether WR model ages could be obtained. The Mg isotopic composition of olivine and WR fractions from both Brachina and NWA 4882 are reported in table 4.2 along with their $^{27}Al/^{24}Mg$ ratios. The $\mu^{26}Mg^*$ of the olivine and WR fractions of Brachina are slightly negative with uncertainties overlapping with the bulk chondritic composition (Schiller et al., 2010) while the $^{27}Al/^{24}Mg$ ratios are below the chondritic value (Lodders, 2003). The olivine and WR fractions of NWA 4882 are strongly subchondritic with respect both to their $\mu^{26}Mg^*$ and $^{27}Al/^{24}Mg$ ratios. The WR fractions from both Brachina and NWA 4882 were regressed together with the bulk chondritic value and yield a $^{26}Al/^{27}Al = (4.6 \pm 1.5) \times 10^{-5}$ with a negative intercept of $\mu^{26}Mg^*_0 = -28.7 \pm 7.5$ ppm 2SE (figure 4.2). Taken relative to CAIs (Connelly et al., 2012; Kirsten K. Larsen et al., 2011), the ^{26}Al-^{26}Mg whole rock age of Brachina and NWA 4882 is 4567.2 ± 0.4 Ma. This is a conservative estimate of the uncertainty on the age due in part to the statistics of small numbers (n = 3) when making the regression.

Table 4.2 ^{26}Al-^{26}Mg systematics of Brachina and NWA 4882 as well as all standards run during the same analytical sessions.

Sample	^{27}Al/^{24}Mg	± 5%	μ^{26}Mg*	2sd	n
Brachina					
Whole Rock	0.062	0.003	-8.16	9.41	4
Olivine 1	0.056	0.003	-7.01	5.55	6
Olivine 2	0.059	0.003	-11.12	3.56	3
NWA 4882					
Whole Rock	0.022	0.001	-21.22	3.94	3
Olivine	0.001	4.8E-05	-24.30	6.01	9
Standards					
DSM-3			-0.10	13.19	79
SPEX			34.18	9.68	5
Allende			15.91	7.88	8
BCR-2			-3.89	3.51	7
DTS-1			-9.30	5.43	4

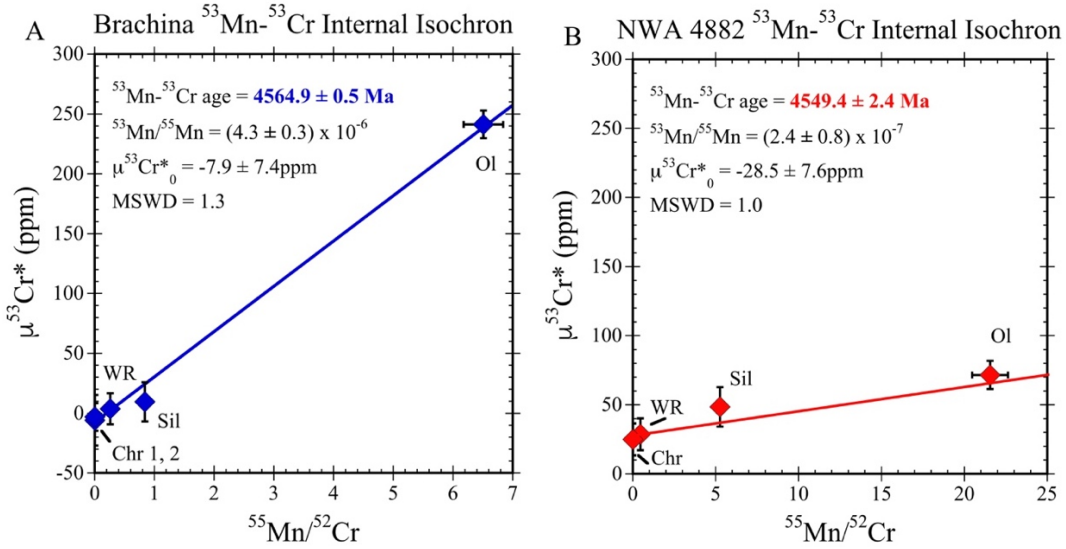


Figure 4.1 ^{53}Mn-^{53}Cr internal isochrons for (A) Brachina and (B) NWA 4882. The different mineral fractions are shown as Ol (olivine), Sil (silicates), Chr (chromite) and WR (whole rock). The chromium isotope data are plotted with their internal 2SE from repeat analyses or the external reproducibility (± 11 ppm), whichever is larger. The data for these brachinites are given in table 4.1.

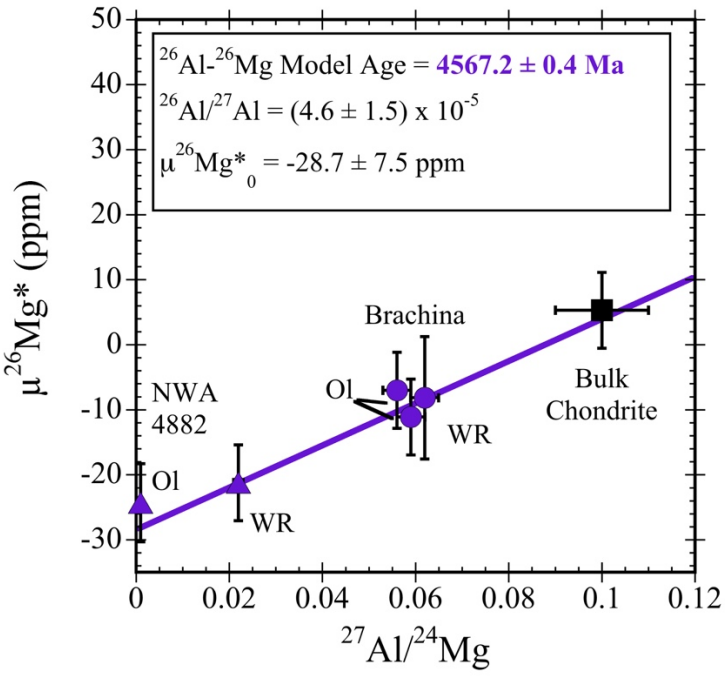


Figure 4.2 ^{26}Al-^{26}Mg systematics in whole rock (WR) and olivine (Ol) fractions for Brachina and NWA 4882. This isochron regression was calculated using only the WR fractions from both brachinites and the bulk chondritic value (Lodders, 2003; Schiller et al., 2010; Teng et al., 2010).

4.4 Discussion

4.4.1 Chronology of Brachina and NWA 4882

Brachinites were first determined to be ancient rocks using ^{129}I-^{129}Xe systematics (Bogard et al., 1983) and fission track dating techniques (Crozaz & Pellas, 1984). The first high-precision age for any brachinite was reported for Brachina by Wadhwa et al., (1998) who reported the ^{53}Mn-^{53}Cr age of 4563.7 ± 0.9 Ma (relative to LEW 86010). Subsequent studies have investigated the impact history of brachinites using Ar-Ar systematics, but no new crystallization ages have been reported for any brachinite. Here we report high-precision ^{53}Mn-^{53}Cr ages for two brachinites, Brachina and NWA 4882. The ^{53}Mn-^{53}Cr ages for these two brachinites differ considerably, with Brachina forming

~2.4 Ma after CAIs and NWA 4882 forming ~15 Ma later. Brachina is one of the oldest known achondrites with few examples of achondrites this ancient in the meteorite record. The only other achondrites with comparably ancient ages include the ungrouped achondrites Asuka 881394 with a U isotope measured Pb-Pb age = 4564.9 Ma (Wimpenny et al., 2019) and NWA 11119 with a U isotope measured Pb-Pb age = 4564.8 Ma (Chapter 2) and the monomict ureilite NWA 766 with a ^{53}Mn-^{53}Cr age = 4564.6 Ma (Yamakawa et al., 2010). While each of these achondrites is distinct in their mineralogy as well as geochemical and isotopic characteristics, this demonstrates the diversity of igneous processes occurring in the first ~3 Ma of Solar System history. The ^{53}Mn-^{53}Cr age of NWA 4882 is 4549.4 ± 2.3 Ma which could represent an original crystallization age or a metamorphic recrystallization age. Each of these possibilities carries their own complications in explaining as will be detailed below. Regardless of whether this age represents a crystallization age or a metamorphic age, this indicates that the brachinite parent body was active for ~15 Ma.

It is understood that ^{26}Al was the predominant heat source for early forming bodies in the Solar System. The products of this internal heating depend on the timing of formation, the composition of material accreted, the mobility of any melt produced and the size of the body. While the mineralogy of the brachinites precludes defining an internal isochron, regression of the WR fractions from both NWA 4882 and Brachina along with the bulk chondritic value allows us to define an estimated ^{26}Al-^{26}Mg model age of 4567.2 ± 0.4 Ma. This model age likely represents the timing of silicate

fractionation on the brachinite parent body. This age is contemporaneous with CAI formation (Connelly et al., 2012) and indicates that the brachinite parent body accreted early and began melting by ~0.5 Ma after Solar System formation.

4.4.2 Implications for the Petrogenesis of the Brachinite Parent Body(ies)

The chronology of these two brachinites poses some interesting questions about the brachinite parent body. The brachinite parent body is believed to be relatively small due in part to the idea that brachinites are primitive achondrites (Nehru et al., 1992). Primitive achondrites only experienced temperatures necessary to initiate silicate melting and thus came from a parent body that a) accreted late after ^{26}Al was no longer a potent heat source, b) the parent body remained small enough not to possess enough ^{26}Al to drive significant melting or c) perhaps that the mobility of the melts were not favorable to promote further parent body melting. However, there does exist evidence that brachinites are not primitive achondrites, but are produced as cumulates via igneous differentiation (Mittlefehldt et al., 2003). This would make the discrepant oxygen isotope systematics difficult to explain as differentiation is known to equilibrate oxygen isotope systematics in differentiated bodies (R N Clayton, 1993; Robert N Clayton & Mayeda, 2017; R. C. Greenwood et al., 2012; Richard C Greenwood et al., 2005). This argument was expanded by (Rumble III et al., 2008) to include the possibility that multiple parent bodies might best explain the oxygen isotopic diversity of brachinites, which vary considerably compared to other achondrites. This would allow for at least some of the brachinites to be cumulates from distinct parent bodies and would negate the complications of making a cumulate rock on a body that did

not differentiate to a degree necessary to homogenize the oxygen isotope composition. The chronology of these brachinites can provide additional constraints to these hypotheses.

If these brachinites are considered cumulate rocks from a single parent body, the chronology would suggest that igneous activity was active on this parent body at least during the first 17 Ma of Solar System history. However, the degree of differentiation and convection on this parent body was not sufficient to homogenize the oxygen isotope composition. This would require that regions on the parent body experienced high degrees of melting, but the melting was not global or at least did not globally mix. If these brachinites were produced in local regions of melting, the ^{26}Al-^{26}Mg model age suggests that silicate fraction began contemporaneously in both regions while the ^{53}Mn-^{53}Cr ages suggest different cooling histories between the two regions of melting. The difference in cooling history could reflect on the relative sizes of the melt regions and/or the availability of melt recharge. Brachina could have originated from a smaller region of melt with limited recharge while NWA 4882 might have come from a larger melt region or perhaps one which experienced later recharge or metamorphic event.

If these brachinites are considered to be primitive achondrites, the implications of the chronology might change. Without high degrees of melting, these achondrites could have come from a common parent body and maintained their distinctive oxygen isotopic compositions. The ^{53}Mn-^{53}Cr age of Brachina and NWA 4882 represent the timing of formation of these primitive residues. However, explaining the chronology of these two brachinites in light of their primitive nature is no less complicated. Brachina's ancient age indicates that the period of incipient melting began and ended within ~2.5 Ma after CAI

formation (Connelly et al., 2012; Glavin et al., 2004). To ensure that melting was minor, the brachinite parent body needed to have effectively mobilized melt upon formation in order to prevent further melting of Brachina's source. Additionally, the nature of these primitive achondrites would suggest a relatively small parent body in order to prevent enough ^{26}Al from accumulating and causing higher internal temperatures. The fact that NWA 4882 has a ^{53}Mn-^{53}Cr age ~15 Ma younger than Brachina would seem at odds with this explanation for the brachinite parent body. Formation of NWA 4882 by impact would alleviate these complications, but NWA 4882 shows no clear evidence of having crystallized from an impact melt. This leaves us to surmise that the ^{53}Mn-^{53}Cr systematics of NWA 4882 likely represent the timing of equilibration during a secondary heating (thermal metamorphism) event. Regardless, the ^{26}Al-^{26}Mg systematics would argue that melting and silicate fractionation in the source regions of Brachina and NWA 4882 was contemporaneous with CAI formation. Finally, it must also be stated that the data presented here does not exclude the possibility of formation of these two objects on distinct parent bodies.

4.5 Conclusions

Brachinites remain an enigmatic group of achondrites. The high precision ^{53}Mn-^{53}Cr systematics reported here indicate that Brachina and NWA 4882 experienced different thermal histories and that the brachinite parent body(ies) was active until at least ~17 Ma after CAI formation. Brachina has an ancient ^{53}Mn-^{53}Cr age of 4564.9 ± 0.5 Ma while NWA 4882 has a ^{53}Mn-^{53}Cr age of 4549.4 ± 2.3 Ma, both relative to D'Orbigny (Amelin, 2008; Brennecka & Wadhwa, 2012; Glavin et al., 2004). Additionally, the ^{26}Al-^{26}Mg

systematics of both brachinites indicate that melting and silicate fractionation on their parent body(ies) was initiated early in the history of the Solar System, contemporaneous with CAIs. The chronology of Brachina and NWA 4882 indicates that the brachinite parent body was one of the earliest forming achondrite parent bodies and provides valuable insights into the types of igneous activity on planetesimals in the early Solar System.

CHAPTER 5

PLANETESIMAL FORMATION AS A KEY TO UNDERSTANDING THE AGE OF THE SOLAR SYSTEM

5.1 Planetesimal Formation

5.1.1 Planetesimals as a Stage in Planet Formation

The processes responsible for the growth of large rocky bodies from aggregates of dust have long puzzled researchers. While the exact mechanisms driving these processes are not well constrained, there have been diligent efforts made at modelling how planets form. In describing how planetesimals, which are the parent bodies of the achondrites, formed in the early Solar System it is useful to consider them as an arrested stage in planet formation. Let us first consider the classical planet formation model before exploring recent advances.

Planet formation is thought to evolve through three main stages which make up the classic formation model. The first stage describes planetesimal formation from the accumulation of dust into fractal aggregates which clump together due to electrostatic forces and grow as dust settles to the midplane of the proto-planetary disk (Blum & Wurm, 2000; Dominik & Tielens, 1997; Kempf et al., 1999; Wurm & Blum, 1998). This allows objects to grow up to a meter in diameter. At this point, models describe the "meter-size barrier" which is a bottleneck in growth and indicates that once objects reach this size, drag forces in the gas should cause them to drift into the Sun on timescales faster than they can further accumulate material (Weidenschilling, 1977). Additionally, as planetesimals grow at different rates their relative velocities increase which should cause

collisions to be a destructive force maximized at the meter size (Cuzzi & Weidenschilling, 2006). This "meter-size barrier" problem must be overcome for rocky bodies to continue growing to sizes that would produce achondrites and terrestrial planets. While this problem has been known for some time, resolutions have been suggested recently that may explain a pathway for continued growth of rocky bodies and will be discussed below.

The second stage of classical planet formation involves planetesimals coagulating through collisions which promote growth up to the planetary embryo stage. Planetary embryos are considered to be lunar to Mars mass objects which are the precursors to terrestrial planets. During this period of growth, gravity begins to affect the bodies during close approaches and alters their orbits in such a way that promotes further collisions. This process is aided by the gravitational focusing factor (Greenzweig & Lissauer, 1992). This leads to the runaway growth stage where bodies grow as a function of their own mass (Greenberg et al., 1978; Wetherill & Stewart, 1989). Oligarchic growth follows, where the accumulation of material behaves according to $M^{-1/3}$ mass of the body. Runaway and oligarchic growth are thought to produce a population of planetary embryos in the inner Solar System. The third and final stage of planet formation involves collisions between embryos that ultimately lead to accretion and formation the terrestrial planets. This process has been successfully modelled by several authors (Agnor et al., 1999; Chambers, 2001; Chambers & Wetherill, 1998; Morbidelli et al., 2012; O'Brien et al., 2006; Raymond et al., 2004).

Planetesimal formation, and thereby achondrite formation, requires overcoming the "meter-size barrier." Three recent studies have suggested possible ways to resolve

this problem. The first of these, Johansen et al., (2007) showed that turbulence within the disk has the potential to create gravitational instabilities which would last on timescales promoting rapid growth. One such modelled result demonstrated that an object with 3.5 times Ceres mass could form within a few orbital periods (Johansen et al., 2007). The second of these studies by Cuzzi et al., (2008) argued that chondrule-sized (cm-sized) particles are concentrated and size-sorted in certain regions of the disk allowing for self-gravitating clumps to form. These self-gravitating clumps could survive long enough in the disk to form planetesimals of 10 – 100 km in size. Additionally, this model helps to explain the preponderance of chondrules in chondrites. Another means of modelling the development of planetesimals was addressed by Morbidelli et al., (2009) who used the present-day Size Frequency Distribution (SFD) of the asteroid belt to model back to what the likely SFD would have been early in Solar System history. Their results indicate that the current SFD of the asteroid belt cannot be modelled with an initial population of km-sized objects as would be the case in the classical planet formation model. Rather, the modelling of Morbidelli et al., (2009) indicates that planetesimals likely started 100s to several 100s of km in size which favors the models of Cuzzi et al., (2008) and Johansen et al., (2007). Therefore, it seems likely that planetesimals were "born big." While there are plenty of studies that argue in favor of the classical model, the chronology of achondrites would indicate that a rapid formation model is necessary.

5.1.2 Achondrite Ages in the Context of Planetesimal Formation

This work contributes to the growing number of chronologic investigations of achondrites. The use of isotope chronometers, such as those described throughout this

work, date the timing of isotopic closure in minerals of interest. These dates can be used to inform the ages of geologic processes on achondrite parent bodies. Additionally, we can use these ages to constrain the timing of parent body formation and evolution. As will be described below, we might take this a step further to inform the timing of CAI formation and through them, the timing of birth of our Solar System.

There are a growing number of achondrites whose ages have been determined using high-precision techniques. In particular, several achondrites have ages reported using multiple chronometers. Planetary materials which have U-corrected Pb-Pb dates and for which initial abundances of one or more short-lived radionuclides have been determined can serve as "age anchors" for other samples for which high-precision relative ages are desired. There are currently four achondrites (D'Orbigny, NWA 6704, NWA 11119, NWA 8661) whose chronology has been investigated using the ^{26}Al-^{26}Mg and ^{53}Mn-^{53}Cr relative chronometers and for which U isotope-corrected Pb-Pb ages have been determined (table 5.1). In light of this, these achondrite can be used to inform the evolution of rocky bodies in the early Solar System as well as the behavior of these isotopic systems in the early Solar System.

The first observation from the chronological data for these achondrites is the coincidence of their crystallization ages. Despite having formed on potentially 5 distinct parent bodies, with NWA 6704 presumably forming in a distinct region of the protoplanetary disk (the outer Solar System?) based on the Δ^{17}O and ε^{54}Cr systematics which resemble carbonaceous chondrites (Sanborn et al., 2019), they appear to have formed contemporaneously. What does this coincidence of crystallization ages tell us about the formation of planetesimals? To first order, this indicates that achondrites were

forming across a variety of parent bodies presumably in different regions of the Solar System at approximately the same time. This implies that the mechanisms of their formation were similar enough to allow this coincidence of ages. For these achondrites to record such early crystallization ages, their parent magmas must have formed and cooled through the closure temperatures of the respective isotopes in the mineral phases of interest almost contemporaenously. This may further indicate the accretion and internal heating of these achondrite parent bodies must have occurred over a similar timeline. Therefore, these achondrite ages suggest that their distinct parent bodies formed at approximately the same time, grew at approximately the same rate, and all reached similar sizes in order to achieve this coincidence of ages.

As described above, current models indicate that planetesimal formation was likely an early and efficient process in the early Solar System. The ages of achondrites corroborate the current models of planetesimal formation and indicate that in the early Solar System, planetesimals were an integral stage in the development of planets. There remain several key questions about achondrite chronology and their implications for parent body development. First, we can consider the question of the earliest possible formation. As discussed above, there is an ever-growing literature which suggests rapid accretion of objects up to the necessary sizes to produce achondrites. Thermal modelling of achondrite parent bodies, which uses ^{26}Al as the primary heat source, demonstrates that planetesimals will readily melt if they form within the first ~2 Ma of Solar System history (Ghosh & McSween, 1998; Hevey & Sanders, 2006; Neumann et al., 2014). In the work of Hevey & Sanders, (2006), all modeled parent bodies of 20 and 50 km radius which accreted at 0, 0.75 and 1.5 Ma reached temperatures sufficient to melt their CI

chondrite-like bulk starting compositions. These modelling efforts agree with the chronology of achondrites and suggest that many achondrite parent bodies grew early and rapidly enough to induce melting. This evidence is strongly demonstrated in the Hf-W ages of iron meteorite which argue for near instantaneous melting of their parent bodies such that a metallic melt was mobilized < 1 Ma after CAI formation (Kleine & Wadhwa, 2017; Kruijer et al., 2014).

The duration of planetesimal formation is difficult to constrain based solely on the chronology of achondrites. After the initial assembly, melting, and subsequent cooling, many planetesimals experienced various degrees of metamorphism and alteration. These processes are the result of reheating of portions of the crust due to further igneous processing of the interiors of the bodies or due to impacts. This can lead to partial to near-complete remelting of portions of the crust. In particular, as the number of bodies grow so does the probability of interactions with other bodies. These interactions disturb the orbits of bodies involved and lead to increased collisions. The effects of these collisions depend on a number of factors (i.e. size of the bodies, relative velocity differences, internal temperatures). These collisions will change the physical, chemical and isotopic compositions of both bodies involved to varying degrees. Craters saturate the surfaces of many planetary bodies, indicating that impacts were a ubiquitous process acting on bodies in the early Solar System. The effects that collisions and impacts have on the chronology of planetesimals can make deciphering the dates difficult.

Prolonged accretion of rocky bodies is recorded in the chondrites and primitive achondrites. Chondrites are meteorites which contain primitive materials such as CAIs, chondrules and matrix. Many chondrites have seen little to no post formation alteration or

metamorphism. This is likely the result of of their accretion after the short-lived heat source ^{26}Al was nearly to completely extinct. The primitive achondrites are a class of achondrites that experienced low degrees of partial melting. Some members have bulk chemical compositions which show only minor modification from bulk chondritic composition. Certain primitive achondrites even contain relict chondrules which argue for incomplete melting and late formation (Mittlefehldt, 2003). The chronology of chondrites and primitive achondrites can place constraints on the timeline of formation of these objects and their parent bodies.

The accretion ages of chondrites can be estimated using the ages determined for the components found in chondrites. Since chondrites are made of components formed at different times, the age of the latest forming components can place limits on the accretion times of their parent bodies. For example, many chondrules have been dated and shown to have a range of ages from ~0 to ~4 Ma after CAI formation (Amelin et al., 2010; Bollard et al., 2017; Villeneuve et al., 2009). This places a minimum age constraint on the timing of assembly of chondrite parent bodies. Additionally, parent body processes such as alteration and impact have been dated which place upper limits on parent body formation (Desch et al., 2018). These lines of evidence indicate that the accretion times of most chondrite parent bodies ranged between ~2-4 Ma after CAI formation.

The chronology of certain primitive achondrites has also been investigated. While brachinites are the only primitive achondrites for which we obtained high precision ages in this work, previous studies have reported ages for Acapulco and silicate inclusions in the winonaite-IAB-iron-silicate group. These ages indicate that primitive achondrites formed over a duration of several million years. The brachinite data presented in this

work indicate that incipient melting on the brachinite parent body began early in Solar System history. Brachina cooled through isotopic closure for the Mn-Cr system ~2 Ma after CAI formation while NWA 4882 did not experience isotopic closure until ~15 Ma later. The best Pb-Pb ages for acapulcoite phosphates indicate formation at ~10 Ma after CAIs (Amelin, 2006). Silicate IAB inclusions have been dated using I-Xe and indicate formation over long timescales starting contemporaneously with formation of CAIs (Bogard et al., 2005). The chronology of primitive achondrites indicates that while some (i.e. the acapulcoites) formed late and might give an upper limit of the timing of parent body formation, other primitive achondrites (i.e. Brachinites and silicate IAB inclusions) formed in the very early. The acapulcoites provide an example of the transition period between achondrites and chondrite lithologies in the waning years of achondrite parent body formation.

In their 2011 paper, Elkins-Tanton et al., discuss a hypothesis that the CV chondrites might have originated on a partially differentiated parent body. The evidence for this came from studies of CV chondrites which found remnant unidirectional magnetism (Carporzen et al., 2011). This effect requires a molten rotating metallic core and is consistent with a magnetic field lasting >10 Ma after CAI formation. In many ways, the work of Elkins-Tanton et al. (2001) is a logical extension from previous "onion-shell" models in which different petrologic grade chondrites of the same type could have originated on the same parent body with the highest-grade metamorphism occurring nearest the center of the body (Taylor et al., 1987; Miyamoto et al., 1981). Elkins-Tanton et al., argue that the outer boundary layer would act as insulation allowing for the trapped internal heat to extensively melt portions of the deep interior while

allowing the outermost portions of the body to remain undifferentiated. Such a scenario could account for some types of primitive achondrites and highly metamorphosed chondrites as well as for certain isotopic similarities across chondrite and achondrite types.

The early forming primitive achondrites also inform planetesimal formation scenarios in that they require arrested growth or delayed accretion in comparison to differentiated achondrites. The chronology of some primitive achondrites indicate early formation, well within the ability of ^{26}Al to melt the interiors (assuming a homogeneous distribution of ^{26}Al and chondritic abundance of Al). This might favor scenarios such as those described by (Cuzzi et al., 2008; Johansen et al., 2007) where material is concentrated in certain parts of the disk such that some regions of the disk may have contained ample material to form planetesimals with enough mass to induce high degrees of melting while in other regions planetesimal formation may have stalled before reaching such a mass.

5.2 The Age of the Solar System

One of the key applications of chronology in planetary science is the determination of the age of our Solar System. This work was pioneered by Patterson (1956) who determined the age of Earth and meteorites to be 4.55 Ga. The age of our Solar System is best defined by the age of the first formed solids to condense from the solar nebula, i.e. calcium-aluminum-rich Inclusions (CAIs). The condensation calculations performed by Grossman, (1972) were the first to convincingly demonstrate that the mineral compositions of CAIs are the result of direct condensation from a gas of

solar composition. With the advent of modern mass spectrometry techniques (Schramm et al., 1970), Lee et al., (1976) were able to demonstrate that these refractory components in the Allende chondrite contained excess of ^{26}Mg which results from their formation during the lifetime of ^{26}Al ($t_{1/2}$ = 0.705 Ma). Allegre et al., (1995) revisited the age of Earth and meteorites using the Pb-Pb method and modern mass spectrometry techniques and found that refractory inclusions in the Allende meteorite had ages of ~4.566 Ga. This was taken as the best estimate for the age of our Solar System. However, the relatively high uncertainties of these early Pb-Pb ages prohibited distinguishing CAI formation from other early events.

Recently, additional improvements in analytical capabilities have allowed refinement of the age of CAIs (Amelin et al., 2009; Amelin, 2006; Connelly et al., 2012). The current best estimate of the timing of CAI formation is the Pb-Pb age of 4567.3 ± 0.3 Ma of a CAI from the carbonaceous chondrite Efremovka (Connelly et al., 2012). However, there still remains uncertainty in whether this is the oldest age of CAI formation and hence, the true age of our Solar System. It is understood that conditions necessary to form CAIs only occurred during a short time interval in the solar nebula, i.e., several 10^5 yrs which is further complicated by the expectation based on dynamical considerations that cm-sized objects spiral into the Sun on timescales of ~10^4 yrs. This is the basis for the "CAI storage" problem which has been addressed in a number of studies (Chambers, 2006; Ciesla, 2007; Desch et al., 2018; Russell et al., 2006; Wood, 1996).

5.2.1 Challenges with Determining the Ages of CAIs

The most powerful chronometer for determining the absolute ages of early Solar System materials is the Pb-Pb system. The power and utility of this system has been described previously in this work. However, there are two pitfalls which make determining the absolute Pb-Pb ages of CAIs difficult. First, as has also been discussed previously this work, it is necessary to measure the $^{238}U/^{235}U$ ratio of any sample for which the Pb-Pb age is to be determined. This is especially important for CAIs that have been shown to record variability in the $^{238}U/^{235}U$ ratio that is sufficient to cause inaccuracies in ages of several millions of years (Brennecka et al., 2010). This is further complicated by low abundances of U and Pb in CAIs as well as their typically small sample sizes. Due to this, at present there exists in the literature only one CAI for which the U isotope measurements have been performed and is thus a correct absolute age. The CAI 22E from the carbonaceous chondrite Efremovka has been dated using U-corrected Pb-Pb method and found to have an age of 4567.3 ± 0.3 Ma (Connelly et al., 2012). Beyond the Pb-Pb system, the short-lived ^{26}Al-^{26}Mg system has been applied extensively to CAIs (Jacobsen et al., 2008; Kita et al., 2013; Larsen et al., 2011; Macpherson et al., 1995).

The utility of the ^{26}Al-^{26}Mg system for CAIs is two-fold. First, CAIs should record the initial $^{26}Al/^{27}Al$ ratio of our Solar System. The distribution of ^{26}Al has implications for the origin and evolution of the Solar System and been the topic of significant debate in the planetary science community, which will be discussed below. Secondly, at the current time there exists only one reported U-corrected Pb-Pb age for a CAI for which an initial (canonical) $^{26}Al/^{27}Al$ ratio is assumed; other CAIs with canonical

initial $^{26}Al/^{27}Al$ ratios are thought to form coevally. In several previous studies, CAIs have been used as age anchors for determining ^{26}Al-^{26}Mg ages (Bouvier et al., 2011b; Hublet et al., 2017; Sanborn et al., 2018; Schiller et al., 2011, 2015; Spivak-Birndorf et al., 2009; Wimpenny et al., 2019).There is evidence that CAIs were initially forming over a short interval of the order of $\sim 10^5$ yr in the early Solar System (Kita et al., 2013; Mishra & Chaussidon, 2014; Thrane et al., 2006). Some CAIs, however, have significantly lower $^{26}Al/^{27}Al$ ratios (such as the FUN CAIs); it not yet known whether these were formed in a distinct nebular environment with much lower ^{26}Al abundance or if they were formed either immediately prior to the injection of ^{26}Al into the early Solar System and formation of most so-called "normal CAIs" (with near-canonical $^{26}Al/^{27}Al$ ratios). Since there is uncertainty about when and where ^{26}Al-poor CAIs formed, we will consider here only the normal CAIs.

There have previously been discrepancies in the ^{26}Al-^{26}Mg relative ages of achondrites reported using different age anchors. To be used as an age anchor the object must meet several criteria: first, it must have a U-corrected absolute Pb-Pb age; second, the abundances of short-lived radionuclide(s) of interest must be determined with sufficient precision in this object; lastly, the U-Pb system as well as the other isotope systems of interest must have achieved isotopic closure at the same time in this object, subsequent to which it did not experience any post-formation alteration or metamorphism. Until recently, only two age anchors have been extensively used to map relative ages based on various short-lived chronometers onto an absolute timescale: the CAI 22E from the carbonaceous chondrite Efremovka (Connelly et al., 2012; Jacobsen et al., 2008; Larsen et al., 2011) and the angrite D'Orbigny (Amelin, 2008; Bouvier et al.,

2011; Brennecka & Wadhwa, 2012; Glavin et al., 2004; Spivak-Birndorf et al., 2009). D'Orbigny has the added benefit that the initial abundances of a variety of different short-lived radionuclides have been determined in this quickly-cooled achondrite (Kleine and Wadhwa, 2017). To use CAIs as age anchors requires taking the initial or "canonical" $^{26}Al/^{27}Al$ as defined by multiple CAIs from multiple previous studies and using the U-corrected Pb-Pb age of the single CAI 22E from Efremovka. Using this method assumes that CAIs all formed at the exactly same time as defined by the CAI 22E.

So then why the discrepancy in ^{26}Al-^{26}Mg ages between the anchors? This could be the result of post-formation alteration of D'Orbigny and as such, could preclude its utility as an age anchor (Sanborn et al., 2015). It is also possible that the current best estimate of the formation age of CAIs based on CAI 22E is in fact not "time-zero" (i.e., the time of formation of the Solar System as defined by the formation of the first refractory solids). In light of some recent studies (including this work), several achondrites now have the most robustly constrained formation ages (i.e., from more than one high-resolution chronometer) than any other objects in the early Solar System. Therefore, we have attempted to utilize these ages to provide an estimate of the true age of CAIs and, thus, an estimate of "time-zero" for the Solar System.

5.2.2 Estimating the Age of the Solar System and Implications for the Distribution of ^{26}Al

At present, there are five achondrites for which both ^{26}Al-^{26}Mg systematics and U-corrected Pb-Pb systematics have been reported. These include the angrite D'Orbigny (Amelin, 2008; Brennecka & Wadhwa, 2012; Spivak-Birndorf et al., 2009); the ungrouped achondrites NWA 6704 (Amelin et al., 2018; Sanborn et al., 2018), NWA

2976 (Bouvier et al., 2011; Brennecka & Wadhwa, 2012), and NWA 11119 (this work); and the eucrite NWA 8661 (this work). One key insight from these chronologic studies is the apparent clustering of achondrite ages at ~4-5 Ma after CAIs. In detail, the ^{26}Al-^{26}Mg relative ages yield a weighted mean age of 4.7 Ma after CAI formation (table 5.2). There is a range in ^{26}Al-^{26}Mg relative ages of these achondrites from the youngest at 5.29 ± 0.13 Ma (NWA 6704) to the oldest at 3.55 ± 0.05 Ma (NWA 11119). These ages are calculated using the difference in the ^{26}Al/^{27}Al ratio of each sample relative to the canonical ^{26}Al/^{27}Al = 5.23 x 10^{-5} from Jacobsen et al., (2008). Another means of determining the age of these achondrites relative to CAIs is to use the U-corrected Pb-Pb ages relative to the U-corrected Pb-Pb age of CAI 22E, which is currently thought to date "time-zero". However, in doing so a discrepancy in the relative ages emerges. The ^{26}Al-^{26}Mg relative ages appear to be consistently younger than those determined using the U-corrected Pb-Pb ages (table 5.2). In fact, the oldest achondrite NWA 11119 (i.e. closest in age to CAIs) has a discrepancy between these relative dates of 1.1 Ma while the youngest achondrite NWA 6704 has a discrepancy of 0.6 Ma. The nature of this age discrepancy has significant implications for the chronology of the early Solar System.

One means of producing these discrepant ages is through heterogeneity in the distribution of ^{26}Al in the early Solar System. While there is significant evidence in support of a homogeneous distribution of ^{26}Al, this has recently been an intense topic of debate in the planetary science community (Kleine & Wadhwa, 2017; and references therein). For the ^{26}Al-^{26}Mg system to be used as a relative chronometer, the distribution of ^{26}Al must have been homogeneous in the reservoir from which the objects being dated originated. Several studies have suggested that this is indeed the case for the CAI-

forming reservoir (Jacobsen et al., 2008; Kita et al., 2013; Macpherson et al., 1995; Wasserburg et al., 2012). This is also inferred for achondrite forming regions based on concordance between the different high resolution chronometers (Amelin et al., 2019; Sanborn et al., 2019). When the ^{26}Al-^{26}Mg relative age between two objects is determined, this assumes the difference in their ^{26}Al/^{27}Al ratios is the result of passage of time. When multiple short-lived chronometers, anchored to different objects yield the same age for an object, this indicates that the assumption is justified. In this dissertation, two achondrites (NWA 11119 and NWA 8661) are reported as having ages that are concordant between three different high-resolution isotope chronometers. Nevertheless, there does exist some evidence to the contrary which is worth discussing. In particular, Larsen et al. (2011) argued for heterogeneity in ^{26}Al based on the variability in the radiogenic ^{26}Mg* among bulk samples of a variety of meteorites. These authors also use an "isochron" that includes data for CAIs and Ameboid-Olivine-Aggregates to argue that the initial $\mu^{26}Mg^*_0$ value (-16 ppm) is higher than would be expected if the initial ^{26}Al/^{27}Al was the canonical 5.23 x 10^{-5} (i.e., $\mu^{26}Mg^*_0$ = -38 ppm). This "isochron" indicates that for chondritic materials (with ^{27}Al/^{24}Mg = 0.101) one would expect to have a $\mu^{26}Mg^*$ = 22 ppm, which is resolvably higher than their reported measurement of bulk CI chondrites ($\mu^{26}Mg^*$ = 4.5 ppm). Together these factors were used to argue against a homogenous distribution of ^{26}Al in the early Solar System which negates the utility of the ^{26}Al-^{26}Mg system as a chronometer. A similar argument was made by Schiller et al., (2015) who used the ^{26}Al-^{26}Mg systematics of angrites to argue that the inner Solar System formed with a reduced inventory of ^{26}Al. By back calculating the initial

($^{26}Al/^{27}Al)_0$, Schiller et al., (2015) determined that the angrites, and by extension the inner Solar System, had a reduced initial ($^{26}Al/^{27}Al)_0$ of ~ 1.3 x 10^{-5}.

Another possible cause of this discrepancy lies with the determination of the Pb-Pb ages and is detailed by Amelin et al., (2009). There are several sources of potential problems that can impact the Pb-Pb age determination, but at least one of these have been rectified (i.e., measurement of the U isotope composition). Other problems involve the potential of fractionating Pb isotopes during the extensive leaching of mineral separates, analytical problems involving mischaracterization of fractionation effects and blank subtraction, deviation from closed system behavior and the potential presence of non-radiogenic Pb of unknown isotopic composition (Amelin et al., 2009). Most of these issues can be eliminated or corrected for if careful sample preparation and data handling are employed.

Finally, it is possible that the U-corrected Pb-Pb age for CAI 22E may not represent "time-zero." There does exist some data that corroborates this interpretation. Bouvier & Wadhwa (2010) reported a ^{26}Al-^{26}Mg model age and a Pb-Pb age for the CAI B1 from the carbonaceous chondrite NWA 2364. The authors did not measure the U isotope composition of this CAI and reported a Pb-Pb age of $4568.2^{+0.2}_{-0.4}$ Ma (assuming a $^{238}U/^{235}U$ = 137.84, based on its measured U/Th ratio and the apparent correlation between $^{238}U/^{235}U$ and U/Th noted by Brennecka et al., 2010), which predates the Efremovka CAI 22E (Connelly et al., 2012) by 0.92 ± 0.41 Ma. These authors additionally reported a $^{26}Al/^{27}Al$ = (5.03 ± 0.26) x 10^{-5} for this CAI, which agrees completely with the canonical $^{26}Al/^{27}Al$ ratio and gives a ^{26}Al-^{26}Mg model age of 4568.14 ± 0.38 Ma relative to the D'Orbigny angrite. While the U isotope composition of the

NWA 2364 CAI B1 was not measured, the work suggests that CAIs could have formed up to ~1 Ma earlier than previously thought. Subsequently, preliminary results have been presented for the ^{26}Al-^{26}Mg systematics and a U-corrected Pb-Pb age for the CAI B4 from the NWA 6691 chondrite; this CAI has a $^{26}Al/^{27}Al = (4.90 \pm 0.05) \times 10^{-5}$ with a U-corrected Pb-Pb age of 4567.9 ± 0.3 Ma (Bouvier et al., 2011; Wadhwa et al., 2014).

The high precision ages of achondrites reported here and in other recent studies provide a means to test the idea that U-corrected Pb-Pb age of the Efremovka CAI 22E may not represent "time zero" for the Solar System (when $^{26}Al/^{27}Al = 5.23 \times 10^{-5}$; Jacobsen et al., 2008). As discussed earlier, these two sets of relative ages are shown in table 5.2 which can be used to test this idea. Specifically, ^{26}Al-^{26}Mg relative ages and their uncertainties were calculated using the $^{26}Al/^{27}Al$ ratios reported for each of these achondrites and comparing them to the canonical $^{26}Al/^{27}Al = 5.23 \times 10^{-5}$ (Jacobsen et al., 2008). Also, the U-corrected Pb-Pb ages of the achondrites compared to the U-corrected age of the Efremovka CAI 22E (Connelly et al., 2012) to obtain another set of relative ages. Comparing the relative ages calculated using these two methods produce discrepant ages. The cause of this discrepancy has been evaluated using the following approach.

The first possible cause of the discrepant ages could result from non-homogeneous distribution of ^{26}Al in the early Solar System, as some authors have argued (Kirsten K. Larsen et al., 2011; Schiller et al., 2015). To evaluate the effect on the relative ages due to non-homogeneous ^{26}Al, the relative ages were calculated by varying the $^{26}Al/^{27}Al$ ratio used as the anchor. The $^{26}Al/^{27}Al$ ratio was varied around the canonical value of $^{26}Al/^{27}Al = (5.23 \pm 0.13) \times 10^{-5}$ by several times the 2SD. This did not improve the discrepancy in the relative ages calculated this way compared to the relative ages

using the reported Pb-Pb ages. This indicates that the discrepancies are not caused by non-homogeneous distribution of ^{26}Al, but must instead might be caused by uncertainty in the true age of the CAIs. To evaluate whether the age discrepancies were caused by the true age of CAIs being misrepresented, the same routine was applied as before. Varying the anchor "age" of CAIs resulted in changes to the age discrepancies which could be further evaluated to understand the true age of CAIs.

As the CAI "age" was varied, new relative ages were calculated for each of the achondrites. The discrepancies between the relative ages using the $^{26}Al/^{27}Al$ ratios and the Pb-Pb ages were used to calculate χ^2 values for each achondrite. Which were then used to calculate a reduced $(\chi)^2$ also known as a Mean Square Weighted Deviation (MSWD). Another way to evaluate the effects of changing the CAI "age" is calculated by using the age discrepancy divided by the square of the uncertainty on discrepancy (i.e. max deviation/sigma). This was repeated for each CAI "age" and the results are shown in figure 5.1. An *a priori* MSWD can be calculated along with the associated tolerance or acceptable uncertainty in the MSWD (σ_{MSWD}). Because we are considering five distinct achondrites, the degrees of freedom for the system is five. This means the maximum σ_{MSWD} = 1.63 (at 95% confidence) indicating the MSWD should be < 2.63 (since an ideal MSWD = 1). Using this MSWD as a target allows the true age of CAIs (CAI_{calc}) to be evaluated based on which "age" used in the calculations provides the best fit to the *a priori* MSWD and lowest max deviation/sigma (figure 5.1). Ages within the tolerance calculated for the *a priori* MSWD range from 4568.0 Ma to 4568.8 Ma. The CAI age which produces the best fit MSWD and lowest max deviation/sigma values is 4568.3 ± 0.3 Ma as shown in figure 5.1. Using this new calculated CAI age (CAI_{calc}) as the age

anchor and performing the same discrepancy calculations gives a MSWD = 1.72 and a max deviation/2SD = 2.07 (table 5.2). This age is older than the Efremovka CAI 22E (Connelly et al., 2012) by 1.0 ± 0.4 Ma and is in complete agreement with the NWA 2364 CAI B1 from Bouvier & Wadhwa, (2010).

Table 5.1 Achondrite $^{26}Al/^{27}Al$, $^{53}Mn/^{55}Mn$ and Pb-Pb Ages

Sample	$^{26}Al/^{27}Al$	2sd	$^{53}Mn/^{55}Mn$	2sd	Pb-Pb age (Ma)	2sd
D'Orbigny	4.0E-7	2.1E-8	3.2E-6	3.9E-8	4563.4	0.3
NWA 2976	3.9E-7	1.6E-8	n/a	n/a	4562.9	0.6
NWA 11119	1.7E-6	9.0E-8	3.5E-6	1.1E-6	4565.4	0.8
NWA 6704	3.2E-6	3.8E-8	2.6E-6	3.4E-7	4562.6	0.3
NWA 8661	4.3E-7	6.0E-8	3.4E-6	5.0E-7	4563.8	0.3

The $^{26}Al/^{27}Al$ and $^{53}Mn/^{55}Mn$ ratios, as well as U-corrected Pb-Pb ages for five achondrites. Data for NWA 11119 and NWA 8661 are from this work (chapters 2 and 3); those for the other achondrites are from (Amelin, 2008; Amelin et al., 2019; Bouvier et al., 2011; Brennecka & Wadhwa, 2012; Connelly et al., 2012; Glavin et al., 2004; Jacobsen et al., 2008; Kleine & Wadhwa, 2017; Sanborn et al., 2019; Srinivasan et al., 2018).

Table 5.2 Calculations for the estimation of the age of the Solar System.

Sample	Δt (Ma) CAI †	2SD	Δt (Ma) CAI‡	2SD	Δt (Ma) CAI_{calc}	2SD
D'Orbigny	5.04	0.05	3.93	0.39	4.93	0.39
NWA 2976	5.05	0.04	4.41	0.66	5.41	0.66
NWA 11119	3.55	0.06	1.88	0.83	2.88	0.83
NWA 6704	5.29	0.13	4.70	0.42	5.70	0.42
NWA 8661	4.96	0.15	3.50	0.42	4.50	0.42
	$\Delta t\ (Ma)\ CAI^{\dagger}_{WM}$	**4.69**	**$\Delta t\ (Ma)\ CAI^{\ddagger}_{WM}$**	**3.93**	**$\Delta t\ (Ma)\ CAI_{calc\text{-}WM}$**	**4.93**
	$2sd_{WM}$	**0.001**	**$2sd_{WM}$**	**0.09**	**$2sd_{WM}$**	**0.09**

The relative ages for different achondrites are calculated using two different high resolution chronometers (i.e., the ^{26}Al-^{26}Mg and the Pb-Pb). Comparison of the reported $^{26}Al/^{27}Al$ ratios of these achondrites to the canonical $^{26}Al/^{27}Al = (5.23 \pm 0.13) \times 10^{-5}$ (Jacobsen et al., 2008)† gives a weighted mean relative of $\Delta t\ CAI^{\dagger}_{WM} = 4.69 \pm 0.001$ Ma. Comparison of the reported Pb-Pb ages of these achondrites relative to the Pb-Pb age of CAI 22E (Connelly et al., 2012)‡ gives a $\Delta t\ CAI^{\ddagger}_{WM} = 3.93 \pm 0.09$ Ma. When the new CAI_{calc} (= 4568.3 ± 0.3 Ma) is used the weighted mean age relative is $\Delta t\ CAI_{calc\text{-}WM} = 4.93 \pm 0.09$ Ma. References are the same as table 5.1.

Table 5.3 Calculations estimating the Solar System initial $(^{53}Mn/^{55}Mn)_0$.

Sample	Δt (Ma) CAI †	2SD	$(^{53}Mn/^{55}Mn)$	2SD	$(^{53}Mn/^{55}Mn)_0$	2SD
D'Orbigny	5.04	0.05	3.22E-06	3.90E-08	8.37E-6	6.30E-7
NWA 11119	3.55	0.06	3.50E-06	1.12E-06	6.85E-6	2.23E-6
NWA 6704	5.29	0.13	2.59E-06	3.40E-07	7.06E-6	1.12E-6
NWA 8661	4.96	0.15	3.40E-06	5.00E-07	8.71E-6	1.48E-6
LEW 86010	10.8	0.42	1.25E-06	7.00E-08	9.79E-6	1.78E-6
					$CAI_{calc\text{-}WM}$	**$2SD_{WM}$**
					8.2E-6	**4.8E-7**

The Δt (Ma) CAI† is calculated using the individual achondrite $^{26}Al/^{27}Al$ relative to the canonical $^{26}Al/^{27}Al = (5.23 \pm 0.13) \times 10^{-5}$ (references for literature data can be found in table 5.1). The $(^{53}Mn/^{55}Mn)$ and 2SD of these achondrites come from ^{53}Mn-^{53}Cr internal isochron regression and can be found in these references (Glavin et al., 2004; Lugmair & Shukolyukov, 1998a; Sanborn et al., 2019) The initial $(^{53}Mn/^{55}Mn)_0$ ratios are calculated using the Δt (Ma) CAI† and literature ^{53}Mn $t_{1/2}$ = 3.7 Ma (Honda & Imamura, 1971b).

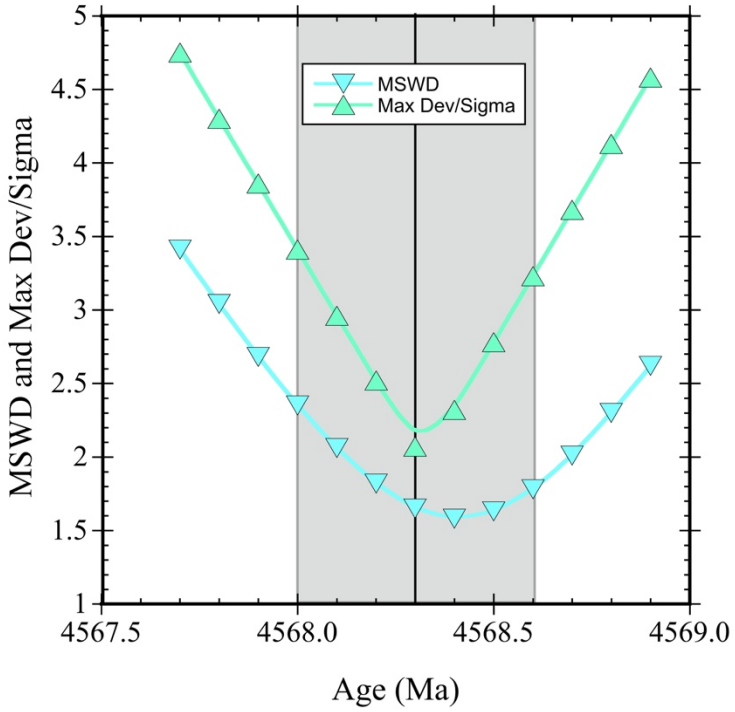


Figure 5.1. Shown here are the variations in MSWD and maximum deviation over the uncertainty as a function of variability in the absolute age. The black line represents the age (with uncertainty in grey) which best fits the data. This plot demonstrates that the best fit age of the Solar System, based on the U-corrected Pb-Pb ages of achondrites, is 4568.3 ± 0.3 Ma.

Another way to evaluate the age of our Solar System is to plot the absolute Pb-Pb age of objects vs their $^{26}Al/^{27}Al$ ratio in natural log form. This type of plot was first published in a review of the short-lived ^{26}Al-^{26}Mg and ^{53}Mn-^{55}Mn systematics in meteoritic materials (Nyquist et al., 2009). On a plot of the absolute age vs the $\ln(^{26}Al/^{27}Al)$, the slope represents the decay constant of ^{26}Al. A similar figure was used by Sanborn et al., (2019) who included the best available achondrite data at the time to evaluate the age of CAIs. Sanborn et al., (2019) suggested that based on the available data, that the true age of CAIs may be closer to the older ages reported for CAIs B1 and B4 from NWA 2364 and NWA 6691, respectively (Bouvier & Wadhwa, 2010; Bouvier et al., 2011; Wadhwa et al., 2014). We have now reported ^{26}Al-^{26}Mg systematics and U-corrected Pb-Pb ages for two new achondrites (NWA 11119 and NWA 8661) in this work. These new achondrites are shown along with all currently available achondrite and CAI data for which U-corrected Pb-Pb ages have been determined are shown in figure 5.2 along with our best estimate for the CAI age calculated here (CAI_{calc}). On this type of plot, the slope represents the decay constant of ^{26}Al ($\lambda^{26}Al$) and should be 0.983 ± 0.33 based on the accepted half-life of 0.705 Ma (Norris et al., 1983). Three different regressions are shown in figure 5.2. The regression shown in red (with slope ($\lambda^{26}Al$) = 1.12 ± 0.09; 95% CI) is made using a CAI weighted mean age (CAI_{WM} age = 4567.9 ± 0.1 Ma) and weighted mean $^{26}Al/^{27}Al = (5.26 \pm 0.13) \times 10^{-5}$ calculated from all available CAI data and achondrite data. The regression shown in blue (slope ($\lambda^{26}Al$) = 0.99 ± 0.16; 95% CI) is made using the new CAI age calculated here of 4568.3 ± 0.3 Ma and all achondrite data. The regression shown in black (slope ($\lambda^{26}Al$) = 0.72 ± 0.34; 95% CI) is

made using only the available achondrite data. The regressions were made using IsoplotR (Vermeesch, 2018).

Figure 5.2 suggests that the true age of CAIs and therefore the best estimate of the age of our Solar System is older than the current estimates based on the ages of Efremovka CAI 22E (Connelly et al., 2012) and Allende CAI SJ 101 (Amelin et al., 2010). This indicates that the ages of the CAIs B1 and B4 from NWA 2364 and NWA 6691, respectively likely represent the age of our Solar System (Bouvier & Wadhwa, 2010; Bouvier et al., 2011; Wadhwa et al., 2014). This conclusion is further illustrated in figure 5.3. As can be seen in this figure, the $^{26}Al/^{27}Al$ relative ages for a number achondrites (obtained by comparing to the canonical $^{26}Al/^{27}Al$ for CAIs) agree within uncertainty of the relative ages obtained using their U-corrected Pb-Pb methods compared to the best estimate presented here for the CAI age of 4568.3 ± 0.3 Ma. This is a further line of evidence that the age of the Solar System is likely older than currently thought and is 4568.3 ± 0.3 Ma. Additionally, this strengthens the argument for homogenous distribution of ^{26}Al in the early Solar System which will be discussed further below.

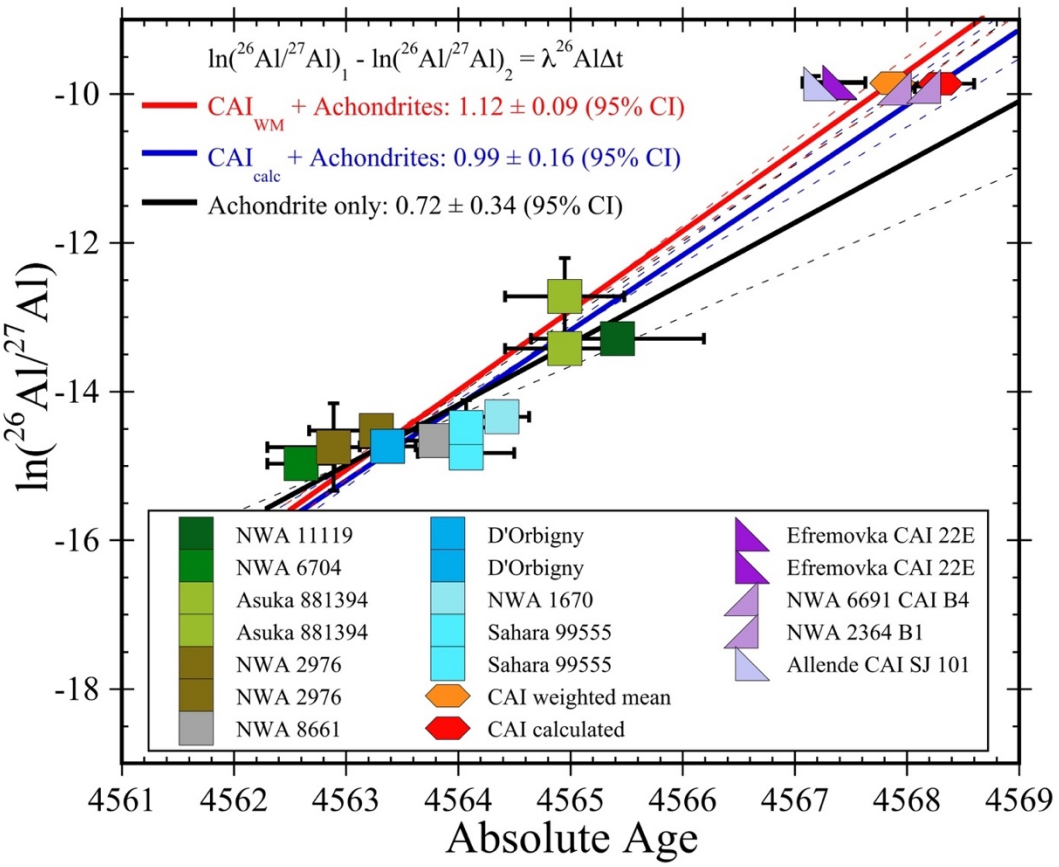


Figure 5.2. The ln(^{26}Al/^{27}Al) values versus the absolute U-corrected Pb-Pb ages for all available achondrites (green-brown are ungrouped; grey is a eucrite; blues are angrites) and CAIs (calculated values as polygons and literature values in purple triangles). The orange polygon (CAI_{WM}) represents the weighted mean of the Pb-Pb ages and weighted mean of ^{26}Al/^{27}Al ratios determined from literature data for CAIs. The red polygon (CAI_{calc}) represents the calculated best estimate CAI age from this study and the weighted mean of ^{26}Al/^{27}Al ratios determined from literature data for CAIs. Achondrites and CAIs listed twice represent different values for the ^{26}Al/^{27}Al ratios or Pb-Pb ages reported in the literature. The ^{26}Al/^{27}Al U isotope compositions, and Pb-Pb ages are from the following literature sources: Amelin, 2008; Amelin et al., 2019; Bouvier et al., 2011; Bouvier et al., 2011; Bouvier & Wadhwa, 2010; Brennecka & Wadhwa, 2012; Connelly et al., 2012; Hublet et al., 2017; Kita et al., 2013; Kleine & Wadhwa, 2017; Larsen et al., 2011; MacPherson et al., 2017; Sanborn et al., 2019; Schiller et al., 2010, 2015; Spivak-Birndorf et al., 2009; Tissot et al., 2017; Wadhwa et al., 2014; Wimpenny et al., 2019.

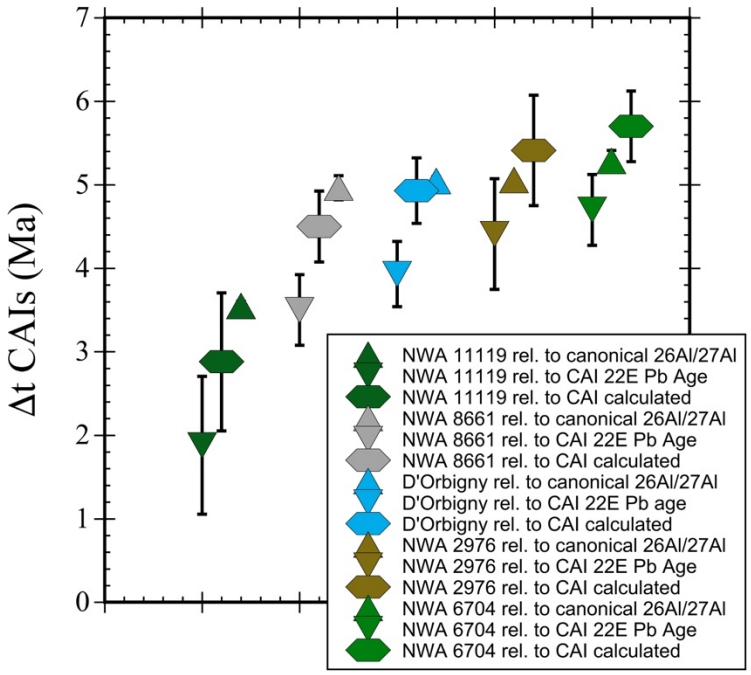


Figure 5.3. The relative ages (Δt in Ma) of a selection of achondrites with U-corrected Pb-Pb ages that are calculated by comparing their 1) $^{26}Al/^{27}Al$ ratio with the canonical value ($^{26}Al/^{27}Al = 5.23 \times 10^{-5}$; Jacobsen et al., 2008) (triangles), 2) absolute U-corrected Pb-Pb age with that of Efremovka CAI 22E (Connelly et al., 2012) (inverted triangles), and 3) absolute U-corrected Pb-Pb age with the new calculated CAI age presented here of 4568.3 ± 0.3 Ma (polygons). This figure demonstrates that the relative ages using the new calculated CAI age are in much better agreement with the relative ^{26}Al-^{26}Mg ages. Data for achondrite U-corrected Pb-Pb ages are from: Amelin, 2008; Amelin et al., 2019; Bouvier et al., 2011; Brennecka & Wadhwa, 2012; Sanborn et al., 2019.

5.3 Initial Abundance of ^{53}Mn in the Early Solar System

Manganese-53 is a short-lived isotope with a half-life of 3.7 Ma (Honda & Imamura, 1971b) that decays to ^{53}Cr. This decay system has utility for dating a number of early Solar System processes and has been used with great success. The first demonstration of variations in ^{53}Cr from the decay of ^{53}Mn was provided in CAIs from Allende by (J. -L Birck & Allègre, 1985). The first exploration of the utility of the ^{53}Mn-^{53}Cr system as a chronometer was presented for a number of different achondrites (Lugmair & Shukolyukov, 1998a). These authors estimated the initial ^{53}Mn/^{55}Mn at the time of CAI formation to be ~9.2 x 10^{-6}. Additionally, they used the ^{53}Cr/^{52}Cr ratio of the HED parent body and calculated the time interval required to evolve to this composition from a source with a chondritic ^{53}Cr/^{52}Cr ratio. This calculation allowed Lugmair & Shukolyukov (1998) to estimate the minimum age of the Solar System to be ~4568.0 Ma. These findings were later refined by Shukolyukov & Lugmair (2006) who estimated a Solar System initial $(^{53}Mn/^{55}Mn)_0 = (8.5 \pm 1.5) \times 10^{-6}$. As will discussed below, these findings agree well with our best estimate of the initial $(^{53}Mn/^{55}Mn)_0$. In a re-evaluation of the applicability of the ^{53}Mn-^{53}Cr chronometer, Trinquier et al., (2008) investigated a number of chondrite and achondrite types and concluded that ^{53}Mn was likely homogeneously distributed in the inner Solar System and therefore can be effectively used as a chronometer. Trinquier et al., (2008) were also able to provide a new estimate of the Solar System initial $(^{53}Mn/^{55}Mn)_0 = (6.28 \pm 0.66) \times 10^{-6}$.

In this study, the initial $(^{53}Mn/^{55}Mn)_0$ is again revisited using all currently available achondrite data. Based on the ^{26}Al-^{26}Mg relative ages of the five achondrites discussed above along with their measured U-corrected Pb-Pb ages, and the published

half-life of ^{53}Mn, we can estimate a Solar System initial $(^{53}Mn/^{55}Mn)_0$ (table 5.3). Taking a weighted mean gives the current best estimate of the Solar System initial $(^{53}Mn/^{55}Mn)_0 = (8.2 \pm 0.5) \times 10^{-6}$. This new estimate is in complete agreement with the previous estimates of Lugmair & Shukolyukov (1998) and Shukolyukov & Lugmair (2006). This conclusion is further strengthened by plotting the $\ln(^{53}Mn/^{55}Mn)$ versus the absolute ages for all available achondrite data from previous studies and this work, along with the best estimates of the initial $(^{53}Mn/^{55}Mn)_0$ and CAI_{calc} age provided here (Fig. 5.4).

As with figure 5.3, if the Pb-Pb ages are concordant with the ^{53}Mn-^{53}Cr system, the slope defined by the data should correspond to the decay constant of ^{53}Mn. This figure demonstrates that all achondrites likely formed on parent bodies that originated in reservoirs with homogenous $^{53}Mn/^{55}Mn$. Figure 5.3 additionally provides support for the best estimates presented here for the age of the Solar System ($CAI_{calc} = 4568.3 \pm 0.3$ Ma) and the Solar System initial $(^{53}Mn/^{55}Mn)_0 = (8.2 \pm 0.5) \times 10^{-6}$ given that the regression using these values and the data for achondrites yields a slope which is indistinguishable from the $\lambda^{53}Mn$ value (Honda and Imanura, 1971).

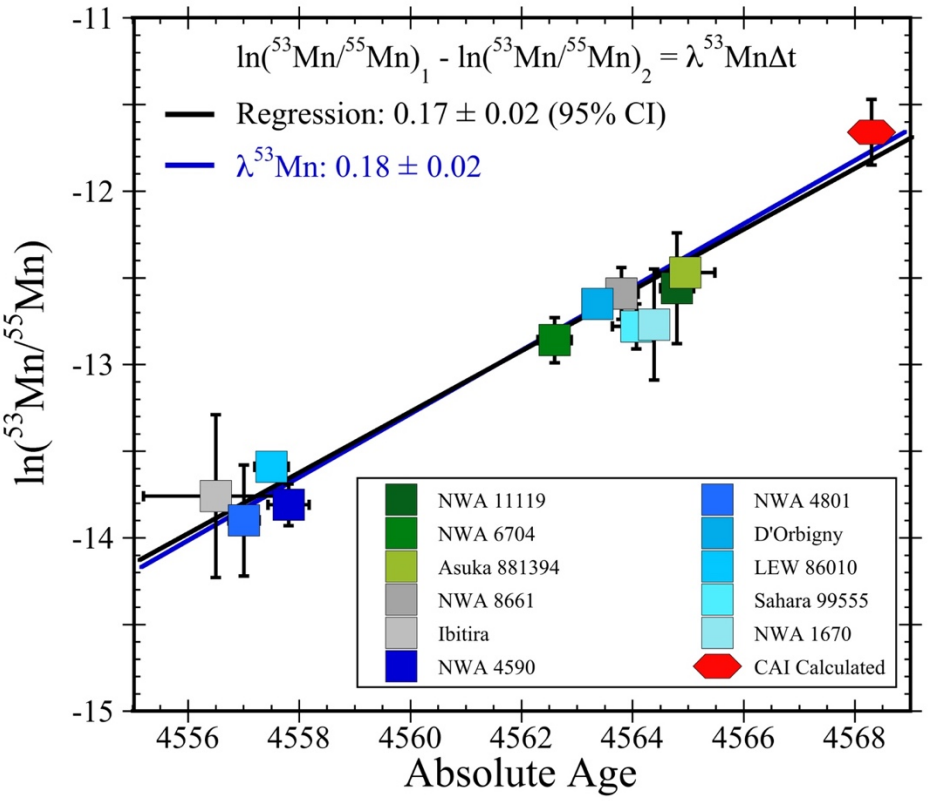


Figure 5.4. The ln(^{53}Mn/^{55}Mn) values versus the absolute U-corrected Pb-Pb ages for achondrites. As in Figure 5.3, colors represent different achondrites (greens are ungrouped; greys are eucrites/eucrite-like; blues are angrites). The red polygon represents the estimates presented here for the CAI_{calc} age and the intial Solar System ln(^{53}Mn/^{55}Mn)$_0$. The black regression is made through only the achondrite data and has a slope indistinguishable from the literature value for λ^{53}Mn (shown in blue). The literature data for ^{53}Mn/^{55}Mn systematics, U isotope compositions, and Pb-Pb ages are from: (Amelin et al., 2019; Amelin, 2008; Brennecka & Wadhwa, 2012; Iizuka et al., 2015; Kleine & Wadhwa, 2017; Lugmair & Shukolyukov, 1998; Sanborn et al., 2019; Schiller et al., 2015; Tissot & Dauphas, 2015; Wadhwa et al., 2009; Wimpenny et al., 2019.

5.4 Conclusions

In this chapter the importance of achondrites is discussed for evaluating the initial distribution of the short-lived radionuclides (^{26}Al and ^{53}Mn) as well as for calculating the age of the Solar System. By evaluating the ^{26}Al-^{26}Mg systematics of these achondrites it can be shown that the Solar System formed with a homogeneous distribution of ^{26}Al ($^{26}Al/^{27}Al = 5.23 \times 10^{-5}$) and the best estimate of the age of our Solar System is 4568.3 ± 0.3 Ma (CAI_{calc}) as shown in figures 5.1 and 5.2. This age is in agreement with two previously reported CAI ages (Bouvier & Wadhwa, 2010; Bouvier et al., 2011; Wadhwa et al., 2014) and suggests that the age of the Solar System is ~1 Ma older than currently thought. As was discussed above, this new age estimate eliminates the age discrepancies seen when comparing ^{26}Al-^{26}Mg relative ages anchored to different objects and argues for a homogeneous distribution of ^{26}Al at the canonical level at the beginning of the Solar System. Additionally, by using the published ages of these achondrites and the known half-life of ^{53}Mn, a new estimate of the Solar System initial $(^{53}Mn/^{55}Mn)_0 = (8.2 \pm 0.5) \times 10^{-6}$ is reported.

REFERENCES

Agnor, C. B., Canup, R. M., & Levison, H. F. (1999). On the Character and Consequences of Large Impacts in the Late Stage of Terrestrial Planet Formation. *ICARUS*, *142*(1), 219–237.

Allegre, C. J., Manhes, G., & Gopel, C. (1995). The Age of the Earth. *Geochimica et Cosmochimica Acta*, *59*(8), 1445–1456. https://doi.org/10.1017/CBO9781139197137.015

Allégre, C. J., Birck, J. L., Fourcade, S., & Semet, M. P. (1975). Rubidium-87/Strontium-87 Age of Juvinas Basaltic Achondrite and Early Igneous Activity in the Solar Syste. *Science*, *187*(4175), 436–439.

Amelin, Y, Connelly, J., Zartman, R. E., Chen, J. H., Go, C., & Neymark, L. A. (2009). Modern U – Pb Chronometry of Meteorites : Advancing to Higher Time Resolution Reveals New Problems. *Geochimica et Cosmochimica Acta*, *73*(17), 5212–5223. https://doi.org/10.1016/j.gca.2009.01.040

Amelin, Yuri. (2006). The Prospect of High-Precision Pb Isotopic Dating of Meteorites. *Meteoritics and Planetary Science*, *41*(1), 7–17. https://doi.org/10.1111/j.1945-5100.2006.tb00189.x

\

Amelin, Yuri. (2008). U-Pb Ages of Angrites. *Geochimica et Cosmochimica Acta*, *72*(1), 221–232. https://doi.org/10.1016/j.gca.2007.09.034

Amelin, Yuri, Kaltenbach, A., Iizuka, T., Stirling, C. H., Ireland, T. R., Petaev, M., & Jacobsen, S. B. (2010). U-Pb Chronology of the Solar System's Oldest Solids with Variable 238U/235U. *Earth and Planetary Science Letters*, *300*(3–4), 343–350. https://doi.org/10.1016/j.epsl.2010.10.015

Amelin, Yuri, Koefoed, P., Iizuka, T., Fernandes, V. A., Huyskens, M. H., Yin, Q. Z., & Irving, A. J. (2018). U-Pb, Rb-Sr and Ar-Ar systematics of the ungrouped achondrites Northwest Africa 6704 and Northwest Africa 6693. *Geochimica et Cosmochimica Acta*, *245*, 628–642. https://doi.org/10.1016/j.gca.2018.09.021

Amelin, Yuri, Koefoed, P., Iizuka, T., Fernandes, V. A., Huyskens, M. H., Yin, Q.-Z., & Irving, A. J. (2019). U-Pb, Rb-Sr and Ar-Ar Systematics of the Ungrouped Achondrites Northwest Africa 6704 and Northwest Africa 6693. *Geochimica et Cosmochimica Acta*, *245*, 628–642. https://doi.org/10.1016/J.GCA.2018.09.021

Anbar, A. D., Roe, J. E., Barling, J., & Nealson, K. H. (2000). Nonbiological Fractionation of Iron Isotopes. *Science*, *288*(5463), 126–128. https://doi.org/10.1126/science.288.5463.126

Barrat, J. A., Greenwood, R. C., Verchovsky, A. B., Gillet, P., Bollinger, C., Langlade, J. A., et al. (2015). Crustal Differentiation in the Early Solar System: Clues from the Unique Achondrite Northwest Africa 7325 (NWA 7325). *Geochimica et Cosmochimica Acta*, *168*, 280–292. https://doi.org/10.1016/J.GCA.2015.07.020

Bennedix, G. K., McCoy, T. J., Keil, K., Bogard, D. D., & Garrison, D. H. (1998). A Petrologic and Isotopic Study of Winonaites : Evidence for Early Partial Melting , Brecciation , and Metamorphism. *Geochimica et Cosmochimica Acta*, *62*(14), 2535–2553.

Birck, J. -L, & Allègre, C. J. (1985). Evidence for the Presence of 53Mn in the Early Solar System. *Geophysical Research Letters*, *12*(11), 745–748. https://doi.org/10.1029/GL012i011p00745

Birck, J. L., & Allègre, C. J. (1978). Chronology and Chemical History of the Parent Body of Basaltic Achondrites Studied by the 87Rb-87Sr Method. *Earth and Planetary Science Letters*, *39*(1), 37–51. https://doi.org/10.1016/0012-821X(78)90139-5

Bischoff, A., Horstmann, M., Barrat, J., Chaussidon, M., Pack, A., & Herwartz, D. (2014). Trachyandesitic Volcanism in the Early Solar System. *Proceedings of the National Academy of Sciences*, *111*(35). https://doi.org/10.1073/pnas.1404799111

Bizzarro, M., Baker, J. A., Haack, H., & Lundgaard, K. L. (2005). Rapid Timescales for Accretion and Melting of Differentiated Planetesimals Inferred from ^{26}Al-^{26}Mg Chronometry. *The Astrophysical Journal*, *632*(1), L41–L44. https://doi.org/10.1086/497638

Blum, J., & Wurm, G. (2000). Experiments on Sticking, Restructuring, and Fragmentation of Preplanetary Dust Aggregates. *ICARUS*, *143*(1), 138–146.

Bogard, D. D., & Garrison, D. H. (2003). 39Ar-40Ar Ages of Eucrites and Thermal History of Asteroid 4 Vesta. *Meteoritics and Planetary Science*, *38*(5), 669–710. https://doi.org/10.1111/j.1945-5100.2003.tb00035.x

Bogard, D. D., Nyquist, L. E., Johnson, P., Wooden, J., & Bansal, B. (1983). Chronology of Brachina. *Meteoritics*, *18*, 269–270.

Bogard, D. D., Garrison, D. H., & Takeda, H. (2005). Ar-Ar and I-Xe Ages and the Thermal History of IAB Meteorites. *Meteoritics and Planetary Science*, *40*(2), 207–224. https://doi.org/10.1111/j.1945-5100.2005.tb00376.x

Bollard, J., Connelly, J. N., Whitehouse, M. J., Pringle, E. A., Bonal, L., Jørgensen, J. K., et al. (2017). Early Formation of Planetary Building Blocks Inferred from Pb Isotopic Ages of Chondrules. *Science Advances*, *3*(8).

Bouvier, A., Brennecka, G. B., & Wadhwa, M. (2011). Absolute Chronology of the First Solids in the Solar System. In *Workshop on the Formation of The First Solids in the Solar System* (pp. 4–5).

Bouvier, Audrey, & Wadhwa, M. (2010). The Age of the Solar System Redefined by the Oldest Pb-Pb Age of a Meteoritic Inclusion. *Nature Geoscience*, *3*(9), 637–641. https://doi.org/10.1038/ngeo941

Bouvier, Audrey, Spivak-Birndorf, L. J., Brennecka, G. A., & Wadhwa, M. (2011). New Constraints on Early Solar System Chronology from Al-Mg and U-Pb Isotope Systematics in the Unique Basaltic Achondrite Northwest Africa 2976. *Geochimica et Cosmochimica Acta*, *75*(18), 5310–5323. https://doi.org/10.1016/j.gca.2011.06.033

Brennecka, G. A., & Wadhwa, M. (2012a). Uranium isotope compositions of the basaltic angrite meteorites and the chronological implications for the early Solar System. *Proceedings of the National Academy of Sciences*, *109*(24), 9299–9303. https://doi.org/10.1073/pnas.1114043109

Brennecka, G. A., & Wadhwa, M. (2012b). Uranium Isotope Compositions of the Basaltic Angrite Meteorites and the Chronological Implications for the Early Solar System. *Proceedings of the National Academy of Sciences*, *109*(24), 9299–9303. https://doi.org/10.1073/pnas.1114043109

Brennecka, G. A., Weyer, S., Wadhwa, M., Janney, P. E., Zipfel, J., & Anbar, A. D. (2010). 238U/235U Variations in Meteorites: Extant 247Cm and Implications for Pb-Pb Dating. *Science*, *327*(5964), 449–451. https://doi.org/10.1126/science.1180871

Brennecka, Gregory A., Borg, L. E., Hutcheon, I. D., Sharp, M. A., & Anbar, A. D. (2010). Natural variations in uranium isotope ratios of uranium ore concentrates: Understanding the238U/235U fractionation mechanism. *Earth and Planetary Science Letters*, *291*(1–4), 228–233. https://doi.org/10.1016/j.epsl.2010.01.023

Campbell, I. H., & Taylor, S. R. (1983). No water, no granites - No oceans, no continents. *Geophysical Research Letters*, *10*(11), 1061–1064. https://doi.org/10.1029/GL010i011p01061

Carporzen, L., Weiss, B. P., Elkins-Tanton, L. T., Shuster, D. L., Ebel, D., & Gattacceca, J. (2011). Magnetic Evidence for a Partially Differentiated Carbonaceous Chondrite Parent Body. *Proceedings of the National Academy of Sciences of the United States of America*, *108*(16), 6386–6389. https://doi.org/10.1073/pnas.1017165108

Catanzaro, E. J., Murphy, T. J., Garner, E. L., & Shields, W. R. (1966). Absolute Isotopic Abundance Ratios and Atomic Weight of Magnesium. *J. Res. Natl. Bur. Stand. ...*, *70*(6), 453–458.

Chambers, J. E. (2001). Making More Terrestrial Planets. *ICARUS*, *152*(1), 205–224.

Chambers, J. E. (2006). Meteoritic Diversity and Planetesimal Formation. *Meteorites and the Early Solar System II*, 487–497.

Chambers, J. E., & Wetherill, G. W. (1998). Making the Terrestrial Planets: N-Body Integrations of Planetary Embryos in Three Dimensions. *ICARUS*, *136*(2), 304–327.

Ciesla, F. J. (2007). Outward Transport of High-Temperature Materials Around the Midplane of the Solar Nebula. *Science*, *318*(5850), 613–615. https://doi.org/10.1126/science.1147273

Clayton, R N. (1993). Oxygen Isotopes in Meteorites. *Annual Review of Earth and Planetary Sciences*, *21*, 115–149.

Clayton, Robert N, & Mayeda, T. K. (2017). Oxygen Isotope Studies of Achondrites. *Geochimica et Cosmochimica Acta*, *60*(11), 1999–2017.

Collinet, M., & Grove, T. L. (2020). Widespread Production of Silica- and Alkali-rich Melts at the Onset of Planetesimal Melting. *Geochimica et Cosmochimica Acta*, *In Press*.

Connelly, J. N., Bizzarro, M., Krot, A. N., Nordlund, Å., Wielandt, D., & Ivanova, M. A. (2012). The Absolute Chronology and Thermal Processing of Solids in the Solar Protoplanetary Disk. *Science*, *338*(6107), 651–655. https://doi.org/10.1126/science.1226919

Crozaz, G., & Pellas, P. (1984). The Formation Age of the Brachina Meteorite. *Earth and Planetary Science Letters*, *71*(1), 195–199. https://doi.org/10.1016/0012-821X(84)90065-7

Cuzzi, J. N., & Weidenschilling, S. J. (2006). Particle-Gas Dynamics and Primary Accretion. In *Meteorites and the early solar system II* (pp. 473–486).

Cuzzi, J. N., Hogan, R. C., & Shariff, K. (2008). Toward Planetesimals: Dense Chondrule Clumps in the Protoplanetary Nebula. *The Astrophysical Journal*, *687*(2), 1432–1447. https://doi.org/10.1086/591239

Day, J. M. D., Ash, R. D., Liu, Y., Bellucci, J. J., Rumble, D., McDonough, W. F., et al. (2009a). Early formation of evolved asteroidal crust. *Nature*, *457*(7226), 179–182. https://doi.org/10.1038/nature07651

Day, J. M. D., Ash, R. D., Liu, Y., Bellucci, J. J., Rumble, D., McDonough, W. F., et al. (2009b). Early Formation of Evolved Asteroidal Crust. *Nature*, *457*(7226), 179–182. https://doi.org/10.1038/nature07651

Day, J. M. D., Walker, R. J., Ash, R. D., Liu, Y., Rumble, D., Irving, A. J., et al. (2012). Origin of Felsic Achondrites Graves Nunataks 06128 and 06129 , and Ultramafic Brachinites and Brachinite-like Achondrites by Partial Melting of Volatile-rich Primitive Parent Bodies. *Geochimica et Cosmochimica Acta*, *81*, 94–128. https://doi.org/10.1016/j.gca.2011.12.017

Desch, S. J., Kalyaan, A., & Alexander, C. M. O. (2018). The Effect of Jupiter's Formation on the Distribution of Refractory Elements and Inclusions in Meteorites. *The Astrophysical Journal Supplement Series*, *238*(1), 11. https://doi.org/10.3847/1538-4365/aad95f

Dominik, C., & Tielens, A. G. G. M. (1997). The Physics of Dust Coagulation and the Structure of Dust Aggregates in Space. *The Astrophysical Journal*, *480*(2), 647–673. https://doi.org/10.1086/303996

Elkins-Tanton, L. T., Weiss, B. P., & Zuber, M. T. (2011). Chondrites as Samples of Differentiated Planetesimals. *Earth and Planetary Science Letters*, *305*(1–2), 1–10. https://doi.org/10.1016/j.epsl.2011.03.010

Gardner-vandy, K. G., Lauretta, D. S., & Mccoy, T. J. (2013). A Petrologic , Thermodynamic and Experimental Study of Brachinites : Partial Melt Residues of an R Chondrite-like Precursor. *Geochimica et Cosmochimica Acta*, *122*, 36–57. https://doi.org/10.1016/j.gca.2013.07.035

Ghosh, A., & McSween, H. Y. (1998). A Thermal Model for the Differentiation of Asteroid 4 Vesta , Based on Radiogenic Heating. *ICARUS*, *134*, 187–206.

Glavin, D. P., Kubny, A., Jagoutz, E., & Lugmair, G. W. (2004). Mn-Cr Isotope Systematics of the D ' Orbigny Angrite. *Meteoritics & Planetary Science*, *700*(5), 693–700.

Goldmann, A., Brennecka, G., Noordmann, J., Weyer, S., & Wadhwa, M. (2015). The Uranium Isotopic Composition of the Earth and the Solar System. *Geochimica et Cosmochimica Acta*, *148*, 145–158. https://doi.org/10.1016/j.gca.2014.09.008

Gomez-Tuena, A., Straub, S. M., & Zellmer, G. F. (2013). An Introduction to Orogenic Andesites and Crustal Growth. *Geologic Society, London, Special Publications*, *385*(8), 1–13.

Goodrich, C. A., & Delaney, J. S. (2000). Fe / Mg – Fe / Mn Relations of Meteorites and Primary Heterogeneity of Primitive Achondrite Parent Bodies. *Science*, *64*(1), 149–160.

Goodrich, C. A., Kita, N. T., Yin, Q., Sanborn, M. E., Williams, D., Nakashima, D., et al. (2017). Petrogenesis and Provenance of Ungrouped Achondrite Northwest Africa 7325 from Petrology , Trace Elements , Oxygen , Chromium and Titanium Isotopes , and Mid-IR Spectroscopy. *Geochimica et Cosmochimica Acta*, *203*, 381–403. https://doi.org/10.1016/j.gca.2016.12.021

Greenberg, R., Wacher, J. F., Hartmann, W. K., & Chapman, C. R. (1978). Planetesimals to Planets: Numerical Simulation of Collisional Evolution. *ICARUS*, *35*(1), 1–26.

Greenwood, R. C., Franchi, I. A., Gibson, J. M., & Benedix, G. K. (2012). Oxygen Isotope Variation in Primitive Achondrites: The Influence of Primordial, Asteroidal and Terrestrial Processes. *Geochimica et Cosmochimica Acta*, *94*, 146–163. https://doi.org/10.1016/j.gca.2012.06.025

Greenwood, Richard C., Burbine, T. H., & Franchi, I. A. (2020). Linking Asteroids and Meteorites to the Primordial Planetesimal Population. *Geochimica et Cosmochimica Acta*, *In Press*. https://doi.org/10.1016/j.gca.2020.02.004

Greenwood, Richard C, Franchi, I. A., Jambon, A., & Buchanan, P. C. (2005). Widespread Magma Oceans on Asteroidal Bodies in the Early Solar System. *Nature*, *435*, 916–918. https://doi.org/10.1038/nature03612

Greenzweig, Y., & Lissauer, J. (1992). Accretion Rates of Protoplanets: II. Gaussian Distributions of Planetesimal Velocities. *ICARUS*, *100*(2), 440–463.

Grossman, L. (1972). Condesation in the Primitive Solar Nebula. *Geochimica et Cosmochimica Acta*, *36*, 597–610.

Hahn Jr., T. M., Lunning, N. G., McSween Jr., H. Y., Bodnar, R. J., & Taylor, L. A. (2017). Dacite formation on Vesta : Partial melting of the eucritic crust, *1196*(6), 1173–1196. https://doi.org/10.1111/maps.12870

Haisch, Jr., K. E., Lada, E. A., & Lada, C. J. (2001). Disk Frequencies and Lifetimes in Young Clusters. *The Astrophysical Journal*, *553*(2), L153–L156. https://doi.org/10.1086/320685

Hevey, P. J., & Sanders, I. S. (2006). A Model for Planetesimal Meltdown by 26Al and its Implications for Meteorite Parent Bodies. *Meteoritics and Planetary Science*, *41*(1), 95–106. https://doi.org/10.1111/j.1945-5100.2006.tb00195.x

Honda, M., & Imamura, M. (1971b). Half-Life of 53Mn. *Physical Review C*, *4*(4), 1182–1188. https://doi.org/10.1103/PhysRevC.4.1182

Hublet, G., Debaille, V., Wimpenny, J., & Yin, Q. (2017). Differentiation and Magmatic Activity in Vesta Evidenced by 26Al- 26Mg Dating in Eucrites and Diogenites. *Geochimica et Cosmochimica Acta*, *218*, 73–97. https://doi.org/10.1016/j.gca.2017.09.005

Huyskens, M. H., Iizuka, T., & Amelin, Y. (2012). Evaluation of Colloidal Silicagels for Lead Isotopic Measurements Using Thermal Ionisation Mass Spectrometry. *Journal of Analytical Atomic Spectrometry*, *27*(9), 1439–1446. https://doi.org/10.1039/c2ja30083d

Iizuka, T., Amelin, Y., Kaltenbach, A., Koefoed, P., & Stirling, C. H. (2014). U-Pb Systematics of the Unique Achondrite Ibitira: Precise Age Determination and Petrogenetic Implications. *Geochimica et Cosmochimica Acta*, *132*, 259–273. https://doi.org/10.1016/j.gca.2014.02.017

Iizuka, T., Yamaguchi, A., Haba, M. K., Amelin, Y., Holden, P., Zink, S., et al. (2015). Timing of Global Crustal Metamorphism on Vesta as Revealed by High-Precision U-Pb Dating and Trace Element Chemistry of Eucrite Zircon. *Earth and Planetary Science Letters*, *409*, 182–192. https://doi.org/10.1016/j.epsl.2014.10.055

Irving, A. J., Kuehner, S. M., Bunch, T. E., Ziegler, K., Chen, G., Herd, C. D., et al. (2013). Ungrouped Mafic Achondrite Northwest Africa 7325: A Reduced, Iron Poor Cumulate Olivine Gabbro from a Differentiated Planetary Parent Body. In *Lunar and Planetary Science Conference* (p. 2164).

Jacobsen, B., Yin, Q. zhu, Moynier, F., Amelin, Y., Krot, A. N., Nagashima, K., et al. (2008). 26Al-26Mg and 207Pb-206Pb Systematics of Allende CAIs: Canonical Solar Initial 26Al/27Al Ratio Reinstated. *Earth and Planetary Science Letters*, *272*(1–2), 353–364. https://doi.org/10.1016/j.epsl.2008.05.003

Johansen, A., & Lambrechts, M. (2017). Forming Planets via Pebble Accretion. *Annual Review of Earth and Planetary Sciences*, *45*(1), 359–387. https://doi.org/10.1146/annurev-earth-063016-020226

Johansen, A., Oishi, J., Mac Low, M.-M., Klahr, H., Henning, T., & Youdin, A. (2007). Planetesimal Formation in Turbulent Circumstellar Disks. *Nature Letters*, *448*(30), 1022–1025. https://doi.org/10.1017/S1743921311020680

Johansen, A., Ormel, C., Bizzarro, M., & Rickman, H. (2014). The Multifaceted Planetesimal Formation Process. In H. Beuther, R. Klessen, C. Dullemond, & T. Henning (Eds.), *Protostars and Planets VI*. University of Arizona Press.

Keil, K. (2014). Brachinite Meteorites: Partial Melt Residues from an FeO-rich Asteroid. *Chemie Der Erde*, *74*(3), 311–329. https://doi.org/10.1016/j.chemer.2014.02.001

Kempf, S., Pfalzner, S., & Henning, T. K. (1999). N-Particle-Simulations of Dust Growth: I. Growth Driven by Brownian Motion. *Icarus*, *141*(2), 388–398.

Kita, N. T., Yin, Q., Pherson, G. J. M. A. C., Ushikubo, T., Jacobsen, B., Nagashima, K., et al. (2013). Al- 26 Mg Isotope Systematics of the First Solids in the Early Solar System. *Meteoritics & Planetary Science*, *48*(8), 1383–1400. https://doi.org/10.1111/maps.12141

Kleine, T., Mezger, K., Palme, H., Scherer, E., & Münker, C. (2005). The W Isotope Composition of Eucrite Metals: Constraints on the Timing and Cause of the Thermal Metamorphism of Basaltic Eucrites. *Earth and Planetary Science Letters*, *231*(1–2), 41–52. https://doi.org/10.1016/j.epsl.2004.12.016

Kleine, T, Mezger, K., Münker, C., Palme, H., & Bischoff, A. (2004). 182Hf-182W Isotope Systematics of Chondrites, Eucrites, and Martian Meteorites: Chronology of Core Formation and Early Mantle Differentiation in Vesta and Mars. *Geochimica et Cosmochimica Acta*, *68*(13), 2935–2946. https://doi.org/10.1016/j.gca.2004.01.009

Kleine, Thorsten, & Wadhwa, M. (2017). Chronology of Planetesimal Differentiation. In L. T. Elkins-Tanton & B. P. Weiss (Eds.), *Planetesimals* (pp. 224–245). Cambridge: Cambridge University Press. https://doi.org/10.1017/9781316339794.011

Koefoed, P., Amelin, Y., Yin, Q.-Z., Wimpenny, J., Sanborn, M. E., Iizuka, T., & Irving, A. J. (2016). U–Pb and Al–Mg Systematics of the Ungrouped Achondrite Northwest Africa 7325. *Geochimica et Cosmochimica Acta*, *183*, 31–45. https://doi.org/10.1016/J.GCA.2016.03.028

Kruijer, T. S., Touboul, M., Fischer-Gödde, M., Bermingham, K. R., Walker, R. J., & Kleine, T. (2014). Protracted Core Formation and Rapid Accretion of Protoplanets. *Science*, *344*(6188), 1150–1154. https://doi.org/10.1126/science.1251766

Kruijer, Thomas S., Burkhardt, C., Budde, G., & Kleine, T. (2017). Age of Jupiter Inferred from the Distinct genetics and Formation Times of Meteorites. *Proceedings of the National Academy of Sciences*, *114*(26), 6712–6716. https://doi.org/10.1073/pnas.1704461114

Larsen, K. K., Wielandt, D., Schiller, M., & Bizzarro, M. (2016). Chromatographic Speciation of Cr(III)-Species, Inter-Species Equilibrium Isotope Fractionation and Improved Chemical Purification Strategies for High-Precision Isotope Analysis. *Journal of Chromatography A*, *1443*(3), 162–174. https://doi.org/10.1016/j.chroma.2016.03.040

Larsen, Kirsten K., Trinquier, A., Paton, C., Schiller, M., Wielandt, D., Ivanova, M. A., et al. (2011). Evidence for Magnesium Isotope Heterogeneity in the Solar Protoplanetary Disk. *Astrophysical Journal Letters*, *735*(2). https://doi.org/10.1088/2041-8205/735/2/L37

Lee, T., Papanastassiou, D. A., & Wasserburg, G. J. (1976). Demonstration of 26Mg Excess in Allende and Evidence for 26Al. *Geophysical Research Letters*, *3*(1), 2–5.

Lee, T., Papanastassiou, D. A., & Wasserburg, G. J. (1977). Mg and Ca Isotopic Study of Individual Microscopic Crystals from the Allende Meteorite by the Direct Loading Technique. *Geochimica Et Cosmochimica Acta*, *41*(10), 1481–1485.

Li, M., & Xiao, L. (2016). Lifetimes and Accretion Rates of Protoplanetary Disks. *The Astrophysical Journal*, *820*(1), 36. https://doi.org/10.3847/0004-637x/820/1/36

Lodders, K. (2003). Solar System Abundances and Condensation Temperatures of the Elements. *The Astrophysical Journal*, *591*(2), 1220–1247. https://doi.org/10.1086/375492

Ludwig, K. R. (1980). Calculation of Uncertainties of U-Pb Isotopic Data. *Earth and Planetary Science Letters*, *46*, 212–220.

Ludwig, K. R. (2012). Isoplot 3.75, A Geochronological Toolkit for Microsoft Excel. *Berkeley Geochronology Center Special Publication No. 5*, (5), 1–72.

Lugmair, G. W., & Galer, S. J. G. (1992). Age and Isotopic Relationships Among the Angrites Lewis Cliff 86010 and Angra dos Reis. *Geochimica et Cosmochimica Acta*, *56*(4), 1673–1694. https://doi.org/10.1016/0016-7037(92)90234-A

Lugmair, G. W., & Shukolyukov, A. (1998a). Early Solar System Timescales According to 53Mn-53Cr Systematics. *Geochimica et Cosmochimica Acta*, *62*(16), 2863–2886. https://doi.org/10.1016/S0016-7037(98)00189-6

Lugmair, G. W., & Shukolyukov, A. (1998b). Early solar system timescales according to53Mn-53Cr systematics. *Geochimica et Cosmochimica Acta*, *62*(16), 2863–2886. https://doi.org/10.1016/S0016-7037(98)00189-6

Macpherson, G. J., Davis, A. M., & Zinner, E. K. (1995). The Dstribution of Aluminum-26 in the Early Solar System - a Reappraisal. *Meteoritics*, *30*(4), 365–386. https://doi.org/10.1111/j.1945-5100.1995.tb01141.x

MacPherson, G. J., Bullock, E. S., Tenner, T. J., Nakashima, D., Kita, N. T., Ivanova, M. A., et al. (2017). High Precision Al–Mg Systematics of Forsterite-Bearing Type B CAIs from CV3 Chondrites. *Geochimica et Cosmochimica Acta*, *201*, 65–82. https://doi.org/10.1016/j.gca.2016.12.006

Mandler, B. E., & Elkins-Tanton, L. T. (2013). The Origin of Eucrites , Diogenites , and Olivine Diogenites: Magma Ocean Crystallization and Shallow Magma Chamber Processes on Vesta. *Meteoritics & Planetary Science*, *48*(11), 2333–2349. https://doi.org/10.1111/maps.12135

Mason, B. (1967). Meteorites. *American Scientist*, *55*(4), 429–455.

McCoy, T. J., Dickinson, T. L., & Lofgren, G. E. (1999). Partial Melting of the Indarch (EH4) Meteorite: A Textural, Chemical, and Phase Relations View of Melting and Melt Migration. *Meteoritics and Planetary Science*, *34*(5), 735–746. https://doi.org/10.1111/j.1945-5100.1999.tb01386.x

McSween, H. Y., Binzel, R. P., De Sanctis, M. C., Ammannito, E., Prettyman, T. H., Beck, A. W., et al. (2013). Dawn; the Vesta-HED Connection; and the Geologic Context for Eucrites, Diogenites, and Howardites. *Meteoritics and Planetary Science*, *48*(11), 2090–2104. https://doi.org/10.1111/maps.12108

Mishra, R. K., & Chaussidon, M. (2014). Timing and Extent of Mg and Al Isotopic Homogenization in the Early Inner Solar System. *Earth and Planetary Science Letters*, *390*, 318–326. https://doi.org/10.1016/j.epsl.2013.12.042

Mittlefehldt, D. W. (2003). Achondrites. *Treatise on Geochemistry*, *52*(7), IUGG447–IUGG453. https://doi.org/10.1029/EO052i007pIU447

Mittlefehldt, D. W. (2015). Asteroid (4) Vesta: I. The Howardite-Eucrite-Diogenite (HED) Clan of Meteorites. *Chemie Der Erde - Geochemistry*. Elsevier GmbH. https://doi.org/10.1016/j.chemer.2014.08.002

Mittlefehldt, D. W., Bogard, D. D., Berkley, J. L., & Garrison, D. H. (2003). Brachinites: Igneous Rocks from a Differentiated Asteroid. *Meteoritics and Planetary Science*, *38*(11), 1601–1625. https://doi.org/10.1111/j.1945-5100.2003.tb00004.x

Miyamoto, M., Fujii, N., & Takeda, H. (1981). Ordinary Chondrite Parent Body - An Internal Heating Model. In *Lunar and Planetary Science Conference* (pp. 1145–1152).

Morbidelli, A., Lunine, J. I., O'Brien, D. P., Raymond, S. N., & Walsh, K. J. (2012). Building Terrestrial Planets. *Annual Review of Earth and Planetary Sciences*, *40*(1), 251–275. https://doi.org/10.1146/annurev-earth-042711-105319

Morbidelli, Alessandro, Bottke, W. F., Nesvorný, D., & Levison, H. F. (2009). Asteroids Were Born Big. *Icarus*, *204*(2), 558–573. https://doi.org/10.1016/j.icarus.2009.07.011

Nehru, C. E., Prinz, M., Delaney, J. S., Dreibus, G., Palme, H., Spettel, H., & Wänke, J. S. (1983). Brachina: A New Type of Meteorite, not a Chassignite. *Journal of Geophysical Research- Solid Earth*, *88*(S01), B237–B244.

Nehru, C. E., Prinz, M., Weisberg, M. K., Ebihara, M., Clayton, R. N., & Mayeda, T. K. (1992). Brachinites: A New Primitive Achondrite Group. *Meteoritics*. https://doi.org/10.1016/j.jpowsour.2005.12.091

Neumann, W., Breuer, D., & Spohn, T. (2014). Differentiation of Vesta : Implications for a Shallow Magma Ocean. *Earth and Planetary Science Letters*, *395*, 267–280. https://doi.org/10.1016/j.epsl.2014.03.033

Norris, T. L., Gancarz, A. J., Rokop, D. J., & Thomas, K. W. (1983). Half-Life of 26Al. *Journal of Geophysical Research- Solid Earth*, *88*(S1), B331--B333. https://doi.org/10.1029/JB088iS01p0B331

Nyquist, L. E., Reese, Y., Wiesmann, H., Shih, C. Y., & Takeda, H. (2003). Fossil 26 Al and 53 Mn in the Asuka 881394 Eucrite: Evidence of the Earliest Crust on Asteroid 4 Vesta. *Earth and Planetary Science Letters*, *214*(1–2), 11–25. https://doi.org/10.1016/S0012-821X(03)00371-6

Nyquist, L. E., Kleine, T., Shih, C. Y., & Reese, Y. D. (2009). The Distribution of Short-lived Radioisotopes in the Early Solar System and the Chronology of Asteroid Accretion, Differentiation, and Secondary Mineralization. *Geochimica et Cosmochimica Acta*, *73*(17), 5115–5136. https://doi.org/10.1016/j.gca.2008.12.031

O'Brien, D. P., Morbidelli, A., & Levison, H. F. (2006). Terrestrial Planet Formation with Strong Dynamical Friction. *ICARUS*, *184*(1), 39–58.

Ott, U., Löhr, H.-P., & Begemann, F. (1985). Noble Gases and the Classification of Brachina. *Meteoritics*, *20*, 69–78.

Ott, U., Begemann, F., & Löhr, H.-P. (1987). Noble Gases in ALH 84025: Like Brachina, Unlike Chassigny. *Meteoritics*, *22*, 476–477.

Patterson, C. (1956). Age of Meteorites and the Earth. *Geochimica et Cosmochimica Acta*, *10*, 230–237.

Raymond, S. N., Quinn, T., & Lunine, J. I. (2004). Making Other Earths: Dynamical Simulations of Terrestrial Planet Formation and Water Delivery. *ICARUS*, *168*(1), 1–17.

Richter, S., Eykens, R., Kühn, H., Aregbe, Y., Verbruggen, A., & Weyer, S. (2010). New Average Values for the 238U/235U Isotope Ratios of Natural Uranium Standards. *International Journal of Mass Spectrometry*, *295*(1–2), 94–97. https://doi.org/10.1016/j.ijms.2010.06.004

Righter, K., & Drake, M. . (1996). Core Formation in Earth's Moon , Mars , and Vesta. *ICARUS*, *529*, 513–529.

Righter, K., & Drake, M. J. (1997). A Magma Ocean on Vesta: Core Formation and Petrogenesis of Eucrites and Diogenites. *Meteoritics and Planetary Science*, *32*(6), 929–944. https://doi.org/10.1111/j.1945-5100.1997.tb01582.x

Roszjar, J., Whitehouse, M. J., Srinivasan, G., Mezger, K., Scherer, E. E., Van Orman, J. A., & Bischoff, A. (2016). Prolonged Magmatism on 4 Vesta Inferred from Hf–W Analyses of Eucrite Zircon. *Earth and Planetary Science Letters*, *452*, 216–226. https://doi.org/10.1016/j.epsl.2016.07.025

Rudnick, R. L. (1995). Making Continental Crust. *Nature*, *378*(6557), 571–578. https://doi.org/10.1038/378571a0

Rumble III, D., Bunch, T. E., Wittke, J. H., & Kuehner, S. M. (2008). Oxygen Isotopic and Petrological Diversity Among Brachinites NWA 4872, NWA 4874, NWA 4882 and NWA 4969: How Many Ancient Parent Bodies? *Lunar and Planetary Science Conference*, *39*, 1974.

Russell, S. S., Hartmann, L., Cuzzi, J. N., Krot, A. N., Gounelle, M., & Weidenschilling, S. J. (2006). Timescales of the Solar Protoplanetary Disk. In *Meteorites and the early solar system II*.

Ruzicka, A., Snyder, G. A., & Tayler, L. A. (1997). Vesta as the HED Parent Body: Implications for the Size of a Core and for Large-Scale Differentiation. *Meteoritics and Planetary Science*, *32*(6), 825–840. https://doi.org/http://www.nature.com/nature/journal/v429/n6989/suppinfo/nature02530_S1.html

Sanborn, M. E., Carlson, R. W., & Wadhwa, M. (2015). 147,146Sm-143,142Nd, 176Lu-176Hf, and 87Rb-87Sr Systematics in the Angrites: Implications for Chronology and Processes on the Angrite Parent Body. *Geochimica et Cosmochimica Acta*, *171*, 80–99. https://doi.org/10.1016/j.gca.2015.08.026

Sanborn, M. E., Wimpenny, J., Williams, C. D., Yamakawa, A., Amelin, Y., Irving, A. J., & Yin, Q.-Z. (2019). Carbonaceous Achondrites Northwest Africa 6704/6693: Milestones for Early Solar System Chronology and Genealogy. *Geochimica et Cosmochimica Acta*, *245*, 577–596. https://doi.org/10.1016/J.GCA.2018.10.004

De Sanctis, M. C., Ammannito, E., Capria, M. T., Tosi, F., Capaccioni, F., Zambon, F., et al. (2012). Spectroscopic Characterization of Mineralogy and its Diversity Across Vesta. *Science*, *336*(6082), 697–700. https://doi.org/10.1126/science.1219270

Schiller, M., Baker, J. A., & Bizzarro, M. (2010). 26Al-26Mg Dating of Asteroidal Magmatism in the Young Solar System. *Geochimica et Cosmochimica Acta*, *74*(16), 4844–4864. https://doi.org/10.1016/j.gca.2010.05.011

Schiller, M., Baker, J., Creech, J., Paton, C., Millet, M. A., Irving, A., & Bizzarro, M. (2011). Rapid Timescales for Magma Ocean Crystallization on the Howardite-Eucrite-Diogenite Parent Body. *Astrophysical Journal Letters*, *740*(1). https://doi.org/10.1088/2041-8205/740/1/L22

Schiller, M., Connelly, J. N., Glad, A. C., Mikouchi, T., & Bizzarro, M. (2015). Early Accretion of Protoplanets Inferred from a Reduced Inner Solar System 26Al =Inventory. *Earth and Planetary Science Letters*, *420*, 45–54. https://doi.org/10.1016/j.epsl.2015.03.028

Schmitz, M. D., & Schoene, B. (2007). Derivation of Isotope Ratios, Errors, and Error Correlations for U-Pb Geochronology Using 205Pb-235U-(233U)-Spiked Isotope Dilution Thermal Ionization Mass Spectrometric Data. *Geochemistry, Geophysics, Geosystems*, *8*(8), 1–20. https://doi.org/10.1029/2006GC001492

Schramm, D. N., Tera, F., & Wasserburg, G. J. (1970). The Isotopic Abundance of 26Mg and Limits on 26Al in the Early Solar System. *Earth and Planetary Science Letters*, *10*(1), 44–59. https://doi.org/10.1016/0012-821X(70)90063-4

Shearer, C. K., Burger, P. V., Neal, C., Sharp, Z., Spivak-Birndorf, L., Borg, L., et al. (2010). Non-Basaltic Asteroidal Magmatism During the Earliest Stages of Solar System Evolution: A View from Antarctic Achondrites Graves Nunatak 06128 and 06129. *Geochimica et Cosmochimica Acta*, *74*(3), 1172–1199. https://doi.org/10.1016/j.gca.2009.10.029

Shields, W., & Murphy, T. (1966). Absolute Isotopic Abundance Ratios and the Atomic Weight of a Reference Sample of Chromium. *J. Res. Natl. Bur. Stand. ...*, *70*(2), 193–198.

Shukolyukov, A., & Lugmair, G. W. (2006). Manganese-chromium isotope systematics of carbonaceous chondrites. *Earth and Planetary Science Letters*, *250*(1–2), 200–213. https://doi.org/10.1016/j.epsl.2006.07.036

Spivak-Birndorf, L., Wadhwa, M., & Janney, P. (2009). 26Al – 26 Mg Systematics in D'Orbigny and Sahara 99555 Angrites : Implications for High-Resolution Chronology using Extinct Chronometers. *Geochimica et Cosmochimica Acta*, *73*(17), 5202–5211. https://doi.org/10.1016/j.gca.2009.02.038

Srinivasan, G., Goswami, J. N., & Bhandari, N. (1999). 26Al in Eucrite Piplia Kalan: Plausible Heat Source and Formation Chronology. *Science*, *284*(5418), 1348–1350. https://doi.org/10.1126/science.284.5418.1348

Srinivasan, P., Dunlap, D. R., Agee, C. B., Wadhwa, M., Coleff, D., Ziegler, K., et al. (2018). Silica-Rich Volcanism in the Early Solar System Dated at 4.565 Ga. *Nature Communications*, *9*(1), 3036. https://doi.org/10.1038/s41467-018-05501-0

Stacey, J. S., & Kramers, J. D. (1975). Approximation of Terrestrial Lead Isotope Evolution by a Two-Stage Model. *Earth and Planetary Science Letters*, *26*(2), 207–221. https://doi.org/10.1016/0012-821X(75)90088-6

Stolper, E. (1977). Experimental Petrology of Eucritic Meteorites. *Geochimica et Cosmochimica Acta*, *41*(5), 587–611. https://doi.org/10.1016/0016-7037(77)90300-3

Strom, K. M., Strom, S. E., Edwards, S., Cabrit, S., & Skrutskie, M. (1989). Circumstellar mMaterial Associated with Solar-Type Pre-Main-Sequence Stars: A Possible Constraint on the Timescale for Planet Building. *Astrophysical Journal*, *97*(5), 1451.

Swindle, T. D., Kring, D. A., Burkland, M. K., Hill, D. H., & Boynton, W. V. (1998). Noble Gases, Bulk Chemsitry, and Petrography of Olivine-Rich Achondrites Eagles Nest and Lewis Cliff 88763: Comparison to Brachinites. *Meteoritics and Planetary Science*, *33*(1), 31–48. https://doi.org/10.1111/j.1945-5100.1998.tb01605.x

Tatsumoto, M., Knight, R. J., & Allegre, C. J. (1973). Time Differences in the Formation of Meteorites as Determined from the Ratio of Lead-207 to Lead-206. *Science*, *180*(4092), 1279–1283. https://doi.org/10.1126/science.180.4092.1279

Taylor, J. G., Maggiore, P., Scott, E. R. D., Rubin, A. E., & Keil, K. (1987). Original Structures, and Fragmentation and Reassembly Histories of Asteroids: Evidence from Meteorites. *Icarus*, *69*(1), 1–13. https://doi.org/10.1016/0019-1035(87)90002-9

Teng, F., Li, W., Ke, S., Marty, B., Dauphas, N., Huang, S., et al. (2010). Magnesium Isotopic Composition of the Earth and Chondrites. *Geochimica et Cosmochimica Acta*, *74*(14), 4150–4166. https://doi.org/10.1016/j.gca.2010.04.019

Thrane, K., Bizzarro, M., & Baker, J. A. (2006). Extremely Brief Formation Interval for Refractory Inclusions and Uniform Distribution of 26 Al in the Early Solar System . *The Astrophysical Journal*, *646*(2), L159–L162. https://doi.org/10.1086/506910

Tissot, F. L. H., & Dauphas, N. (2015). Uranium Isotopic Compositions of the Crust and Ocean: Age Corrections, U Budget and Global Extent of Modern Anoxia. *Geochimica et Cosmochimica Acta*, *167*, 113–143. https://doi.org/10.1016/j.gca.2015.06.034

Tissot, F. L. H., Dauphas, N., & Grove, T. L. (2017). Distinct 238U/235U Ratios and REE Patterns in Plutonic and Volcanic Angrites: Geochronologic Implications and Evidence for U isotope Fractionation During Magmatic Processes. *Geochimica et Cosmochimica Acta*, *213*, 593–617. https://doi.org/10.1016/j.gca.2017.06.045

Touboul, M., Sprung, P., Aciego, S. M., Bourdon, B., & Kleine, T. (2015). Hf-W Chronology of the Eucrite Parent Body. *Geochimica et Cosmochimica Acta*, *156*, 106–121. https://doi.org/10.1016/j.gca.2015.02.018

Trinquier, A., Birck, J. L., Allègre, C. J., Göpel, C., & Ulfbeck, D. (2008). 53Mn-53Cr Systematics of the Early Solar System Revisited. *Geochimica et Cosmochimica Acta*, *72*(20), 5146–5163. https://doi.org/10.1016/j.gca.2008.03.023

Trinquier, Anne, Birck, J., & Allegre, C. J. (2007). Widespread ^{54} Cr Heterogeneity in the Inner Solar System. *The Astrophysical Journal*, *655*(2), 1179–1185. https://doi.org/10.1086/510360

Trinquier, Anne, Trinquier, A., Elliott, T., Ulfbeck, D., Coath, C., Krot, A. N., & Bizzarro, M. (2009). Origin of Nucleosynthetic Isotope Heterogeneity in the Solar Protoplanetary Disk. *Science*, *324*(5925), 374–376. https://doi.org/10.1126/science.1168221

Urey, H. C. (1955). The Cosmic Abundances of Potassium, Uranium, and Thorium and the Heat Balances of the Earth, the Moon, and MArs. *Proceedings of the National Academy of Sciences*, *41*, 127–144.

Usui, T., Jones, J. H., & Mittlefehldt, D. W. (2015). A Partial Melting Study of an Ordinary (H) Chondrite Composition with Application to the Unique Achondrite Graves Nunataks 06128 and 06129. *Meteoritics & Planetary Science*, *50*(4), 759–781. https://doi.org/10.1111/maps.12392

Vermeesch, P. (2018). IsoplotR : A Free and Open Toolbox for Geochronology. *Geoscience Frontiers*, *9*(5), 1479–1493. https://doi.org/10.1016/j.gsf.2018.04.001

Villeneuve, J., Chaussidon, M., & Libourel, G. (2009). Homogeneous Distribution of 26Al in the Solar System from the Mg Isotopic Composition of Chondrules. *Science*, *325*(5943), 985–988. https://doi.org/10.1126/science.1173907

Wadhwa, M., Shukolyukov, A., & Lugmair, G. W. (1998). 53Mn-53Cr Systematics in Brachina: A Record of One of the Earliest Phases of Igneous Activity on an Asteroid. *Lunar and Planetary Science Conference XXIX*, *29*, #1480 (abstract).

Wadhwa, M., Amelin, Y., Bogdanovski, O., Shukolyukov, A., Lugmair, G. W., & Janney, P. (2009). Ancient Relative and Absolute Ages for a Basaltic Meteorite: Implications for Timescales of Planetesimal Accretion and Differentiation. *Geochimica et Cosmochimica Acta*, *73*(17), 5189–5201. https://doi.org/10.1016/j.gca.2009.04.043

Wadhwa, M., Kita, N. T., Bullock, E. S., G.J., M., & A., B. (2014). High Precision Al-Mg Isotope Systematics for an Almost Pristine Refractory Inclusion: Implications for the Absolute Age of the Solar System. In *Lunar and Planetary Science Conference* (pp. 26–27).

Warren, P. H. (1997). Magnesium Oxide-Iron Oxide Mass Balance Constraints and a more Detailed Model for the Relationship Between Eucrites and Diogenites. *Meteoritics and Planetary Science*, *32*(6), 945–963. https://doi.org/10.1111/j.1945-5100.1997.tb01583.x

Warren, P. H. (2011). Stable-Isotopic Anomalies and the Accretionary Assemblage of the Earth and Mars : A Subordinate Role for Carbonaceous Chondrites. *Earth and Planetary Science Letters*, *311*(1–2), 93–100. https://doi.org/10.1016/j.epsl.2011.08.047

Warren, P. H., & Gessler, P. (2001). Bluewing 001 : A New Eucrite with Extremely Unequilibrated Pyroxene, Cognate (?) Eucritic Xenoliths, and Stannern-like Geochemistry. In *Lunar and Planetary Science Conference* (pp. 4–5).

Wasserburg, G. J., Wimpenny, J., & Yin, Q. Z. (2012). Mg Isotopic Heterogeneity, Al-Mg Isochrons, and Canonical 26Al/27Al in the Early Solar System. *Meteoritics and Planetary Science*, *47*(12), 1980–1997. https://doi.org/10.1111/maps.12014

Weber, I., Morlok, A., Bischoff, A., Hiesinger, H., Ward, D., Joy, K. H., et al. (2016). Cosmochemical and Spectroscopic Properties of Northwest Africa 7325-A Consortium Study. *Meteoritics and Planetary Science*, *51*(1), 3–30. https://doi.org/10.1111/maps.12586

Weidenschilling, S. J. (1977). Aerodynamics of Solid Bodies in the Solar Nebula. *Royal Astronomoy Society*, *80*, 57–70.

Wetherill, G. W., & Stewart, G. R. (1989). Accumulation of a Swarm of Small Planetesimals. *ICARUS*, *77*(2), 330–357.

Wimpenny, J., Sanborn, M. E., Koefoed, P., Cooke, I. R., Stirling, C., Amelin, Y., & Yin, Q. Z. (2019). Reassessing the Origin and Chronology of the Unique Achondrite Asuka 881394: Implications for Distribution of 26Al in the Early Solar System. *Geochimica et Cosmochimica Acta*, *244*, 478–501. https://doi.org/10.1016/j.gca.2018.10.006

Windmark, F., Birnstiel, T., Güttler, C., Blum, J., Dullemond, C. P., & Henning, T. (2012). Planetesimal formation by sweep-up: How the bouncing barrier can be beneficial to growth. *Astronomy and Astrophysics*, *540*, 1–17. https://doi.org/10.1051/0004-6361/201118475

Wood, J. A. (1996). Unresolved Issues in the Formation of Chondrules and Chondrites. In R. H. Hewins, R. Jones, & E. R. D. Scott (Eds.), *Chondrules and the Protoplanetary Disk*. Cambridge University Press.

Wurm, G., & Blum, J. (1998). Experiments on Preplanetary Dust Aggregation. *ICARUS*, *132*(1), 125–136.

Wurm, G., Paraskov, G., & Krauss, O. (2005). Growth of planetesimals by impacts at ~25 m/s. *Icarus*, *178*(1), 253–263. https://doi.org/10.1016/j.icarus.2005.04.002

Yamaguchi, A., Jeffrey, G., & Keil, K. (1997). Metamorphic history of the eucritic crust of 4 Vesta. *Journal of Geophysical Research*, *102*, 381–386.

Yamakawa, A., Yamashita, K., Makishima, A., & Nakamura, E. (2009). Chemical separation and mass spectrometry of Cr, Fe, Ni, Zn, and Cu in terrestrial and extraterrestrial materials using thermal ionization mass spectrometry. *Analytical Chemistry*, *81*(23), 9787–9794. https://doi.org/10.1021/ac901762a

Yamakawa, A., Yamashita, K., Makishima, A., & Nakamura, E. (2010). Chromium isotope systematics of achondrites: Chronology and isotopic heterogeneity of the inner solar system bodies. *Astrophysical Journal*, *720*(1), 150–154. https://doi.org/10.1088/0004-637X/720/1/150